

**TOOL FOR QUALITY TESTING OF RAW MATERIAL OF PERMANENT MAGNETS**

By

Muhammad Jawad Zaheer

A THESIS

Submitted to  
Michigan State University  
in partial fulfillment of the requirements  
for the degree of

MASTER OF SCIENCE

Electrical Engineering

2012

## **ABSTRACT**

### **TOOL FOR QUALITY TESTING OF RAW MATERIAL OF PERMANENT MAGNETS**

By

Muhammad Jawad Zaheer

Permanent magnets are used extensively in synchronous machines that produce high power density, wide speed range and high efficiency. It is important therefore to determine the quality of the magnetic material before the assembly and magnetization in the electrical machines. In this thesis, different types of magnetometers are reviewed before pulsed field magnetometer system is chosen due to its simplicity, quick and smaller size to measure the magnetic hysteresis for characterization. A pulsed magnetometer is useful for testing high-performance magnets due to their ability to produce higher magnetic fields. The basic geometry, coil winding configuration and input currents of the pulsed field magnetometer are calculated using FEM and MATLAB/Simulink. The whole coil arrangement combined with power electronic circuitry is designed and built while the control is implemented using LabView.

The second part of the work is to distinguish between good and bad raw material of the permanent magnets used in PMAC machines. For this, the magnetic field is applied to good raw material magnet such that the negative peak forces the magnet operating point to fall slightly above or close to the knee of the hysteresis curve. It is used as reference and compared to the magnets with some amount of impurities. On the whole, the pulsed field magnetometer, coupled with minor loops and recoil lines, is used as a successful technique to distinguish between good and bad raw material of the permanent magnets used in PMAC machines.

## **ACKNOWLEDGEMENTS**

I wish to express my infinite gratitude to my advisor, Dr. Elias Strangas, whose advice and help have been invaluable to me throughout my work. I would also like to thank Dr. Edward Rothwell and Dr. Bingsen Wang for their time and effort in being part of my committee.

I would like to extend special thanks to those at General Motors, especially John Agapiou and Thomas Perry, who funded the project and helped make this research possible. I would also like to thank the ECE department members, whose help was much appreciated, including Brian Wright, Gregg Mulder, Roxanne Peacock, Meagan Kroll, and Pauline Van Dyke.

I would also like to thank all of my previous and current colleagues as well as my friends at MSU. They are Sajjad Zaidi, Abdul Rahman Tariq, Carlos Nino, Shanelle Foster, Arslan Qaiser, Andrew Babel, Eduardo Montalvo Ortiz, Reemon Haddad, Jorge Cintron-Rivera, Shahid Nazrulla, Hassan Aqeel Khan, Afshan Huma and many others.

Last but not the least, my special thanks to my parents and brothers for their constant support and prayers, and who had been waiting to share the happiness and sorrows of the lives.

# TABLE OF CONTENTS

LIST OF TABLES.....	vi
LIST OF FIGURES.....	vii
Chapter 1 Introduction .....	1
1.1- Overview and Problem .....	1
1.2- Proposed Solution.....	2
1.3- Background: .....	3
1.4- Thesis Organization:.....	5
Chapter 2 Theory .....	7
2.1- Magnetic Characteristics: .....	7
2.1.1- Major Hysteresis Loop:.....	7
2.1.2- Minor Hysteresis Loops: .....	10
2.1.3- Demagnetization: .....	11
2.1.4- Recoil Lines: .....	12
2.1.4.1- Effect of Temperature .....	14
2.1.5- Eddy Currents: .....	16
2.1.6- Demagnetization Factor .....	18
2.2- Types of Magnetometer: .....	20
2.2.1- Hysteresis graph .....	21
2.2.2- Vibrating Sample Magnetometer .....	25
2.2.3- SQUID Magnetometer .....	28
2.2.4- Pulsed Field Magnetometer .....	30
Chapter 3 Design and Simulation .....	34
3.1- Design Objectives.....	34
3.2- Finite Element Analysis: .....	35
3.2.1- Equations used in the FEM:.....	35
3.2.2- FEM based Design .....	39
3.3- MATLAB/Simulink: .....	53
3.3.1- Saturable Transformer hysteresis characteristics .....	53
3.3.2- Model Parameterization and circuit.....	58
3.3.3- Results/Waveforms .....	60
Chapter 4 Experimental Setup.....	64
4.1- Hardware (Power Electronics) .....	64
4.2- Software Implementation .....	69
4.2.1- LabView .....	69
4.2.2- MATLAB .....	70
4.3- Experimental Procedure .....	71
4.3.1- Calibration of Helmholtz Coil .....	71
4.3.2- Testing Procedure .....	72

4.3.3-	TestingProcedureforgoodandbadrawmaterial .....	75
4.3.4-	SetofTests .....	76
Chapter 5	Experimental Results .....	77
5.1-	Magnetometer .....	77
5.2-	Sample Magnets.....	80
5.2.1-	Nickel Plated - N42 .....	80
5.2.2-	Aluminum Coated.....	84
5.2.3-	BlackPaintCoated.....	87
Chapter 6	Conclusions and Future Work.....	91
6.1-	Conclusions: .....	91
6.2-	Future Work Modifications:.....	93
BIBLIOGRAPHY	.....	96

## LIST OF TABLES

Table 3.1: Hysteresis parameters .....	59
Table 5.1: Comparison of magnet characteristics between the specs provided by the K&J Magnetics and measured using pulsed field magnetometer .....	81
Table 5.2: Comparison of residual remanence at different temperature and damping resistors for Nickel plated magnets.....	83
Table 5.3: Comparison of residual remanence at different temperature for Aluminum coated magnets.....	87
Table 5.4: Comparison of residual remanence at different temperature for Black painted magnets.....	.90

## LIST OF FIGURES

Figure 2.1: Major Hysteresis loop for the magnet .....	9
Figure 2.2: Minor Hysteresis loop for the magnet .....	10
Figure 2.3: Demagnetization curve and working line .....	12
Figure 2.4: Demagnetization curve and recoil lines of the permanent magnet.....	13
Figure 2.5: Magnet at (a) 20 <sup>0</sup> C and (b) 100 <sup>0</sup> C .....	15
Figure 2.6: Shape of magnet and demagnetization field.....	19
Figure 2.7: Measurements in Closed and Open Circuit Magnetometer .....	21
Figure 2.8: Characterization of permanent magnets using Hysteresisgraph .....	22
Figure 2.9: Scheme of Vibrating Sample Magnetometer with electromagnet field source .....	27
Figure 2.10: SQUID Magnetometer .....	29
Figure 2.11: Coil Arrangement of Pulsed Field Magnetometer.....	30
Figure 3.1: (a) Actual dimensions of the final design of coil arrangement. (b) Problem domain definition for finite element analysis in FLUX 2D .....	40
Figure 3.2: Magnetic field lines shown at one-time instance.....	41
Figure 3.3: Pulsed Current through the excitation coil.....	42
Figure 3.4: Induced voltages across the search coil .....	43
Figure 3.5: Induced voltages across the Helmholtz coil .....	45
Figure 3.6: Axial-component of the magnetic flux density.....	47
Figure 3.7: Axial-component of the magnetic field strength .....	49
Figure 3.8: (a) current (b) induced voltage in search coil (c) induced voltage in H coil (d) magnetic flux density (e) magnetic field strength .....	50
Figure 3.9 Electrical Model of the PSB saturable transformer .....	56
Figure 3.10 Hysteresis Loops .....	54
Figure 3.11 Internal minor loops .....	57
Figure 3.12: Simulink Circuit .....	58
Figure 3.13 Modeled hysteresis major loops.....	60
Figure 3.14: Excitation Current .....	61
Figure 3.15: Magnetization Current.....	61
Figure 3.16: Magnetic Flux Density vs time with different damper resistors .....	62

Figure 3.17: Hysteresis with different damper resistors .....	65
Figure 4.1: Power Electronics Circuitry .....	66
Figure 4.2: Control Circuitry from data acquisition to control the contactors .....	66
Figure 4.3: Actual coil arrangement showing excitation coil, search coil and Helmholtz coil with the sample magnet at the center .....	68
Figure 4.4: Control Circuitry from data acquisition to control the contactors .....	69
Figure 4.5: Initial Hysteresis loop without knowledge of initial conditions converted to symmetrical hysteresis after removing the offsets .....	73
Figure 4.6 Testing Sequence for the magnet .....	74
Figure 5.1: Comparison between Finite Element Analysis and Experimental Results without placing the magnet at the center of the coil i.e. in the air .....	78
Figure 5.2: Nickel plated- N42 with 46.2mF capacitance at 425 V .....	81
Figure 5.3: Hysteresis for Nickel Plated-N42 with 46.2mF capacitance at 300V with different damping resistance and temperature .....	82
Figure 5.4: Complete hysteresis for Aluminum coated magnet at 425V at room temperature ..	84
Figure 5.5: Hysteresis for Aluminum coated magnet at 425V at different temperatures using capacitance of 38.5mF .....	85
Figure 5.6: Complete hysteresis for Black paint coated magnet at 425V at different temperatures and capacitance .....	88
Figure 5.7: Complete hysteresis for Black Paint coated magnet at 425V at different temperatures .....	89

# Chapter 1

## Introduction

### 1.1- Overview and Problem

From computers to airplane to cell phones, permanent magnets have been playing a vital in various fields for many decades. They are used in the imperatively for the generation, distribution and conversion of electrical energy as well as in the field of telecommunications and biomedical applications. Permanent magnets are extensively used in synchronous machine that produces high power density, wide speed range and high efficiency.

Raw permanent magnet material used in PMAC machines is assembled in an unmagnetized state. Permanent magnets are later magnetized through an external magnetizer. Once they are installed, they cannot be removed. Thus, if the quality of the magnets is inadequate, the rotor assembly is unusable. It is important therefore to determine the quality of the magnetic material before the assembly and magnetization.

A pulsed magnetometer is useful for testing high-performance magnets because it can produce high magnetic fields that are sufficient to magnetically saturate them.

## 1.2- Proposed Solution

The quality of raw material of the permanent magnets will be characterized in three steps. First step comprises of full characterization of standard cylindrical shaped magnets and use it as baseline. For this step, pulsed field magnetometer system is built where pulsed current is discharged through the excitation coil and induced voltages are measured due to change of flux through the air and the magnet in the  $0^{\circ}$  and  $180^{\circ}$  direction. These measured induced voltages will be used to calculate the magnetic field intensity and magnetic flux density in the magnet and later used to plot the measured hysteresis loop. This characterization will be mainly focused on the first and second quadrant of the hysteresis graph, at the remanence and coercivity of the magnets; and the effect of temperature on them. Since the pulsed field magnetometer system is an open-loop circuit system, the demagnetization and eddy current errors have to be accounted for. The measured hysteresis loop will be compared with the actual hysteresis loop obtained from the manufacturer and corrected until the measured hysteresis loop resembles the actual hysteresis loop obtained in a high accuracy device. For this project, a hysteresisgraph will be used at the GM Research laboratories. Then, this full characterization will be used as our baseline to the second step.

Second step of the characterization consists of quick characterization of the cylindrical shaped sample magnets and use it as second reference. In this step, the pulsed field magnetometer is again used to measured hysteresis loop that will be compared with our baseline hysteresis loop in the first step. Other important properties of the magnet characteristics are the minor loops and recoil lines of the magnet in the second quadrant.

Due to the demagnetization caused by the pulsed current in the reversed direction, the magnet operates on a minor loop different from the major hysteresis loop. In general, the minor loop is estimated by a recoil line that is constructed based on the original major hysteresis loop, known slope and operating point of magnet [1]. The magnets containing bad raw material will have lower coercivity than the good raw materials of the magnet. Due to lower coercivity, the knee of the hysteresis curve will move rightwards, closer to the vertical magnetic flux density axis as the bad raw material influence increases. If the working condition remains same, the working point could fall below the knee and follows different recoil line. The demagnetization and eddy current errors are again accounted for and this quick characterization will be served as our second and main reference for the third step.

After the system is built, the last step is the quick characterization of the bulk of samples and correlates it with the second reference. Different pattern of faults, based on the minor loops and recoil lines, is used as a simple and quick method to differentiate between good and bad raw material.

### **1.3- Background:**

The magnetic characterization of the material is defined by its intrinsic properties, such as saturation magnetization, magnetic anisotropy and Curie temperature, and its hysteresis phenomena. We can apply fluxmetric technique in which a current is passed through the coil that increases the magnetic field. This variation in field produces a change of flux that induces voltage in the coils wrapped around the magnet. The magnetization of the magnet is acquired by integrating this induced voltage [1- 4].

According to the *Biot–Savart law* the sum of external and internal currents we get:

$$\nabla \times B = \mu_0(J_e + J_m) \dots (1.1)$$

Where  $\mu_0 = 4\pi \times 10^{-7} \text{ NA}^{-2}$  is the magnetic constant (also called magnetic permeability in vacuum). The magnetic field,  $H$ , is thus defined through the equation:

$$\nabla \times \left( \frac{B}{\mu_0} - M \right) = \nabla \times H = J_e \dots (1.2)$$

The magnetic field is directly controlled by means of the external currents. In the presence of materials the induction is:

$$B = \mu_0(H + M) \dots (1.3)$$

The measuring unit is *Tesla (T)* for  $B$  and  $(A/m)$  for  $H$  and  $M$ . In the absence of magnetic material,  $M = 0$ ,  $B = H$  and the magnetic flux density field and the magnetic field intensity are equivalent quantities.

*Faraday's Law* is used to relate the induced emf,  $e$ , in a coil to the rate of change of its flux linkage around a single turn conductor linking flux,  $\Phi$ :

$$e = -\frac{\partial \Phi}{\partial t} \dots (1.4)$$

If electric field,  $E$ , is defined as the voltage per unit length of the conductor, then (1.3) can be modified for an area,  $dA$ , that is bounded by the loop,  $dl$ :

$$\oint E \cdot dl = -\frac{\partial}{\partial t} \int B \cdot dA \dots (1.5)$$

Equation (1.5) can be rewritten as:

$$\nabla \times E = - \frac{\partial B}{\partial t} \dots (1.6)$$

We can define the term  $J = M$  as magnetic polarization, a quantity expressed in *Tesla*, and we can rewrite the equation as:

$$B = \mu_0 H + J \dots (1.7)$$

#### **1.4- Thesis Organization:**

The rest of this thesis is arranged as follows: Chapter 2 presents the characteristics of permanent magnets and types of magnetometers. It gives an overview of the hysteresis, eddy currents, recoil lines and demagnetization properties of the permanent magnets. Different types of magnetometers; hysteresisgraph, vibrating sample magnetometer, Squid magnetometer and pulsed field magnetometers are also discussed in the same chapter. This chapter will take an in depth review of pulsed field magnetometer design taken from the paper [5] written by P. Bretchko and R. Ludwig and discuss the correction of eddy currents and demagnetization factor.

Chapter 3 discusses the pulsed field magnetometer model design in the finite element analysis using Magsoft's Flux2D. The initial results and findings are presented in this section. This chapter also discusses the work done on MATLAB/Simulink using transformer as magnet and effect of recoil lines based on resistance, capacitance.

Chapter 4 presents the hardware and software design of the pulsed field magnetometer system. It will give a detail overview of the power electronics used in the project. A LabView

program is used as an interface that controls the charging and discharging of the capacitors. National Instrument DAQ card is used as a communication interface between the hardware and LabView. The measured data is then post processed using Matlab.

Chapter 5 shows the results. Several experiments were done using three different types of neodymium-iron-boron magnets. Two of them were provided by the General Motor facility and one of them is from K&J magnetics. The capacitors are charged up to different levels voltages at 300V, 400V, 430V. Different resistances were added as damper so that the original magnets are above the knee of the hysteresis. To emulate a fault, the magnets are heated at different temperatures of 50<sup>o</sup>C, 70<sup>o</sup>C, 100<sup>o</sup>C; and 150<sup>o</sup>C. Effects of these disturbances are observed at recoil lines, remanence and coercivity of the magnets; which are used to distinguish the quality of raw material. Chapter 6 discusses the future work and modifications in the design to achieve better results.

# Chapter 2

## Theory

In this chapter we provide necessary background information on different magnetic characteristics and different types of magnetometers available to evaluate these characteristics.

### 2.1- Magnetic Characteristics:

#### 2.1.1 - Major Hysteresis Loop:

A magnetic field has two distinct properties; magnetic field intensity,  $H$ , and magnetic flux density,  $B$ . The hysteresis loop of permanent magnet is constructed by plotting an applied magnetic field to the induced magnetic flux density in the magnet. The horizontal axis represents the magnitude of the applied magnetic field while the vertical axis represents the measured induced magnetic flux in the magnet as shown in Figure 2.1 [2, 5].

Starting from the unmagnetized magnets, the values of  $H$  and  $B$  are zero. As the line shows, the greater the amount of magnetic field applied, the stronger is the magnetic flux density. The initial slope is very steep but it slowly decreases. As the magnetic field is continuously increased, a point comes where additional increase in the magnetizing field produces very little

or no increase in magnetic flux density. This point reached is known as magnetic saturation,  $B_s$  for the material.

When the magnetic field is increased in the reverse direction, the hysteresis follows a different curve on the return path. When the applied magnetic field reaches zero, there is a difference in the value of magnetic flux density from the original curve. This point on the curve is known as remanent flux density or remanence,  $B_r$ . The applied magnet field intensity is further reduced in the opposite direction, until it drives magnetic flux density to zero. The value of the magnetic field that causes the magnetic flux density to reach zero is known as the coercivity of the material,  $H_c$ . The value of  $H_c$  represents the magnet's resistance to demagnetization. The applied magnetic field is reduced further until it reaches the negative saturation point.

The direction of field is again reversed towards the positive direction and the curve follows a different loop as compared to the initial curve from the unmagnetized position. This whole process represents the major loop of the hysteresis.

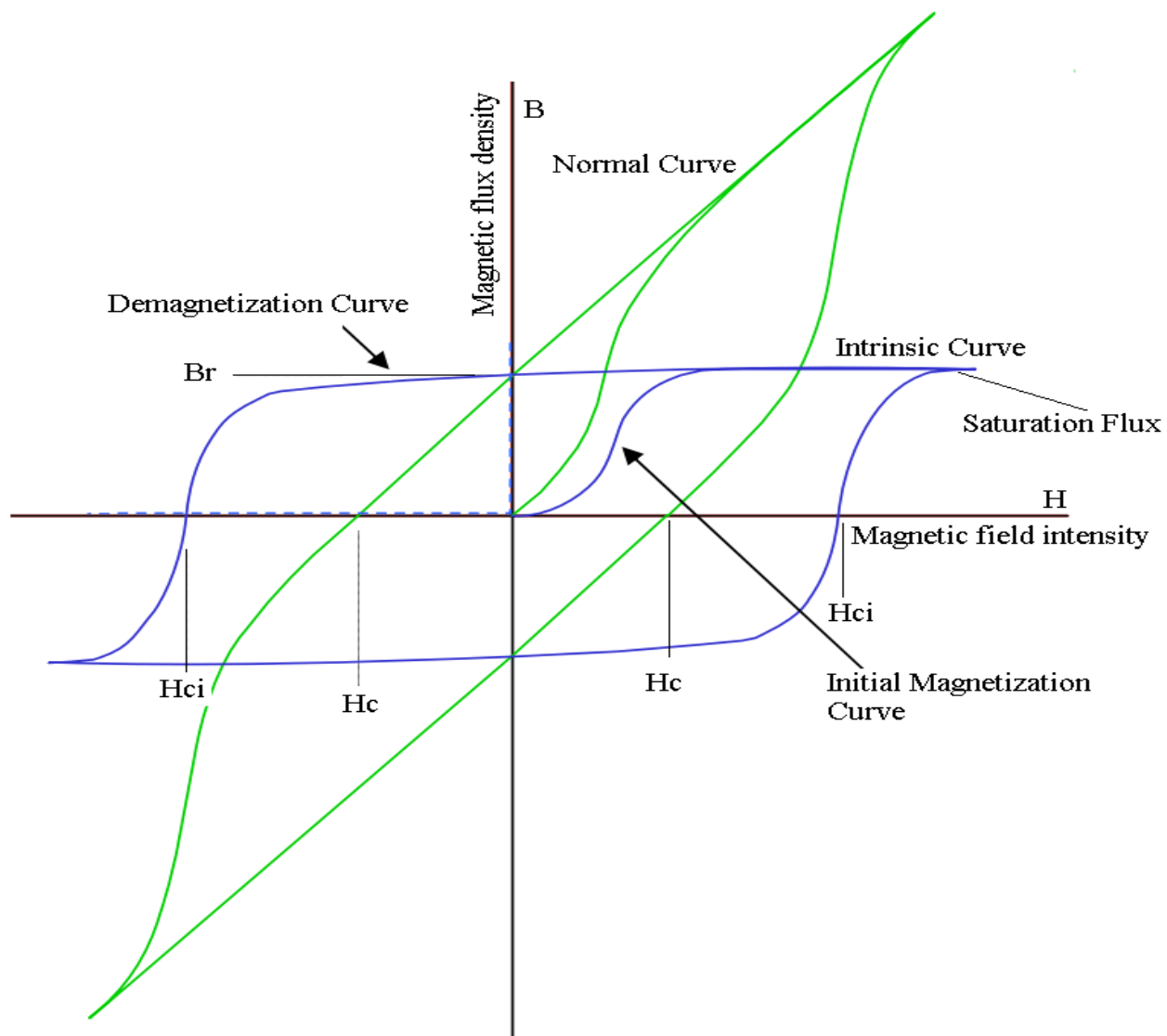


**Figure 2.1: Major Hysteresis loop for the magnet “For interpretation of the references to color in this and all other figures, the reader is referred to the electronic version of this thesis.”**

The Normal curve is the plot of magnetic field,  $H$  versus magnetic flux density,  $B$ , where  $B$  is the sum of the applied field and the field contributed by the magnet. The Intrinsic curve is obtained

by subtracting the magnitude of the applied magnetic field,  $\mu_0 H$ , at each point, thus leaving only the field contributed by the magnet.

**2.1.2- Minor Hysteresis Loops:**

If the applied magnetic field is stopped at some arbitrary point on the normal hysteresis curve before it reaches the saturation and then the direction of the applied field,  $H$ , is reversed to that of the normal loop, the loop formed inside the major hysteresis loop is known as the minor loops as shown in Figure 2.2.

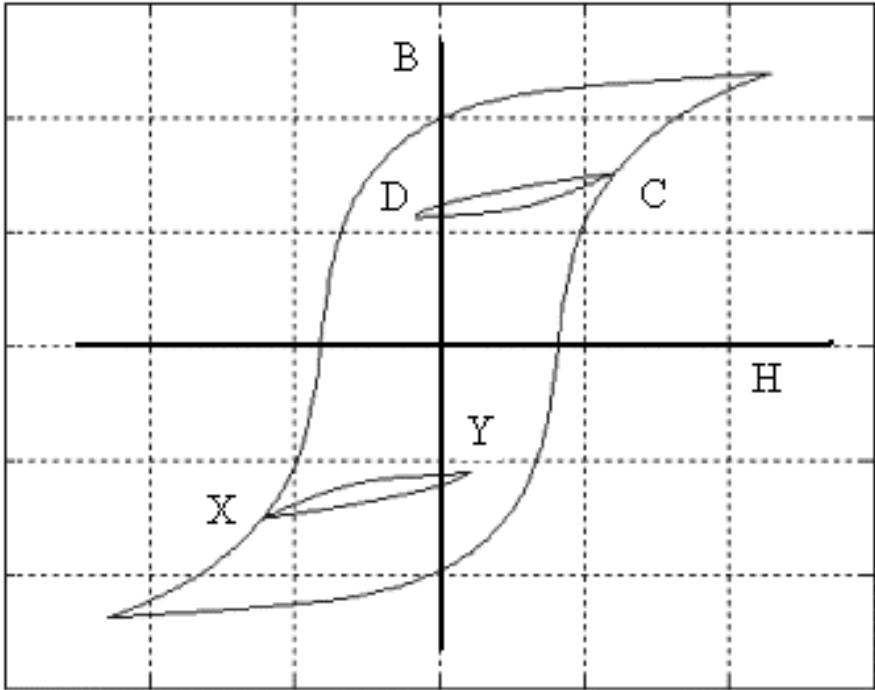


**Figure 2.2: Minor Hysteresis loop for the magnet**

If the starting point of the minor loop is chosen anywhere on the descending portion of the normal loop, point X, then the minor loop ascends towards the point Y after the reversing the applied field. Upon another reversal to the direction of the applied field, it follows the

counterclockwise direction back towards the same initial point X on the normal loop. On the contrary, if the initial point of the minor loop is chosen anywhere on the ascending portion of the normal loop, point C, and then the descending portion of the minor loop would follow till point D on the first reversal of applied field, before coming back towards the initial point C upon second reversal of the direction of the applied field. It can be seen that the area of a minor loop falls inside the area enclosed by the normal hysteresis loop.

### **2.1.3- Demagnetization:**

The phenomenon in which the magnetic flux decreases in the second quadrant of the hysteresis loop when the magnetic field is increased in the opposite direction is known as demagnetization and the curve is called demagnetization curve. As it can be seen in the Figure 2.3, there is a rapid change in the slope of the intrinsic curve. This point is known as the knee of the curve. The maximum permeability of the material occurs at this knee.

If there are no currents present in the circuit, the working line where the machine operates goes through the origin as shown in Figure 2.3. If there are currents present, the working line has a negative offset depending on the current value. The intersection point of the working line and the BH curve is the working point.

This working point is very important when designing because if the working point falls below the knee on the curve, the magnet will become demagnetized. Therefore, the magnet should always be operating above the knee of the curve to operate in safe linear region and avoid any risk of demagnetization.

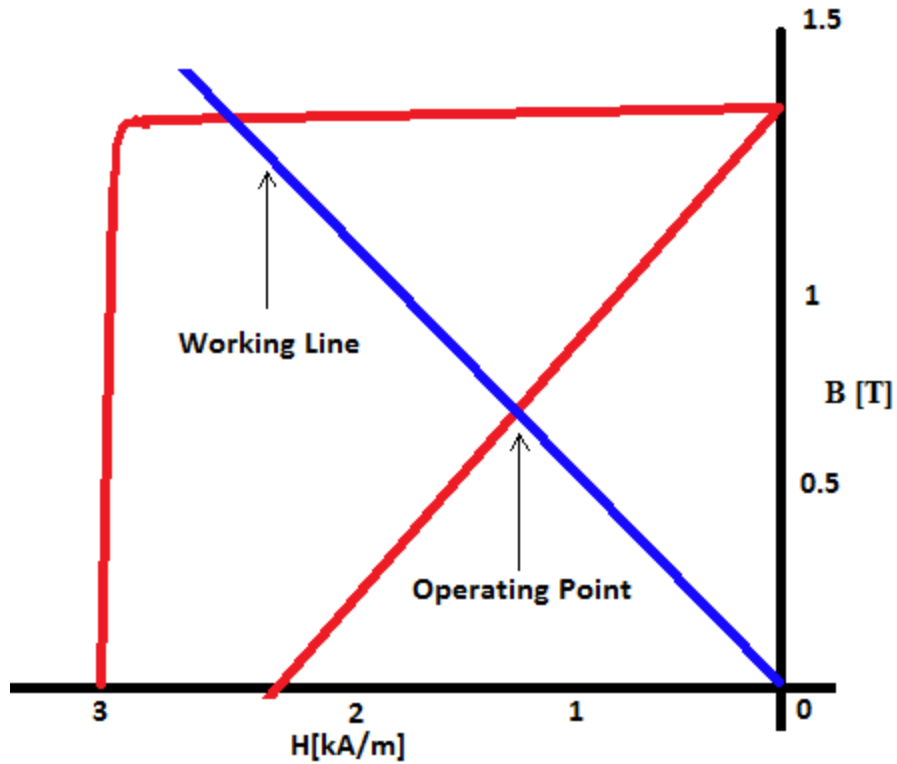
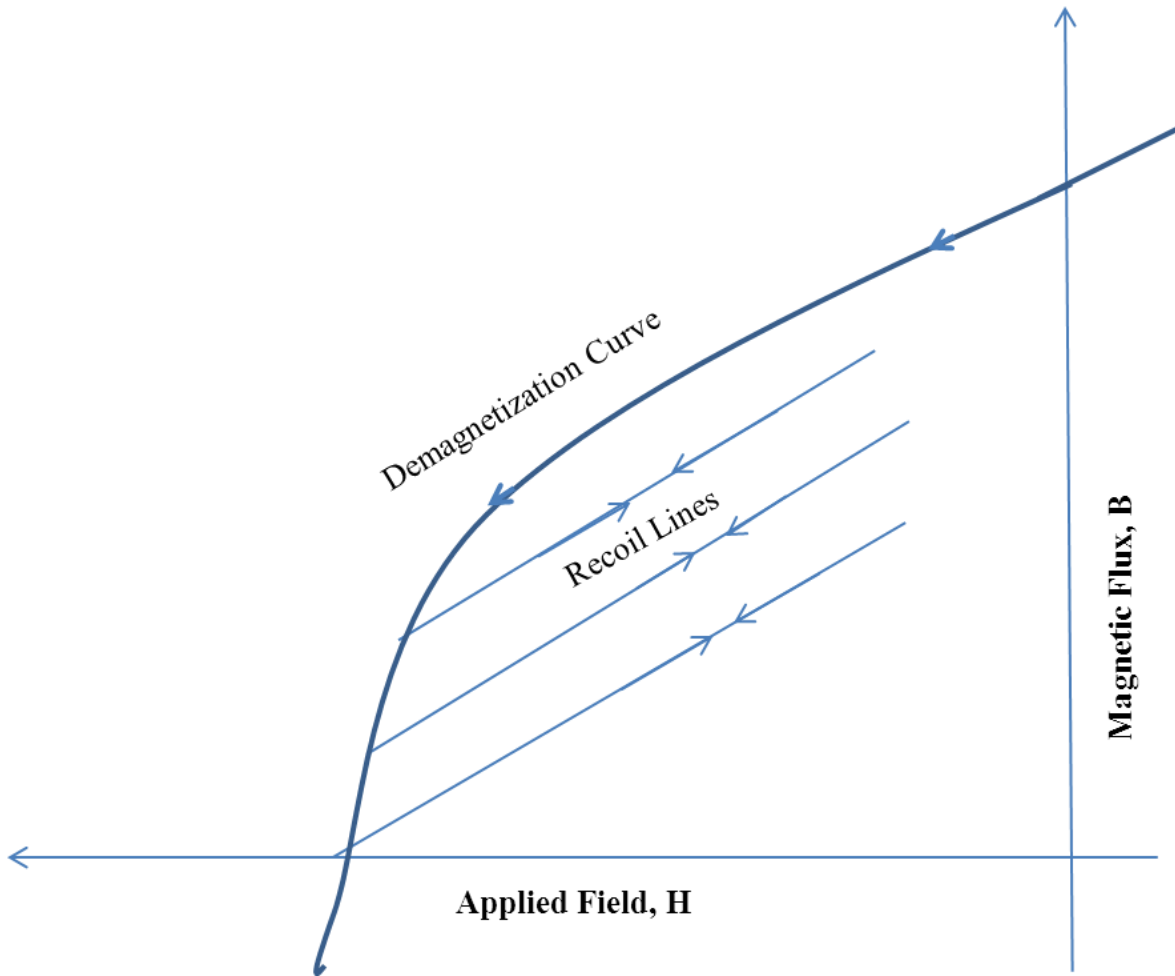


Figure 2.3: Demagnetization curve and working line

#### 2.1.4- Recoil Lines:

When the current/field is passing through the second quadrant of the loop known as demagnetization curve and the direction of current/field is reversed, then the magnetic flux density increases along recoil lines within the main loop as shown in Figure 2.4.



**Figure 2.4: Demagnetization curve and recoil lines of the permanent magnet**

Between the initial point and the magnetic flux density axis, such lines are reversible, in fact, it produces a thin loop of negligible area and it is usual to consider only the mean recoil line and its slope. The slope of recoil lines does not depend on the value of magnetic flux density from which they originate within the 2nd quadrant. The slope of the recoil lines is known as relative recoil permeability,  $\mu_{rec}$ , expressed as

$$\mu_{rec} = \frac{\Delta B}{\mu_0 \Delta H} \dots (2.1)$$

The point where the recoil line meets the magnetic flux density axis is called the residual remanence.

#### **2.1.4.1- Effect of Temperature**

The effect of temperature on the demagnetization curve as well as on the recoil lines of the magnet are shown in the Figure 2.5. When there is an increase in temperature, the knee move rightwards, closer to the vertical magnetic flux density axis. If the working condition remains same, then the working point could also fall below the knee.

At 20<sup>o</sup>C temperature, the normal curve intersects the load lines that represent the operating point of the magnet, denoted by the red dot. When the temperature is increased to 60<sup>o</sup>C, the magnet is close to the maximum operating temperature because the operating point is slightly right to the knee of the normal curve.

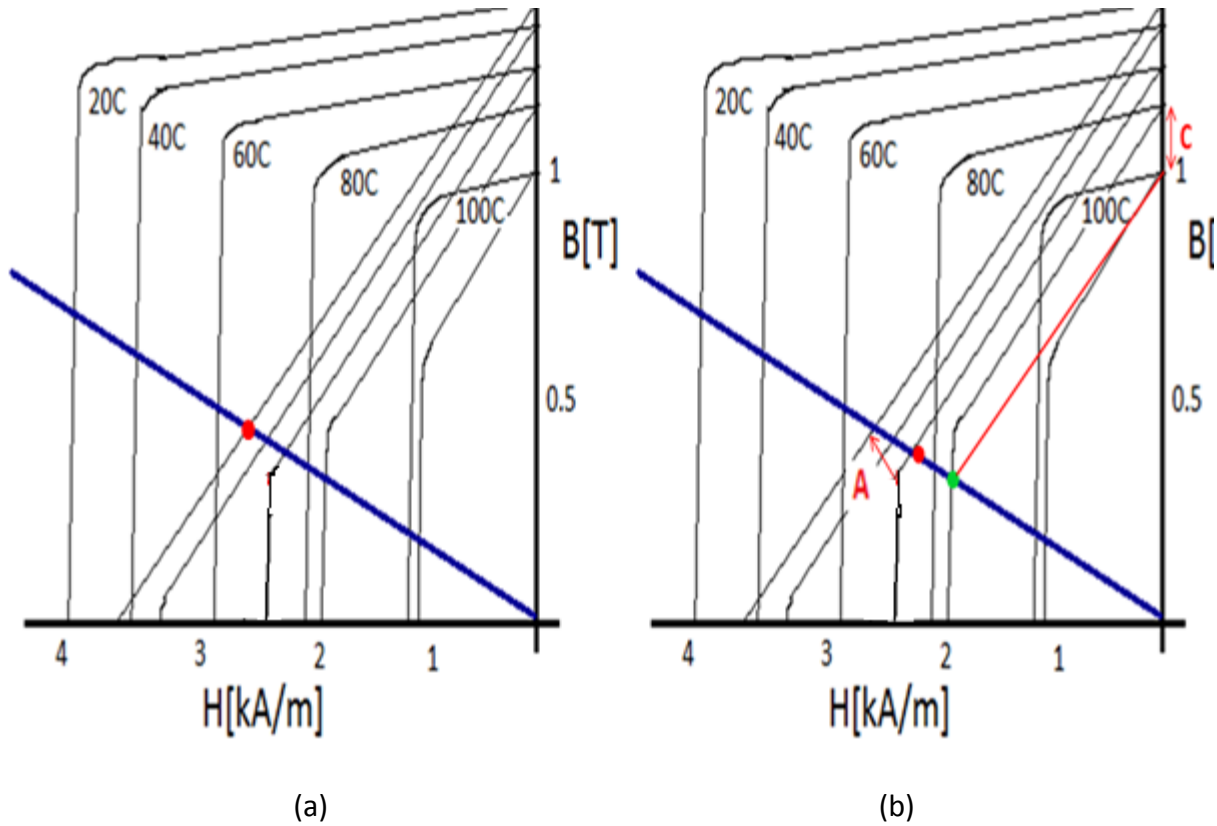


**Figure 2.5: Magnet at (a) 20°C and (b) 80°C**

Beyond this temperature, the magnet starts to demagnetize irreversibly. If the magnet is heated up to 80°C, the operating point moves to the green dot that is below the knee of the normal curve. This operating point has been reduced by a distance C, as shown in the Figure 2.5b.

When the magnet is cooled back to room temperature, it does not rise back up the knee but it will be dropped by a distance A, shown in the Figure 2.5b. The red dot represents the new operating point once the magnet cools back to 20°C which is lower than the original operating point at 20°C.

### 2.1.5 - Eddy Currents:

Eddy currents are electric currents induced in conductors when they are exposed to a changing magnetic field; either due to deviations of the field with time or due to relative motion of the field source and conductor [6]. This causes circulating flow of current within the body of the conductor and thus according to *Ampere's law* induce magnetic fields. Eddy currents are not just limited at the boundaries, but also where applied field intensity experiences a change in the magnitude or direction. The stronger the applied magnetic field or the greater the electrical conductivity of the conductor or faster the field changes, the stronger is the magnitude of induced currents.

The swirling current in the conductor is due to electrons experiencing a Lorentz force that is perpendicular to their motion. *Lenz's law* states that "the electromagnetic field induced in an electric circuit always acts in such a direction that the current it drives around a closed circuit produces a magnetic field which opposes the change in magnetic flux". In the case of a varying applied field, the induced field will always be in the opposite direction to that applied. The same will be true when a varying external field is increasing in strength. However, when a varying field is falling in strength, the induced field will be in the same direction as that originally applied, in order to oppose the decline.

The eddy currents have undesired effects in the magnets. The magnetic field, created by the eddy currents, destroys the high field quality in the good field region that is required for this type of magnet. Power loss due to eddy currents leads to heating of the conductive magnet

components. The *Lorentz* forces due to fast changes of high magnetic fields may also lead to extra stresses in the material.

Taking the curl of both sides of *Ampere's law* and introducing the material equation we obtain under the assumption that the conductivity,  $\sigma$ , is uniform in space:

$$\nabla \times \nabla \times \vec{H} = \nabla \times \vec{j} = \sigma(\nabla \times E) \dots (2.2)$$

Applying the vector relation to the left-hand side and introducing Faraday's law on the right-hand side leads to

$$\nabla^2 \vec{H} = \sigma \mu \frac{\partial \vec{H}}{\partial t} \dots (2.3) \quad \text{with} \quad \mu = \mu_0 \mu_r \dots (2.4)$$

Where

$\mu_0$  is the permeability of air

$\mu_r$  is the relative permeability

This is the magnetic diffusion equation where  $\kappa$  is known as the magnetic diffusivity.

$$\kappa = \frac{1}{\sigma \mu} \dots (2.5)$$

The expression shows that higher the conductivity (i.e. large eddy currents), the lower the diffusivity, i.e., the diffusion process is slow. Large  $\mu$  means large stored energy, which takes a longer time to be stored.

Having solved the differential equation for the field  $H$  (under certain boundary conditions), the eddy current density can be calculated by *Ampere's law* and consequently the power loss as well. Diffusion equations can also be derived in a similar way for the magnet vector potential,  $A$ , with the definition

$$B = \nabla \times A \dots (2.6)$$

Having found the vector potential by solving the corresponding diffusion equation (under the chosen boundary conditions) one can calculate the current density,  $J$ , by the equation:

$$\vec{J} = -\sigma \vec{E} = -\sigma \frac{\partial \vec{A}}{\partial t} \dots (2.7)$$

#### **2.1.6- Demagnetization Factor**

When a ferromagnetic sample magnet is placed in the coil, magnetic induction,  $B$ , is born. The magnetic field and magnetic flux density vectors are parallel to each other and additive. When a field is applied to a permanent magnet intrinsic induction,  $J$ , is born.

If the permanent magnet is removed from the established field or the direction of the magnetic field is changed rapidly, free poles within the magnet sample are established. Due to the result of pole formation within a magnet, the magnetization of the material due to these free poles itself generates a magnetic field in the opposite direction from the direction of the applied field as shown in Figure 2.4. This opposite direction field is known as a demagnetization field,  $H_d$  and exists between the free poles.

The field potential in this case is due to some of the magnetization,  $J$ , returning internally. The magnitude of this demagnetization field is proportional to the magnitude of the magnetization  $J$  and is 180 degree opposed to  $J$ . It is expressed as:

$$H_d = -\frac{NJ}{\mu_0} = 4\pi N_d I \dots (2.8)$$

Where

$N_d$  is the demagnetization factor

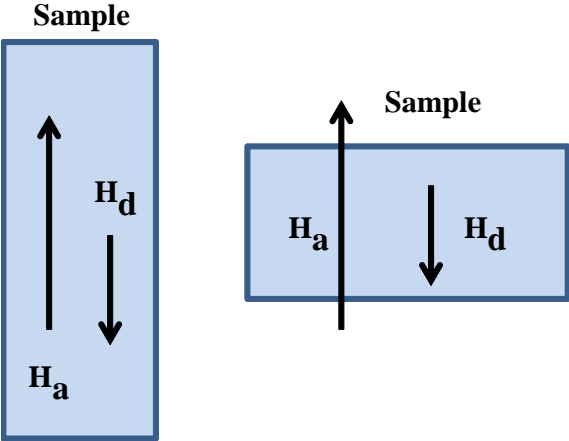


**Figure 2.6: Shape of magnet and demagnetization field**

The demagnetizing factor,  $N_d$ , depends upon the geometry of the magnet and the spacing of the poles. If the magnet is in a closed magnetic circuit,  $H_d$  will be zero since the free poles do not exist. For a magnet in an open circuit condition or for a magnet circuit containing an air gap the effect of demagnetization field will be to lower the magnetization  $J$ .

## 2.2- Types of Magnetometer:

Magnetometers are essential to establish hysteresis loop and characterize the quality of permanent magnets. There are two major categories of magnetometers measuring hysteresis loop; closed circuit and open circuit as shown in Figure 2.7 [3, 4]. When the flux path lies entirely within a strong magnetic material, except possibly for a small amount of leakage flux, the circuit is said to be closed. Lines of magnetic induction  $B$  are continuous and form closed loops. The region occupied by these closed loops is called a magnetic circuit. If the flux passes partially through a nonmagnetic material, usually air, the circuit is said to be open. Hysteresisgraph and SQUID are closed circuit methodologies, while vibrating sample magnetometer and pulsed field magnetometer represent open-loop circuit methodology.

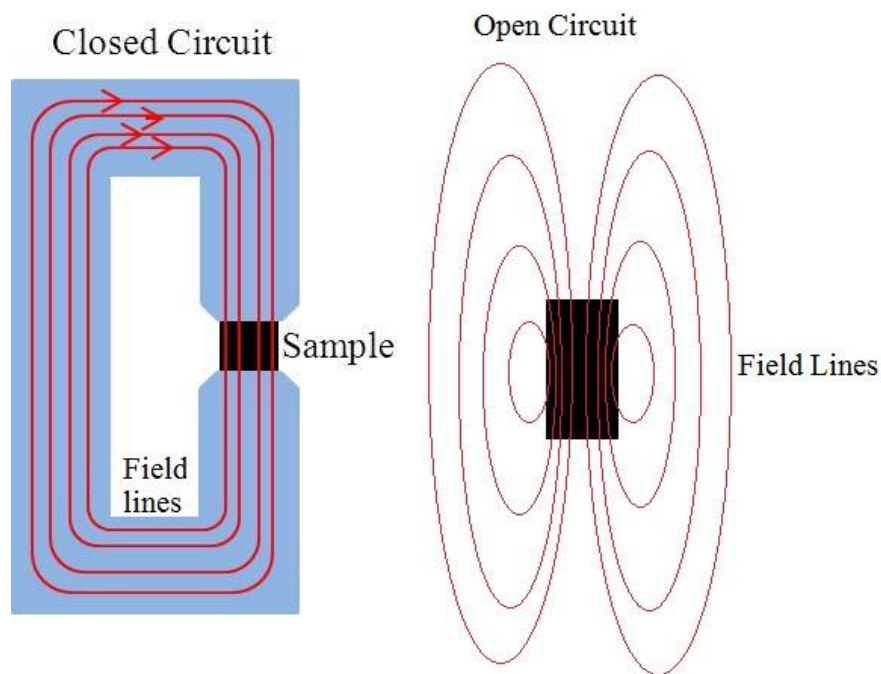


**Figure 2.7: Measurements in Closed and Open Circuit Magnetometer**

All these different types of magnetometers are discussed below:

### **2.2.1 Hysteresisgraph**

The Hysteresisgraph method is a closed magnetic circuit technique that uses fluxmetric methods. The general procedure is to vary the current through the primary winding and measure its magnitude, while simultaneously integrating the output voltage from the secondary winding with a fluxmeter. Electromagnets provide both the exciting field and the soft return path for the flux. Sample geometry and field magnitude are an important parameters to accurately measure the accuracy and reproducibility of this method [2, 6, 7].

Figure 2.8 provides the essential scheme of a Hysteresisgraph for permanent magnet testing [2]. The iron core acts as a channel and amplifies the field produced by means of a couple of windings located close to the gap. One of the two poles is flexible to accommodate the sample in the gap. The diameter,  $D_o$ , of the core is large so the sample can easily fit in. This diameter predicts the cost of the apparatus and depends on the power supply.

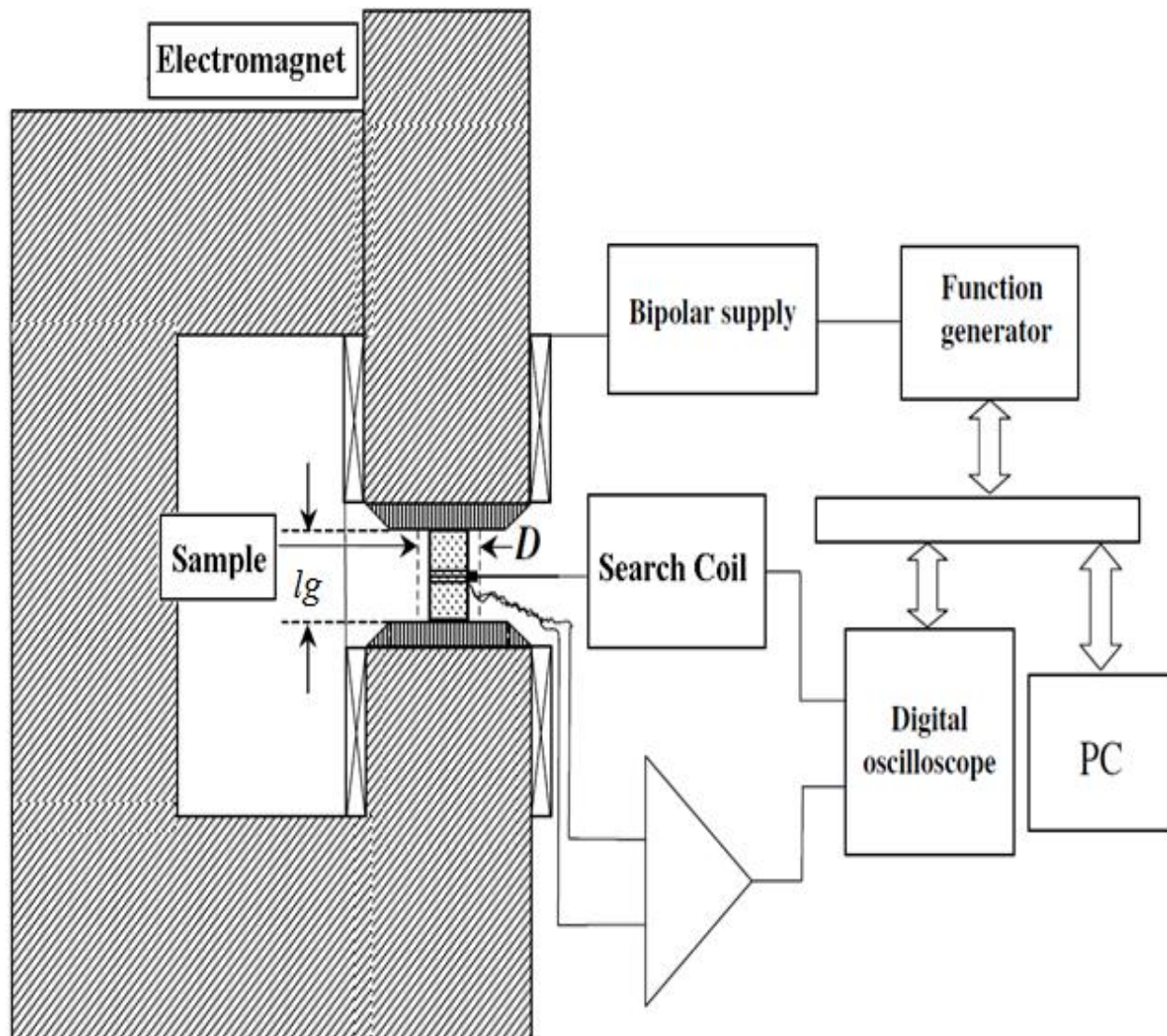


**Figure 2.8: Characterization of permanent magnets using Hysteresisgraph [2].**

The soft core used in the design acts as a short circuit for the magneto motive force generated by the specimen and the magneto motive force,  $NI$ , impressed by the windings all appears across the specimen. Such a field is uniform and equal to [1]

$$H = H_g = \frac{NI}{l_g} \dots (2.9)$$

Where

$l_g$  is the gap length.

The measured induction in the sample is

$$B = J_s - H_g \mu_0 = \frac{\int V \cdot dt}{NA} \dots (2.10)$$

The test specimen is normally shaped as a cylinder, having either rectangular or circular cross-section, with smooth and as parallel as possible end faces and uniform cross-sectional area within 1% [2].

The secondary winding with high number of turns is used to detect the flux derivative. Air flux compensation is made in the usual way, either by automatic compensation using a J-coil, which provides zero signals in the absence of the sample, or by numerical subtraction in the course of signal analysis.

The tangential field at the sample surface  $H$  is detected by means of a Hall plate or a coaxial H-coil. Time integration is required in the second case. In the simplest approach, the secondary winding has known number of turns and calibrated turn–area  $N_2 A_2$  and the flux derivative is

$$\frac{\partial \phi_2}{\partial t} = (N_2 \left( A_2 \mu_2 \left( \frac{\partial H}{\partial t} \right) + A_s \left( \frac{\partial J}{\partial t} \right) \right) \dots (2.11)$$

where

$A_s$  is the cross-sectional area of the specimen.

Another way of measuring  $H$  is by measuring current through the windings. The current is calculated usually from measuring the voltage drop across a low-value shunt resistor in series.

The two voltages are plotted as x and y signals to give the hysteresis loop of the sample material. The plot may be produced directly using an x-y recorder, but more commonly the voltages are converted to digital values using an analog-to-digital (A/D) converter and a computer. The hysteresis loop may then be plotted on the computer screen and/or on a printer, using the software that controls the A/D converter or some other program.

Before beginning the measurement, the fluxmeter controls should be adjusted for minimum drift, and the fluxmeter should be reset to give zero output. If only a complete hysteresis loop is needed, it is best to start the integration at the maximum field (+ or -). The field is then varied from its maximum value, through zero, to its maximum value in the opposite direction, and then back to its original value. Use of a bipolar power supply allows the magnetizing current to be varied smoothly through zero. The field sweep may be manually controlled, or controlled by a computer driving a programmable power supply.

Since the zero setting of the fluxmeter will not in general coincide with the demagnetized state of the sample, the plotted loop will be displaced from zero in the y direction. A constant value must be added to (or subtracted from) each measured y value to center the loop about the x axis.

Finally, it is necessary to convert the recorded voltages to values of field and flux density, using the dimensions of the sample, the value of the series resistor in the primary circuit, the number of turns in the two windings, and the calibration factor of the fluxmeter. Signal acquisition by

means of a two-channel digital oscilloscope or voltmeter, A/D conversion and digital treatment of the signal are performed, so that  $B(t)$  and  $H(t)$  are determined.

### **2.2.2 Vibrating Sample Magnetometer**

The Vibrating Sample Magnetometer (VSM) is based on the flux change in a coil when a magnetized sample is vibrated within an assembly of detecting coils with open magnetic circuit. The sample, commonly a small disk, is attached to the end of a nonmagnetic rod, the other end of which is fixed to a loudspeaker cone or to some other kind of mechanical vibrator as shown in Figure 2.9. The VSM measures the magnetic moment  $m$  and the magnetic dipole moment  $j = \mu_0 m$  in the presence of a static or slowly changing external magnetic field [1, 9, 10, 11].

The vibration can be obtained by impressing a vibrating motion on the sample, so as to produce an AC signal while making a DC measurement. The drive is either carried out by an electric motor or by a transducer similar to a loudspeaker system. The specimen is suspended between the poles of the electromagnet and oscillates vertically to the field direction; it must be carefully centered between the pickup coils.

The oscillating magnetic field of the moving sample induces an alternating emf in the pickup coils, whose magnitude is proportional to the magnetic moment of the sample, vibration amplitude and frequency. The coil design ensures that it is independent of variations in the field generated by the electromagnet.

The (small) alternating emf is amplified, usually with a lock-in amplifier which is sensitive only to signals at the vibration frequency. The lock-in amplifier must be provided with a reference signal at the frequency of vibration [1]. These can be measured separately using

- a capacitor with one set of fixed plates and one set of movable plates
- a pick-up coil and a permanent magnet,
- an electro-optical sensing system.

The coil arrangement of Figure 2.8 is very commonly used. The apparatus is calibrated with a specimen of known magnetic moment, which must be of the same size and shape as the sample to be measured, and should also be of similar permeability. The driving system may be mechanical, through a crank and a small synchronous motor, or in a recent commercial instrument, with a linear motor. In this case the vibration frequency is generally below 40Hz, and the vibration amplitude is a few millimeters. The amplitude is fixed by the geometry of the mechanical system or by the drive signal to the linear motor.

The maximum available field in the gap of the electromagnet is limited in the VSM, because space must be allowed for the vibrating rod and the pickup coils. Therefore, care is necessary to minimize vibration of the sensing coils in the field, and to keep the measuring field from influencing other parts of the system.

A fundamental feature of the vibrating system considers the stability of frequency and amplitude of the oscillation applied to the sample. A reference signal is therefore generated in a couple of coils by a permanent magnet attached to the vibrating rod at a distant position from

the measuring pickup coils; it is amplified and compared by software with the target signal. Any difference is numerically compensated and the driving signal of the lock-in amplifier is modified in order to recover the programmed vibration frequency and amplitude. Typically, the vibration frequency can range between 10 Hz and 100 Hz. A complete hysteresis loop can be traversed in several minutes, a far longer time than required with the Hysteresisgraph method. Thus, the measurement time is typically long.

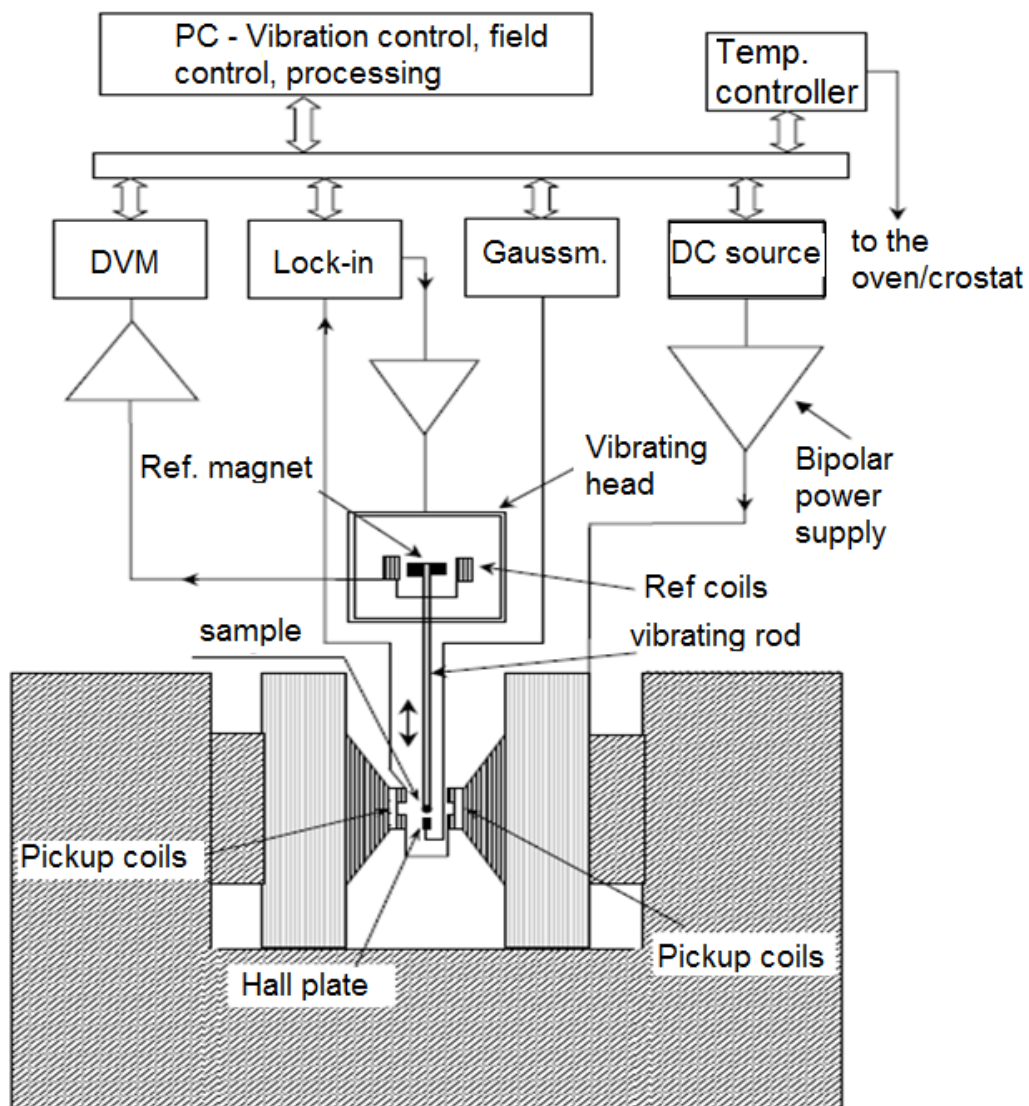


Figure 2.9: Scheme of Vibrating Sample Magnetometer with electromagnet field source [2].

### 2.2.3 SQUID Magnetometer

Superconducting Quantum Interference Devices (SQUID) are very sensitive magnetometers used to measure extremely weak magnetic fields, based on superconducting loops and point-contact junction designed to measure extremely low currents. SQUID magnetometers can detect fields from several femtotesla up to 9 T [2, 3, 4, 11]. The SQUID itself can be quite small, but the need for liquid-helium coolant makes the complete instrument rather bulky and heavy. The power consumption of several watts is due almost entirely to the radio-frequency electronics.

The materials are cooled below a superconducting transition temperature where the materials lose all resistance to the flow of electricity. At this point, the materials are known as superconductors and the interactions between electric currents and magnetic fields are observed. If a line of magnetic flux becomes threaded through a ring made of a superconducting material, a current is induced in the ring. In the absence of any further disturbances the current would continue flowing forever.

The superconducting ring is interrupted by a “weak-link,” though a thin layer of insulator. A super current can flow through the weak link, but is an oscillating function of the magnetic field intensity. In other words, as the field increases, the super current first rises to a peak, then falls to zero, then increases again and so on [2]. These periodic variations are exploited to measure the current in the superconducting ring and hence the ambient magnetic field

There are two types of SQUID: RF SQUID and DC SQUID [3]. In RF SQUID, the ring is inductively coupled to a radio-frequency circuit that both supplies a known bias field and serves as the

detector output. Changes in the ring current alter the resonant frequency of the circuit; as a result, the output signal changes periodically as the field varies. Changes in the field can be measured simply by counting the peaks and valleys. Alternatively, a feedback loop can be employed to lock the radio-frequency circuit onto a single peak, continually adjusting the bias field to compensate for changes in the external field. The feedback current is then a measure of the ambient field.

DC SQUID is based on the tunneling of superconducting electrons across a very narrow insulating gap, called a Josephson junction, between two superconductors. When the two weak links are matched properly through design, the current in the ring has DC response to the flux through it. The superconducting ring in a SQUID is typically a toroid a few millimeters in diameter made of a metal such as lead or niobium. The weak link is a narrow construction in the superconductor or a point-contact junction [2].

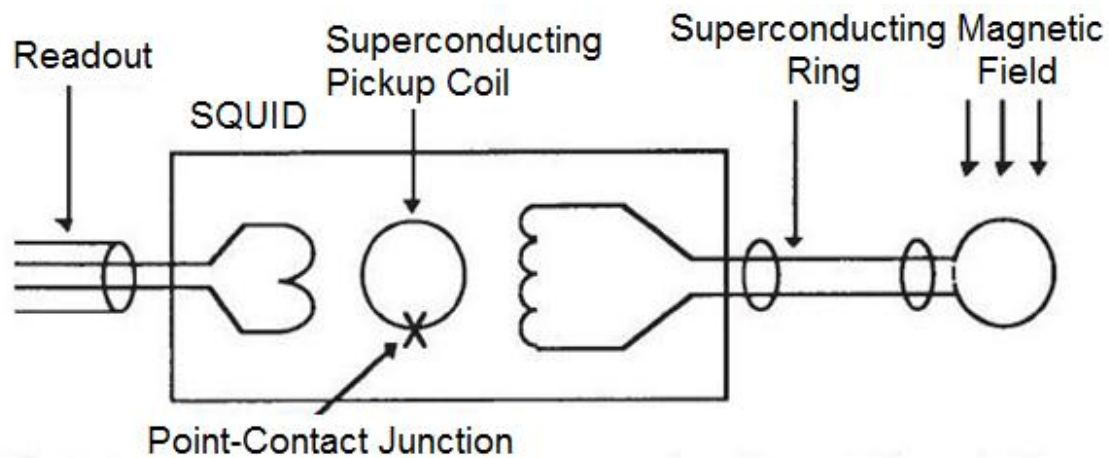
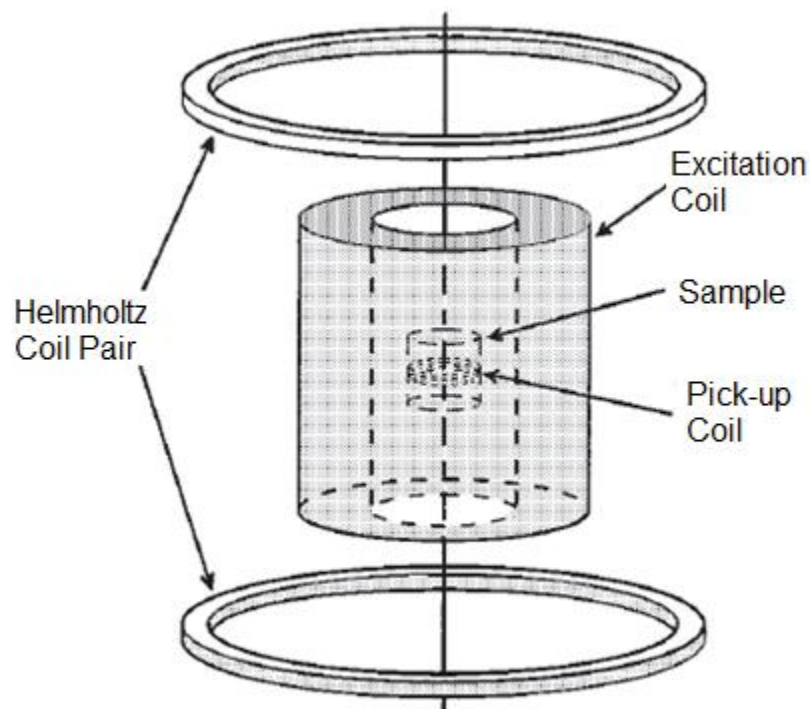


Figure 2.10: SQUID Magnetometer [2]

## 2.2.4 Pulsed Field Magnetometer

A pulsed field magnetometer can be used for measuring the hysteresis loop on hard magnetic material. The pulsed excitation current only lasts few milliseconds and can generate the magnetic flux density of about 6.2T [1,4, 13- 17]. It is suited for fast and reliable measurement of the hysteresis loops of hard magnetic materials. Figure 2.11 shows a coil arrangement of a pulsed field magnetometer.



**Figure 2.11: Coil Arrangement of Pulsed Field Magnetometer [1]**

The breakdown of pulsed field magnetometer components consists of [4]:

- Charging Unit: The charging unit should generate a reproducible and selectable charging voltage. It determines the repeatability of the achieved field in the pulse magnet.

- **Energy Source:** Energy storage, typically capacitor battery, is used. The capacitor is generally charged to a selectable voltage and discharged through the resistive air-core coil. The capacitance determines the costs of such a system, the maximum sample size and the time constant. The battery must have the capability to reverse the voltage so that the full loop of hysteresis can be measured.
- **Excitation Coil:** The excitation current is discharged into resistive air-core coil. The inductivity of this pulse magnet determines the pulse duration. Due to high energy discharge, the coils can heat up and care must be taken between successive measurements.
- **Pick up Coils:** A careful design of the pick-up system is very important in order to achieve a high degree of compensation and consequently a good sensitivity. The pulsed field magnetometer consists of one or two pick-up coil system. The search pick up coil is wound tightly around the sample and used to measure the magnetic flux density in the sample. The search coil picks up not only the magnetic field due to external excitation but also due to permanent magnet that is characterized.

A pair of Helmholtz coils is positioned symmetrically with respect to the middle plane of the excitation coil. The absolute value of the excitation field  $H$  in the center of coil is obtained by multiplying the readings from the Helmholtz coil by a calibration constant. In DC systems, a sensor coil is usually placed close to the sample. Unfortunately, this does not work for an open loop system, where there is no external closed magnetic path. Because of this, the magnetic field from sample would couple to the excitation field and the reading will be corrupted. The Helmholtz coil is quite large and there is not a significant portion of flux lines from a sample

that are linked with the coil so the majority of the field in the Helmholtz coil is due to excitation field.

For some applications the pick-up system should be cooled in order to hold a stable temperature, which is especially important for a room-temperature system with a high repetition rate.

- Software Implementation:

This consist either of a data-acquisition system that can communicate with the analog front end. The main purpose of this board is to amplify and integrate the signals from the Helmholtz and pick up search coils and to form a transistor-transistor logic compatible trigger signal. The software should also be able to establish a graphical user interface. The software is then used to measure the hysteresis curve of the sample.

The magnetic field in the sample is composed of the excitation field and the demagnetization field, which is estimated based on the demagnetization factor [1, 15]

$$H = H_o + H_d = H_o - N_d M \dots (2.12)$$

All the magnetic fields calculated using the induced voltages are in fact the average of the corresponding fields, where the averaging is performed over the surface area of the pickup coils i.e. search coil for Magnetization,  $M$ , and Helmholtz coils for excitation field,  $H_o$ .

The magnetic flux density from the induced voltages across the search coil is calculated by [1]:

$$B = \mu_0(H + M) = \mu_0\{H_o + (1 - N_d)M\} \dots (2.13)$$

Therefore, the magnetization of the sample is expressed as:

$$M = \frac{1}{\mu_0} \left( \frac{B - \mu_0 H}{1 - N_d} \right) \dots (2.14)$$

The intrinsic magnetic flux density,  $B_i$ , is written as:

$$B_i = \mu_0 M = \frac{B - \mu_0 H}{1 - N_d} \dots (2.15)$$

The magnetic field in the sample is expressed as:

$$H = \frac{H_0 - N_d \frac{B}{\mu_0}}{1 - N_d} \dots (2.16)$$

# Chapter 3

## Design and Simulation

### 3.1- Design Objectives

Before the start of pulsed field magnetometer design phase, several design objectives are laid down that help characterize the magnets. First objective is to make sure that several different cylindrical shaped magnets can be accommodated in the system. The magnets have to be completely saturated and the rare-earth magnets have high saturation flux density of about 1.2 – 1.5 T. Therefore, to make sure that the magnets are completely saturated, the minimum magnetic flux density generated by the field has to be 4 T. The minimum field intensity that will require the magnet to reach the saturation should be higher than 4A/m. Lastly, to establish and observe the recoil, the current should be oscillating. The negative peak of the current should produce enough magnetic fields that will force the magnet operating point to fall below the knee of the curve.

The Finite Element Method and Simulink models are developed to accomplish these design objectives that are explained in the following sections.

### 3.2- Finite Element Analysis:

This section explores a pulsed field magnetometer design modeled in Magsoft's Flux 2D software for Finite Element Analysis (FEM). The FEM is a very popular tool for the design and analysis of electromagnetic devices [20, 21]. The main objective of using the FEM is to determine the dimensions of the excitation coil, search coil and Helmholtz coil; capacitance of the capacitive bank; current needed to produce at least twice the magnetic flux density and magnetic field strength to saturate the permanent magnet sample.

The pulsed field magnetometer design is an iterative process. Once the design variables such as geometry of the coils, capacitance and voltage limits are set, the magnetic flux density and magnetic field strength are evaluated and compared. Initial design is obtained from the paper discussed above and most of the FEA iterations are performed after this for the fine tuning and optimization.

#### 3.2.1 Equations used in the FEM:

The finite element analysis is run under transient magnetic mode coupled with circuitry that charges and discharges the capacitors into the air-core excitation coil. Transient magnetic application of FEM deals with the time dependent electromagnetic fields that are related by the following Maxwell's equations [20]:

$$\nabla \times \vec{E} = -\frac{\partial \vec{B}}{\partial t} \dots (3.1)$$

$$\nabla \cdot \vec{B} = 0 \dots (3.2)$$

$$\nabla \times \vec{H} = \vec{J} \dots (3.3)$$

$$\vec{J} = \sigma \vec{E} \dots (3.4)$$

$$\nabla \times \vec{B} = \mu \vec{H} \dots (3.5)$$

Where

$\vec{E}$  is the field intensity (V/m)

$\vec{B}$  is the magnetic flux density (T)

$\vec{H}$  is the magnetic field intensity (A/m)

$\vec{J}$  is the current density (A/m<sup>2</sup>)

$\sigma$  is the electrical conductivity of the medium (S)

$\mu$  is the permeability (H/m)

In Cartesian coordinate system, it is defined as:

$$\nabla \equiv \vec{a}_x \frac{\partial}{\partial x} + \vec{a}_y \frac{\partial}{\partial y} + \vec{a}_z \frac{\partial}{\partial z} \dots (3.6)$$

$\vec{a}_x, \vec{a}_y, \vec{a}_z$  are unit vector along their respective axes.

Equation (3.5) refers to magnetic properties of the material. Magnetic flux density and magnetic field intensity can be expressed as functions of each other by the following relationships

$$\vec{B} = \mu\vec{H} = \mu_0\mu_r\vec{H} \dots (3.7)$$

Where

$\mu_0$  is the permeability of free space=  $4\pi \times 10^{-7}$  H/m

$\mu_r$  is the relative permeability

In the presence of permanent magnets, equation 3.7 becomes

$$\vec{B} = \mu_0\mu_r\vec{H} + \vec{B}_r \dots (3.8)$$

$$\vec{H} = \frac{\vec{B}}{\mu_0} - \vec{H}_c \dots (3.9)$$

Where

$B_r$  is the remanent magnet flux density of permanent magnets

$H_c$  is the coercive magnetic field of permanent magnets

FEA meshing divides the machine geometry into small elements. Magsoft's Flux 2D is used for all simulations that uses the magnetic vector potential, A for solving electromagnetic fields.

Equation (3.1) implies presence of electric scalar potential, V and it is related with A by

$$\vec{E} = -\frac{\partial \vec{A}}{\partial t} - \nabla V \dots (3.10)$$

Combining equations 3.3, 3.4, 3.9 and 3.10, results in the following equation:

$$\nabla \times (\nu_0 [\nu_r] \nabla \times \vec{A} - \vec{H}_c) + [\sigma] \frac{\partial \vec{A}}{\partial t} + \nabla V = 0 \dots (3.11)$$

Where

$\nu_r$  is the relative reluctivity of the medium

$\vec{A}$  is the magnetic vector potential (Wb/m)

V is the electric scalar potential

Equation (3.11) is solved by FEA in transient magnetic application [19]. In the FEM design, the material properties are described and assigned to the respective faces of the geometry in the FEM software application. Different mesh sizes are also defined in the software depending upon the concentration of the magnetic flux density in different areas. The magnet material, magnetization direction and parameters of the electrical circuit components are defined as well. Time steps of time dependent quantities are also mentioned in transient magnetic solution. The solution is run for a specified time and finally, the results such as induced voltages; current; inductance; magnetic flux density; magnetic field strength; etc. are obtained by post processing.

For every iteration, one or more machine design parameters are varied and its effect is noted on the desired output parameter. Parameterization (multiple variation steps) for certain design parameters is also used in some FEM simulations.

### 3.2.2 FEM based Design

The final design of the magnetometer is shown in figure 3.1a. On the right side, the domain for the finite element modeling is shown exploiting the axial symmetry of the structure. The pulsed field magnetometer comprises of an air-core excitation coil with an inner diameter of 3 in and a length of 5 in. The air-core has the resistance of about 24 m $\Omega$  and contains 90 turns. The cylindrical shaped sample of radius 0.75 in and thickness of 1 in is placed at the center of the air-core excitation coil as shown in figure 3.1a. The search coil used to measure the magnetic flux density is wound around the sample while a pair of Helmholtz coil or H coil records the applied the magnetic field strength is placed on the top and below of the excitation coil. The search coil consists of 7 turns while the H coil consists of 2 turns per coil. The resistance and inductances of the coils are modeled to get the realistic results.

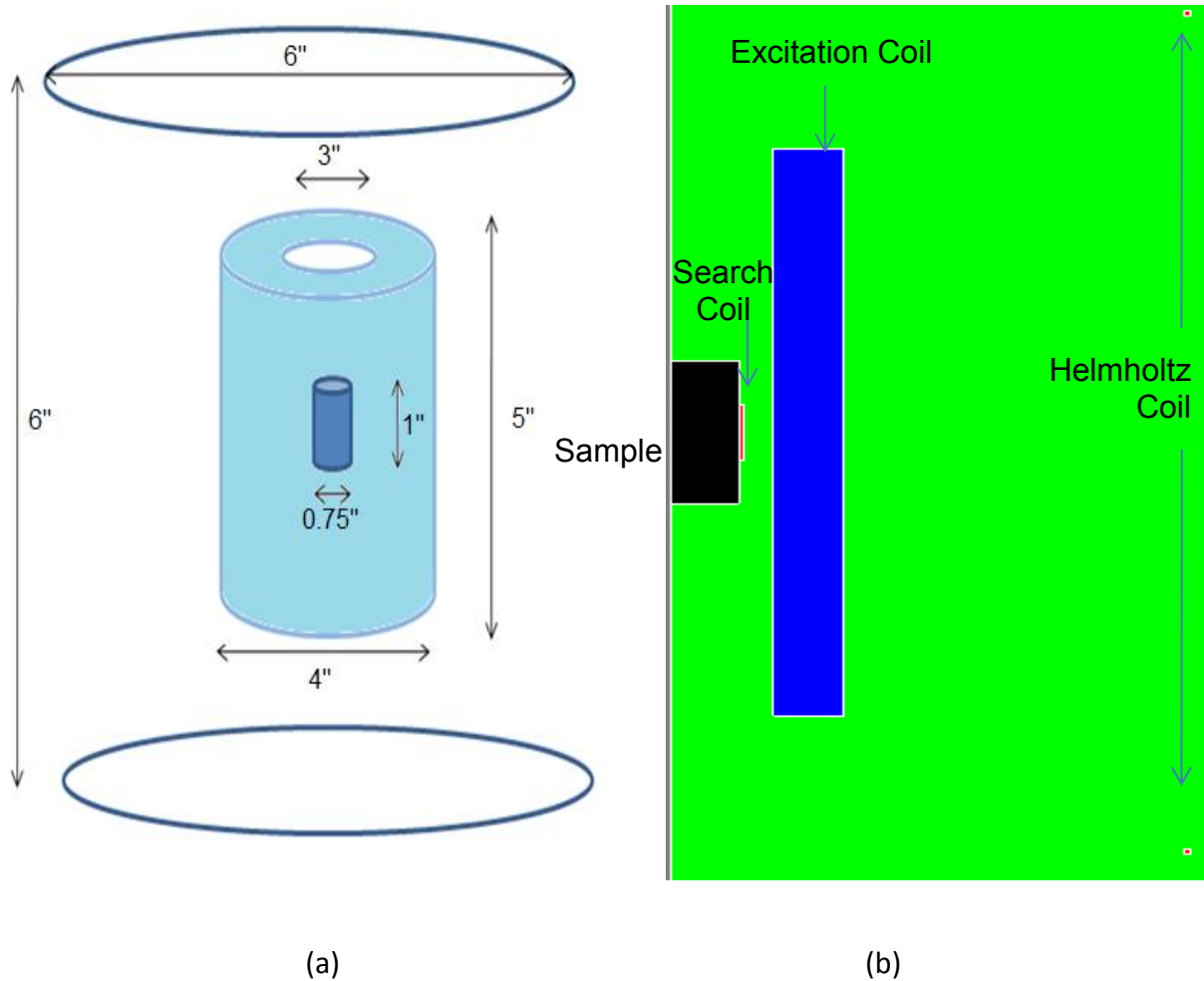


**Figure 3.1: (a) Actual dimensions of the final design of coil arrangement. (b) Problem domain definition for finite element analysis in FLUX 2D.**

The electrical coupling model connects the capacitive bank to the air-core excitation coil. The excitation field is generated by discharging a large capacitor bank into the resistive air-core coil. The capacitor bank consists of a total capacitance of 46.2 mF and charged up to 425 Volts. Figure 3.2 shows different magnetic flux density color shades at different places as well as the magnetic field lines at one time instance. The maximum flux is concentrated at the center of the sample. It can be seen that the magnetic flux density is fairly evenly distributed around the

whole magnet, which shows the whole part of magnet is completely saturated. As the distances increases from the center, the amount of magnetic flux density decreases accordingly.

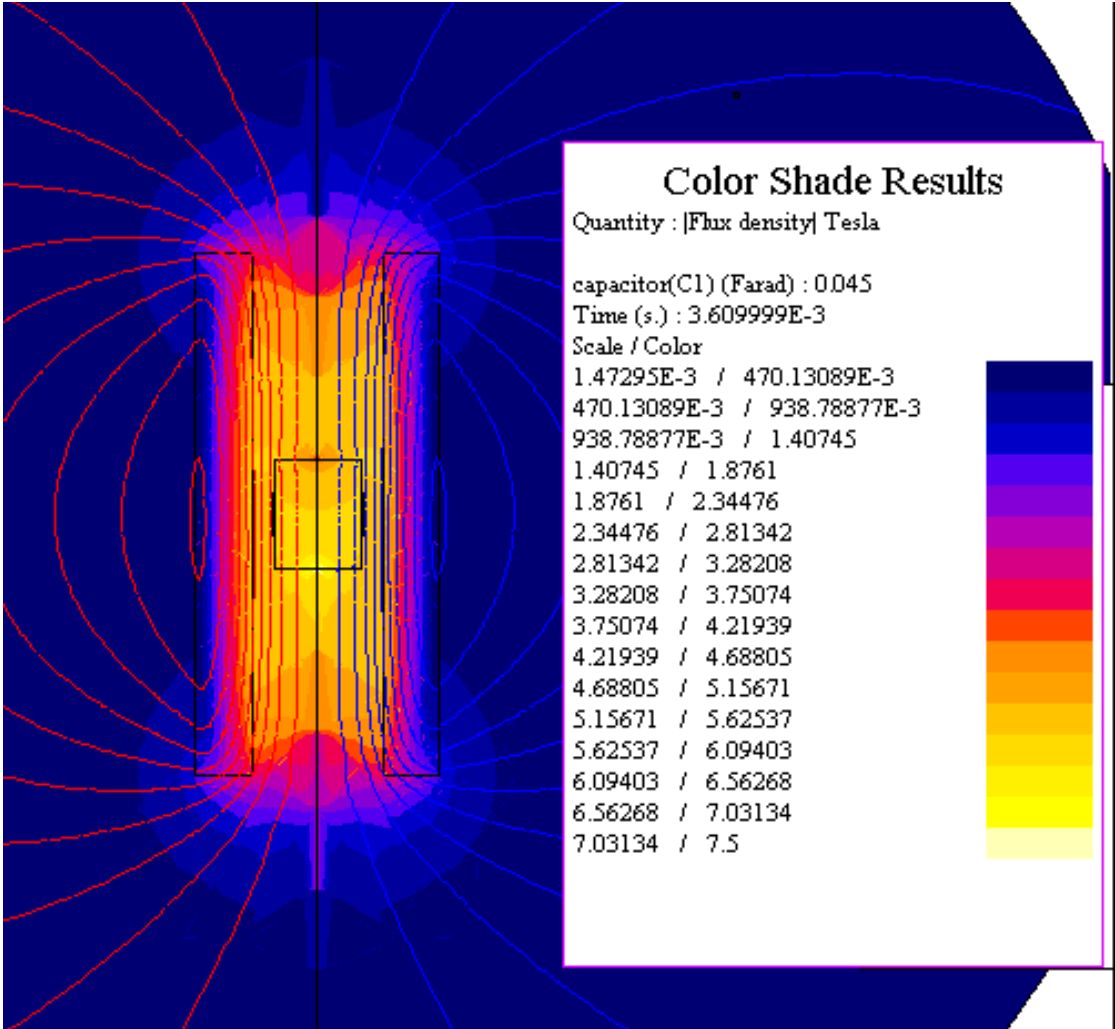


**Figure 3.2: Magnetic field lines shown at one-time instance**

The 46.2mF capacitors are charged up to different values of voltages; 250V 300V, 350V, 400V and 425V while all other variables are kept constant. Figure 3.3 shows the energized pulsed current passing through the excitation coil at different voltage levels. It is seen that the current goes up to 6.9 kA when the capacitors are charged up to 425V. The pulse period is about 13ms

and it lasts for about 43ms. As the charged voltage of the capacitor decreases, the amount of current discharge also decreases. The simulation iterations were repeated in the same manner by removing the magnet from the center and the effects were observed in the air. The amount of current discharge from the capacitors remains the same as expected.

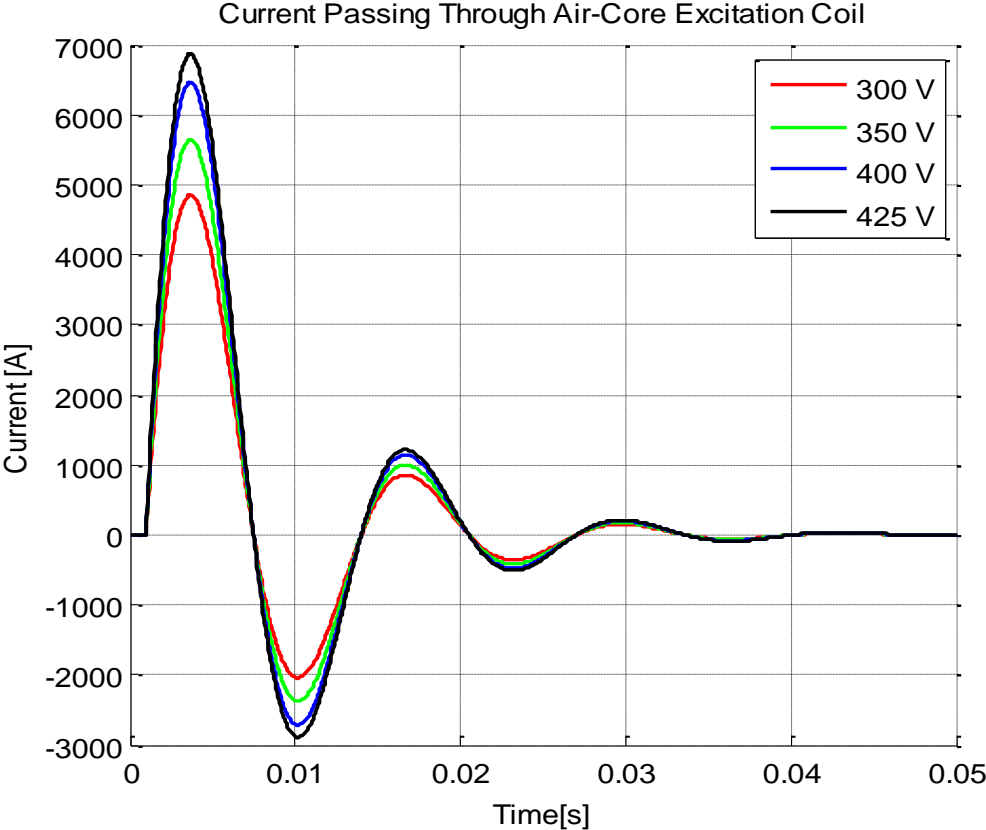
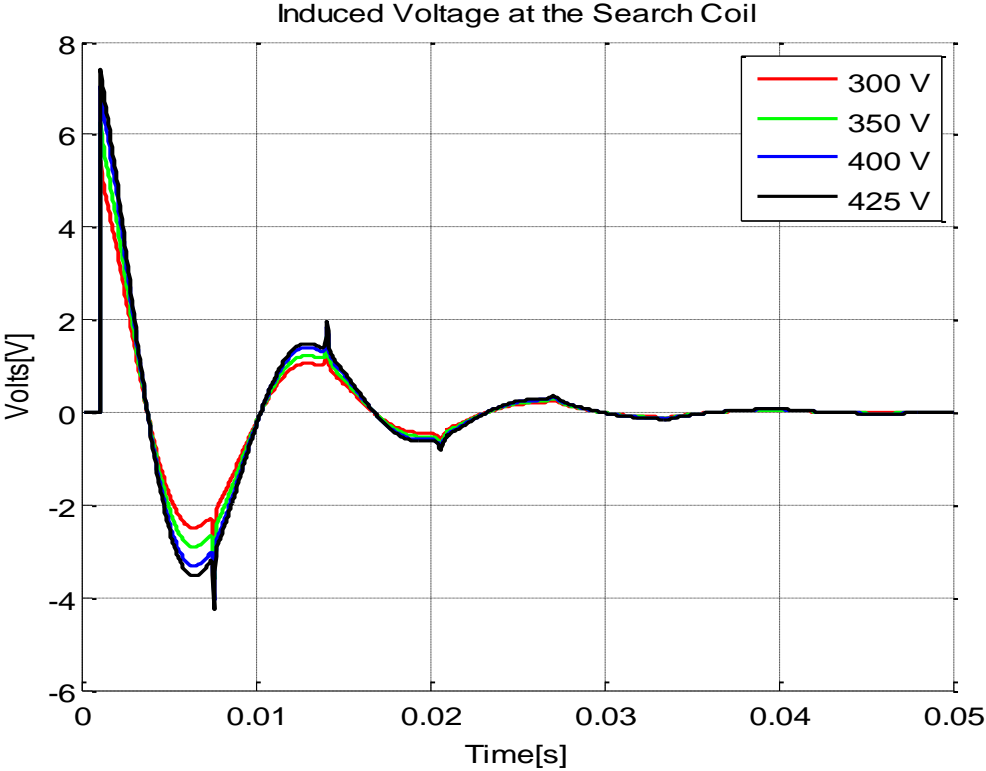


**Figure 3.3: Pulsed Current through the excitation coil**

The huge amount of pulsed current changes the magnetic field in the surroundings. This change in the magnetic field lines produces a change of flux, which induces a voltage due to Faradays law of induction in the search coil wrapped around the magnet. Figure 3.4 shows the induced voltages in the search coil with respect to time. The maximum voltage induced in the search coils is about 7.3V. The discontinuous peaks in the middle are due to the effects of magnet.

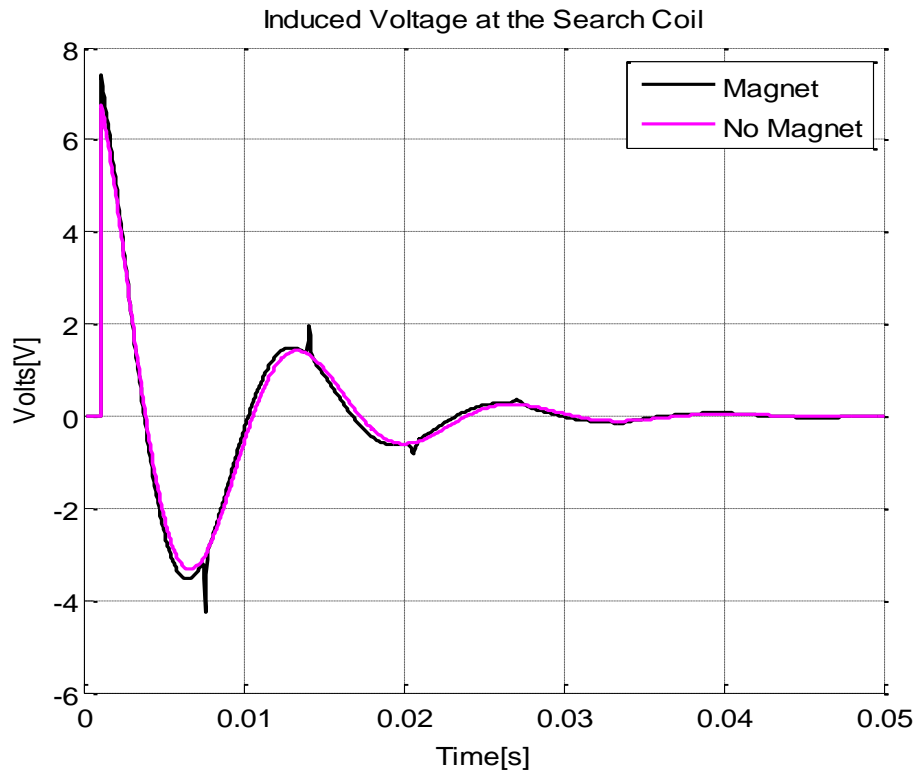
Figure 3.4b is the comparison between the presence of magnet and non-presence of the magnet. When the magnet is not present, the induced voltage waveform is smooth while some peaks are observed when magnet is present. The peak increases as more current/energy is discharged through the excitation coil.



(a) With different charged voltages with the presence of magnet at the center

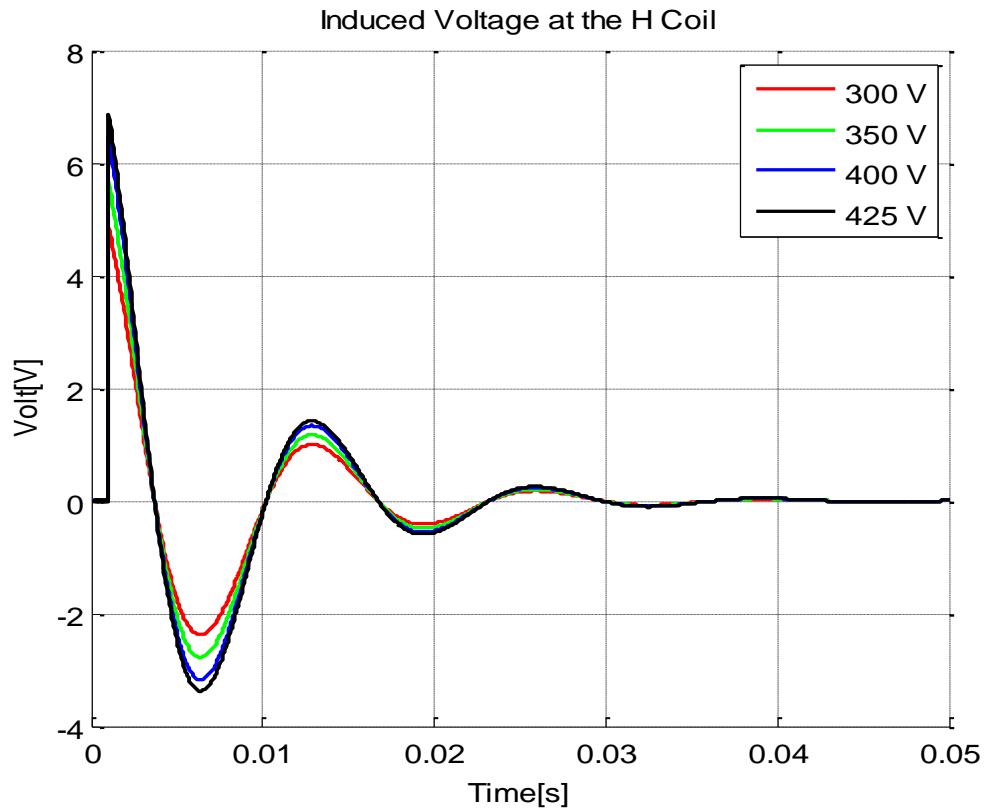
**Figure 3.4:** shows the induced voltages across the search coil

Figure 3.4 (cont'd)



(b) At charged voltage of 425V with and without the presence magnet at the center

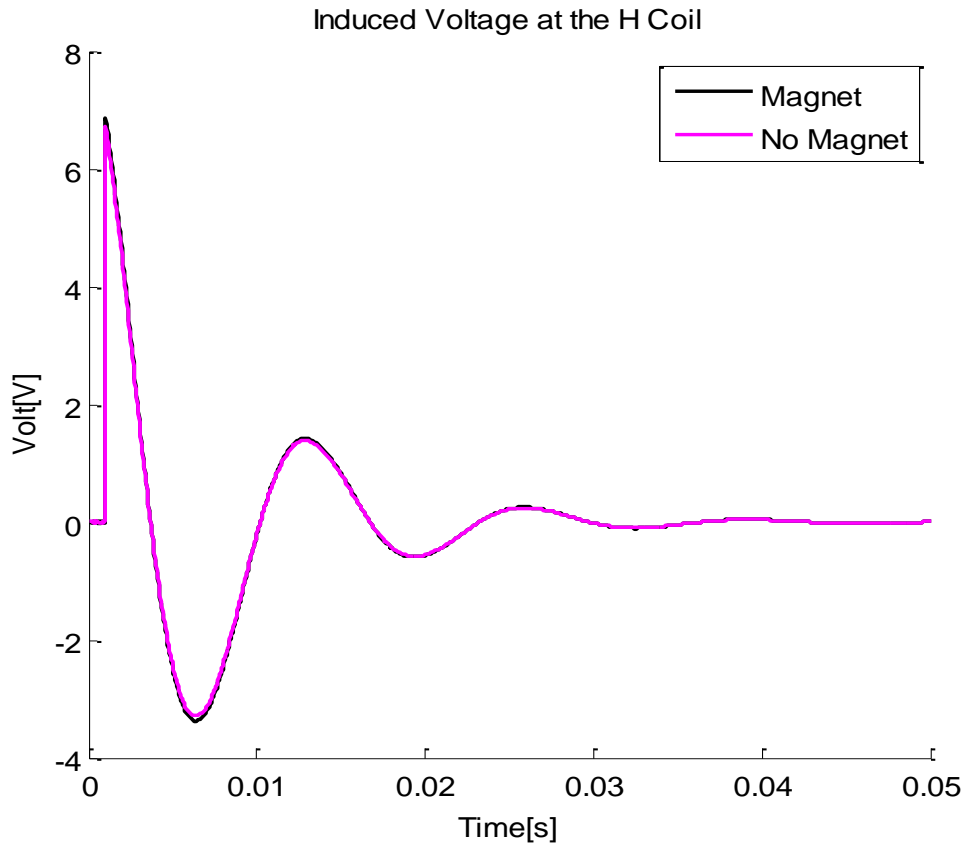
The change in the magnetic field and the change of flux also induce a voltage in the Helmholtz coil which is shown in Figure 3.5. As the current increases, the amount of induced voltages increases as expected. The induced voltage in the H coil is much smoother and has no peaks as compared to the induced voltages in the search coil. It shows that the effect of magnet is not seen in the H coil. It is also confirmed from the figure 3.5b that shows the induced voltage with and without the presence of the magnet.



*(a) At different voltages with magnet at the center*

**Figure 3.5:** shows the induced voltages across the Helmholtz coil

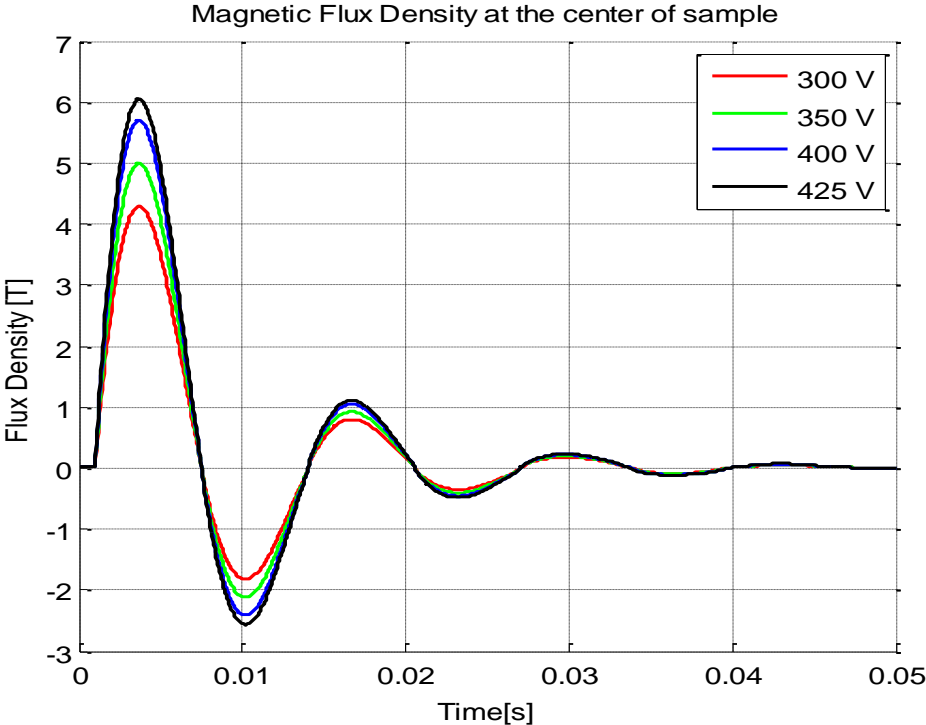
Figure 3.5 (cont'd)



(b) At 425V with and without the magnet at the center

The magnetic flux density and magnetic field strength can be calculated using the induced voltages above. The FEM design software has the capability of calculating the magnetic flux density and magnetic field strength itself. The software is used to measure these parameters. Figure 3.6 shows the corresponding axial component of the magnetic flux density with respect to time at the center of the sample at different voltages. As voltage increases, the magnetic flux density increases correspondingly. Figure 3.6b shows the difference in the waveforms of magnetic flux density at the center of the coil with and without the presence of magnet. Due to

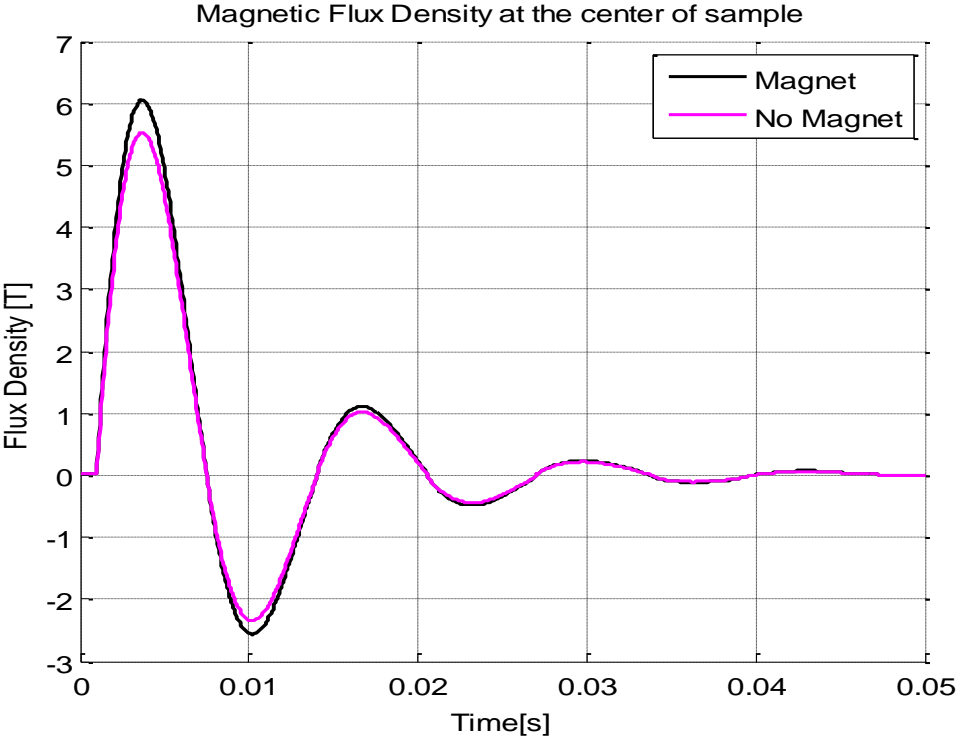
the presence of magnet, the magnetic flux density created is more due the remaneance of the magnet.



(a) At different voltages with the presence of magnet at the center

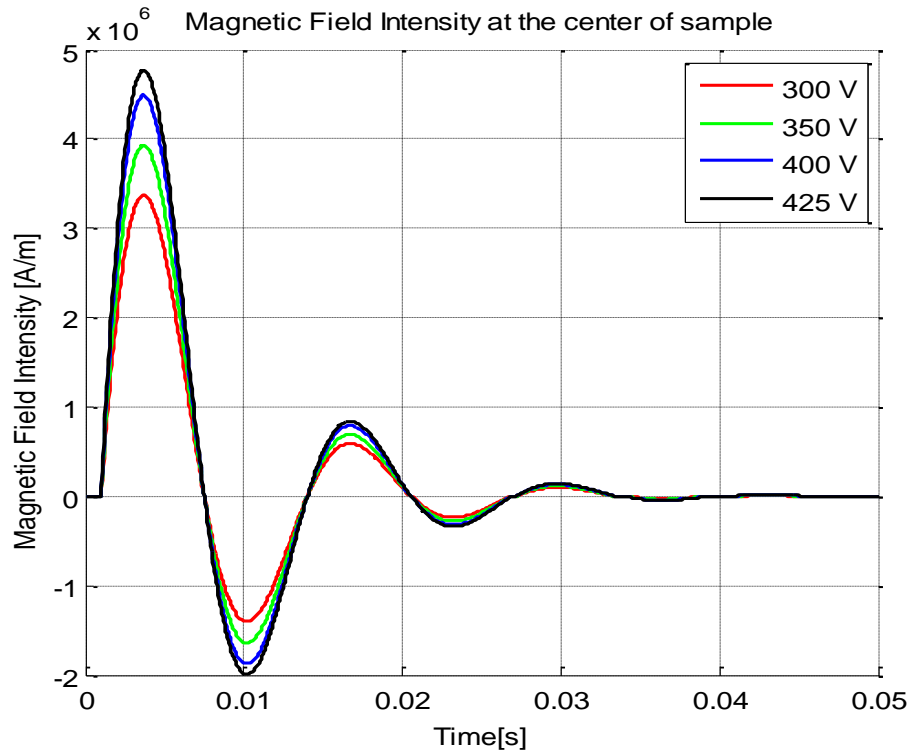
**Figure 3.6: Axial-component of the magnetic flux density**

Figure 3.6 (cont'd )

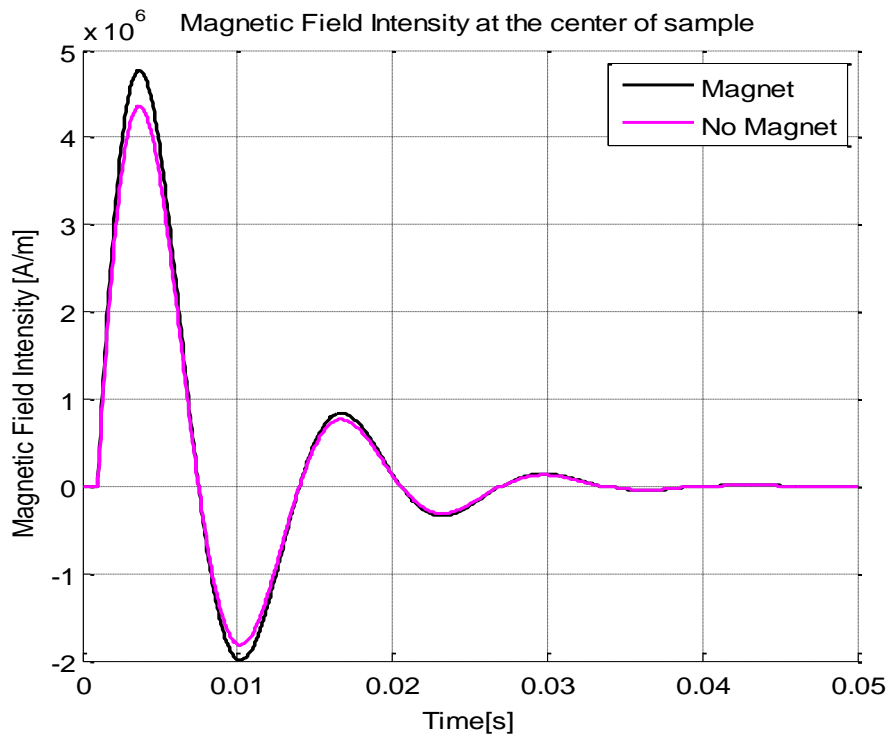


(b) At 425V with and without the presence of magnet at the center

The FEM design software is also used to measure the axial component of the magnetic field strength with respect to time at the center of the sample at different voltages shown in Figure 3.7. As voltage increases, the magnetic field strength also increases similarly. Figure 3.7b shows the difference in the waveforms of magnetic field strength at the center of the coil with and without the presence of magnet. The difference is caused due to losses in the magnet such as eddy currents and conductivity.



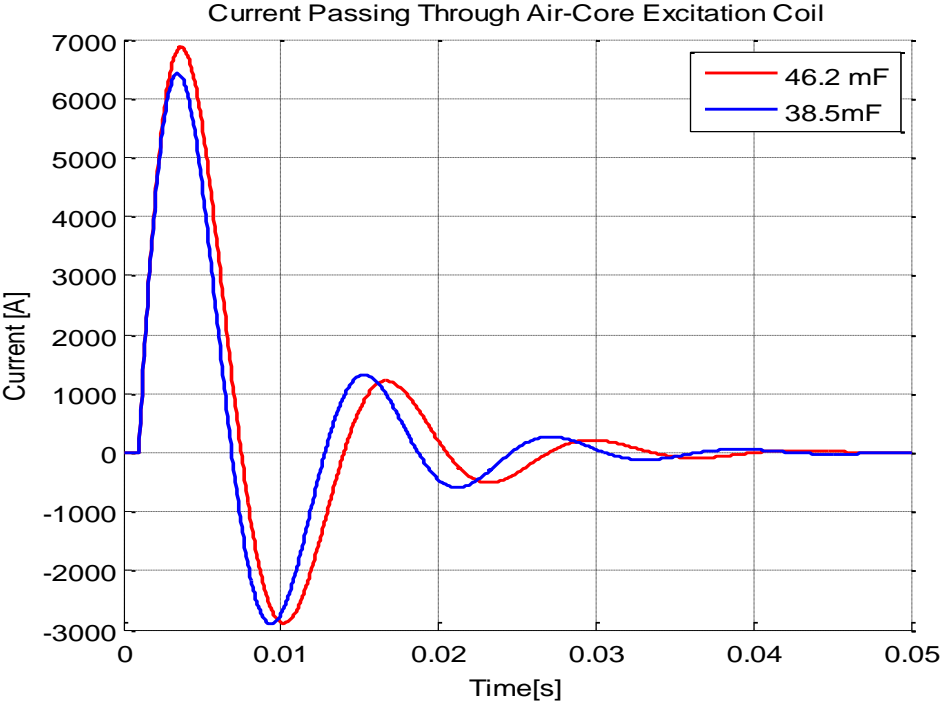
(a) At different voltages with magnet at the center



(b) at 425V with and without the magnet at the center

**Figure 3.7: Axial-component of the magnetic field strength**

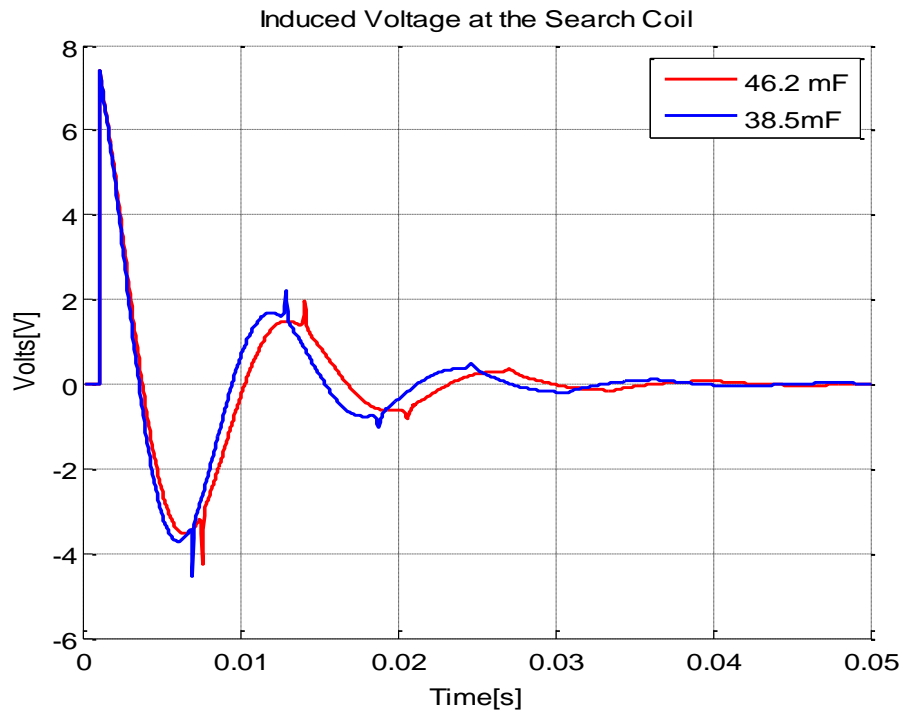
Another important feature we need to observe is the effect of capacitance on the magnetic field and magnetic flux density. The maximum peak current reduces as the capacitance of the capacitive bank reduces from 46.2mF to 38.5mF while the voltage is kept constant at 425 V. The waveform of the current discharge with respect to time is shown in Figure 3.8. It can be observed that the discharge rate is faster with lower capacitance. The time period reduces from 14ms to 12.5ms. The magnitude of induced voltage in the search coil reduces very little while the peaks remain of the same magnitude that shows that the effect of magnet is about the same. The magnitude of the induced voltage also has little effect. The magnitudes of magnetic flux density and magnetic field strength have been reduced but are still strong enough to saturate the magnet completely.



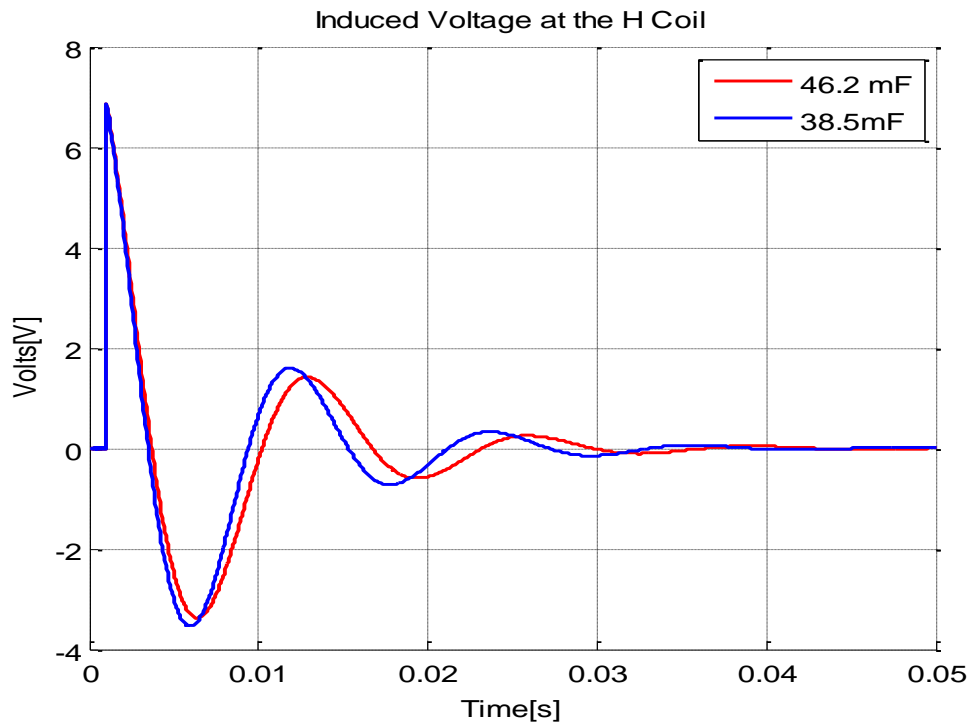
(a)

**Figure 3.8: (a) current (b) induced voltage in search coil (c) induced voltage in H coil (d) magnetic flux density (e) magnetic field strength**

Figure 3.8 (cont'd)

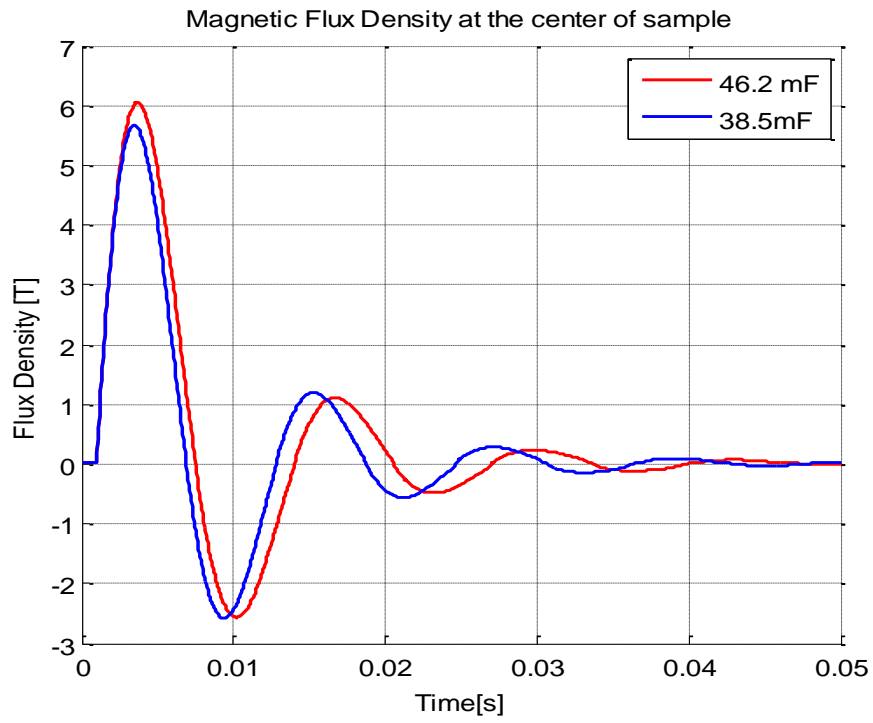


(b)

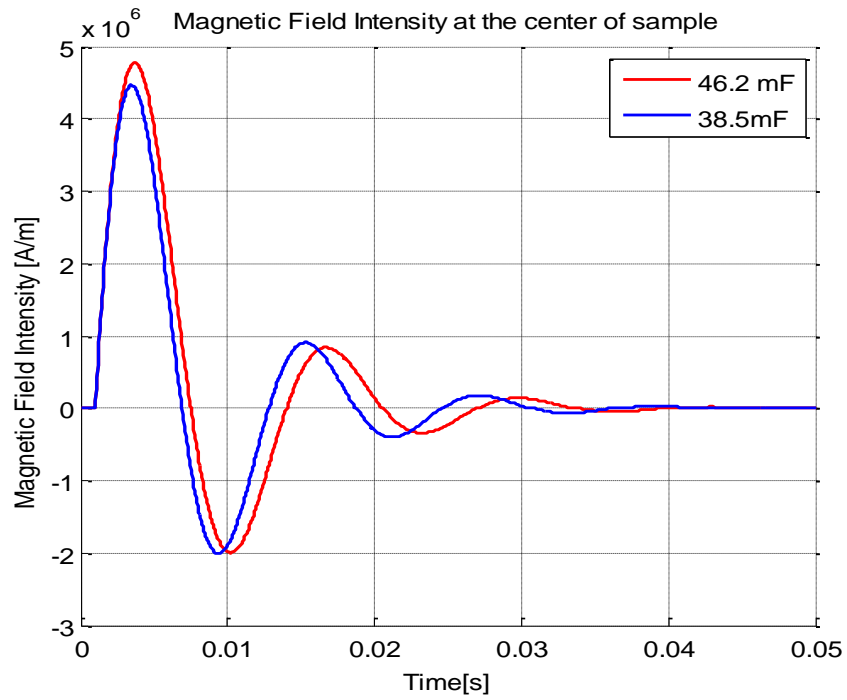


(c)

Figure 3.8 (cont'd)



(d)



(e)

### **3.3- MATLAB/Simulink:**

This section explores the hysteresis properties of the magnets. The main disadvantage of the FEM software is the absence of the magnetic hysteresis properties. The non-linear magnetic properties of the magnets in the FEM software are modeled by only  $H_c$  and  $B_r$ . Due to the absence of ability to model hysteresis in commercial Finite Element Program; the MATLAB/Power System Blockset (PSB) is used as a simulation tool that uses static hysteresis model for the saturable transformer block [22, 23]. In this technique, saturable transformer is assumed as magnet and its hysteresis properties are defined.

The model defines a relation between flux,  $\Phi$ , and the magnetization current. It is useful under transient conditions and can be represent minor loops. The model exhibit all the main features of hysteresis and is extended to represent also the saturation characteristic.

The same power electronics methodology is used as in FEM, where capacitors are charged up to certain level of voltage and discharged through an air-core excitation coil modeled using the saturable transformer primary coils. The magnetic properties of saturable transformers are same as the magnetic properties of the same magnets. The secondary coils in the saturable transformer are assumed as the search coil that is wrapped around the magnet.

#### **3.3.1- Saturable Transformer hysteresis characteristics**

The electrical model for 1phase saturable transformer is shown in Figure 3.9 that takes into account the winding resistances and the leakage inductances as well as the magnetizing characteristics of the core, which is modeled by a resistance,  $R_m$ , simulating the core active

losses and  $L_{sat}$ , simulating the saturable inductance. The electrical model is built with simulink blocks that are specified using the hysteresis design tool of the powergui block. The magnetizing current,  $I$ , is computed from the flux,  $\Phi$ , obtained by integrating voltage across the magnetizing branch. The static model of hysteresis defines the relation between flux and the magnetization current evaluated in DC, when the eddy current losses are not present.

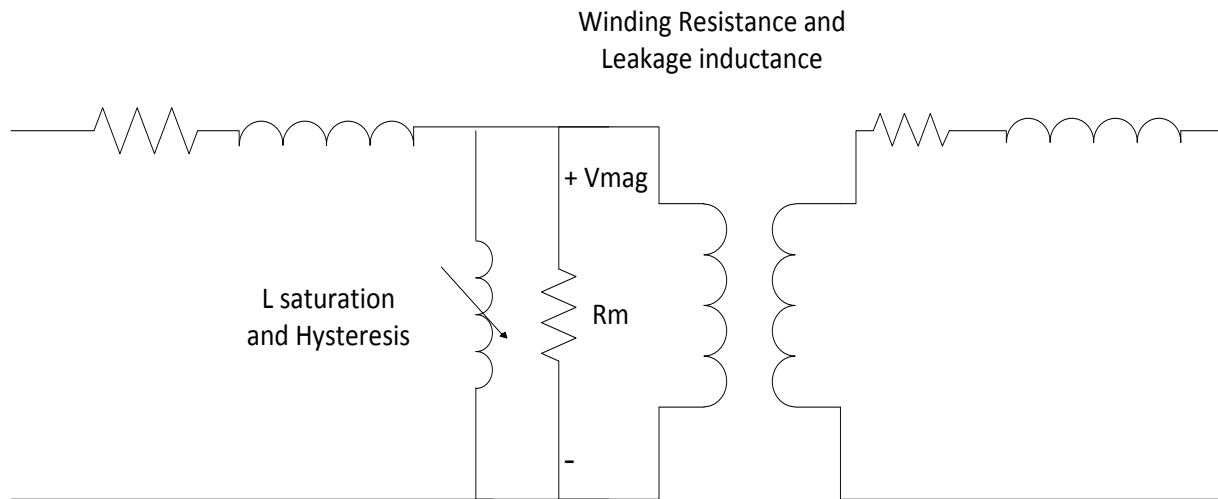


**Figure 3.9 Electrical Model of the PSB saturable transformer**

The hysteresis model uses a semi empirical characteristic, using an arctangent analytical expression  $\Phi(I)$  and its inverse  $I(\Phi)$  to represent the operating point trajectories [21]. The analytical expression parameters are obtained by curve fitting empirical data defining the major loop and the single-valued saturation characteristic. The minor loops are derived from the major loop ascending (i.e  $d\Phi/dI > 0$ ) or descending (i.e  $d\Phi/dI < 0$ ) trajectories. The basic analytical expression  $\Phi(I)$  representing a major loop half cycle is given by :

$$\Phi = -sgn[a * \arctan(-sgn * bI + c) - sgn * aI + e]$$

Where

$\text{sgn} = 1$  for ascending trajectory and  $-1$  for a descending trajectory,

$\alpha$  is the residual flux( $\Phi_r$ )

$c$  is the coercive current( $I_c$ )

$b$  is the slope ( $d\Phi/dI$ )

$a$  and  $e$  represent saturation point coordinates,  $I_s$  and  $\Phi_s$ .

The model uses inverse relation  $I(\Phi)$  during simulation as the input is  $\Phi$  instead.

The hysteresis design tool of the powergui block is used to fit the hysteresis major loop of a particular core type to basic parameters. These parameters are defined by the remanent flux ( $\Phi_r$ ), the coercive current ( $I_c$ ), and the slope ( $d\Phi/dI$ ) at  $(0, I_c)$  point as shown in the Figure 3.10.

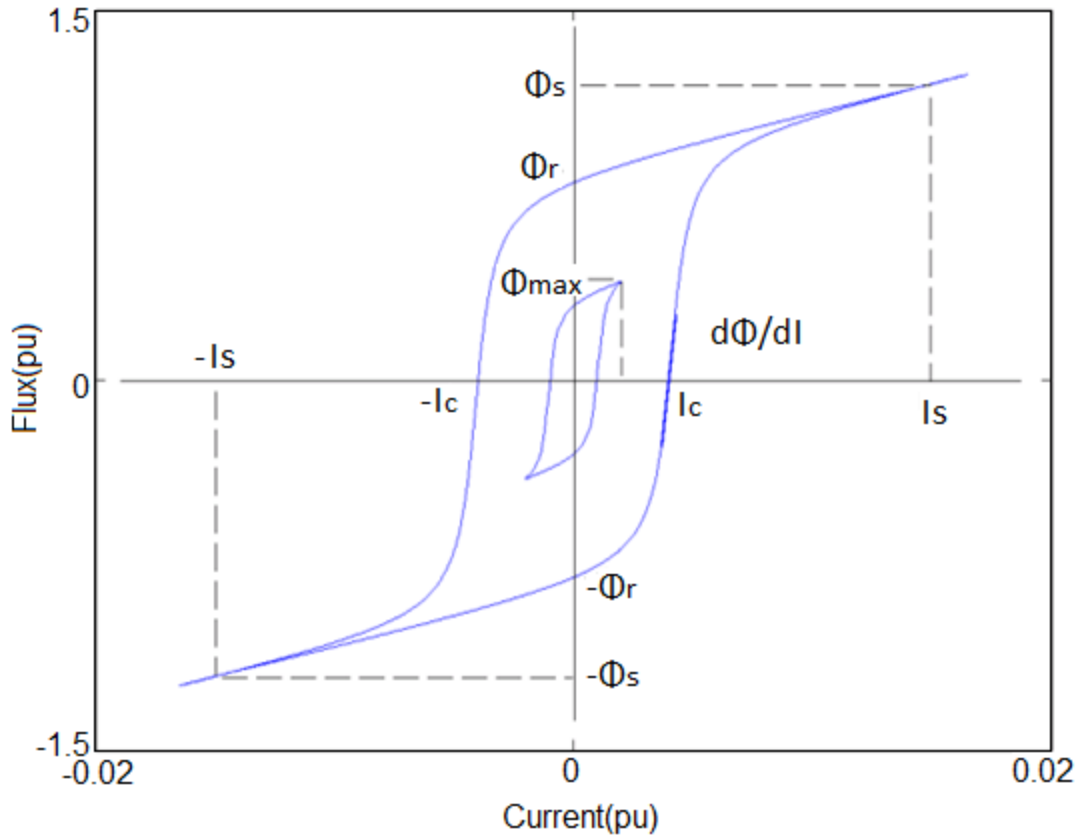


**Figure 3.10 Hysteresis Loops [22]**

The fundamental characteristics of the hysteresis model are defined as [22]:

1. A symmetrical variation of the flux produces a symmetrical current variation between  $I_{\max}$  and  $+I_{\max}$ , resulting in a symmetrical hysteresis loop whose shape and area depend on the value of  $\Phi_{\max}$ . The major loop is produced when  $\Phi_{\max}$  is equal to the saturation flux ( $\Phi_s$ ). Beyond that point the characteristic reduces to a single-valued saturation characteristic that is asymptotic to the air core inductance ( $L_s$ ).

2. In transient conditions, an oscillating magnetizing current will produce minor asymmetrical loops, as shown in the next figure, and all points of operation are assumed to be within the major loop.
3. Inside a minor loop, the magnetizing curve depends only on the last two reversal points and each curve tends to return to the reversal point previous to the last (e.g. the evolution 1-2-3-4-3-5-2-6-1) in the above figure 3.11

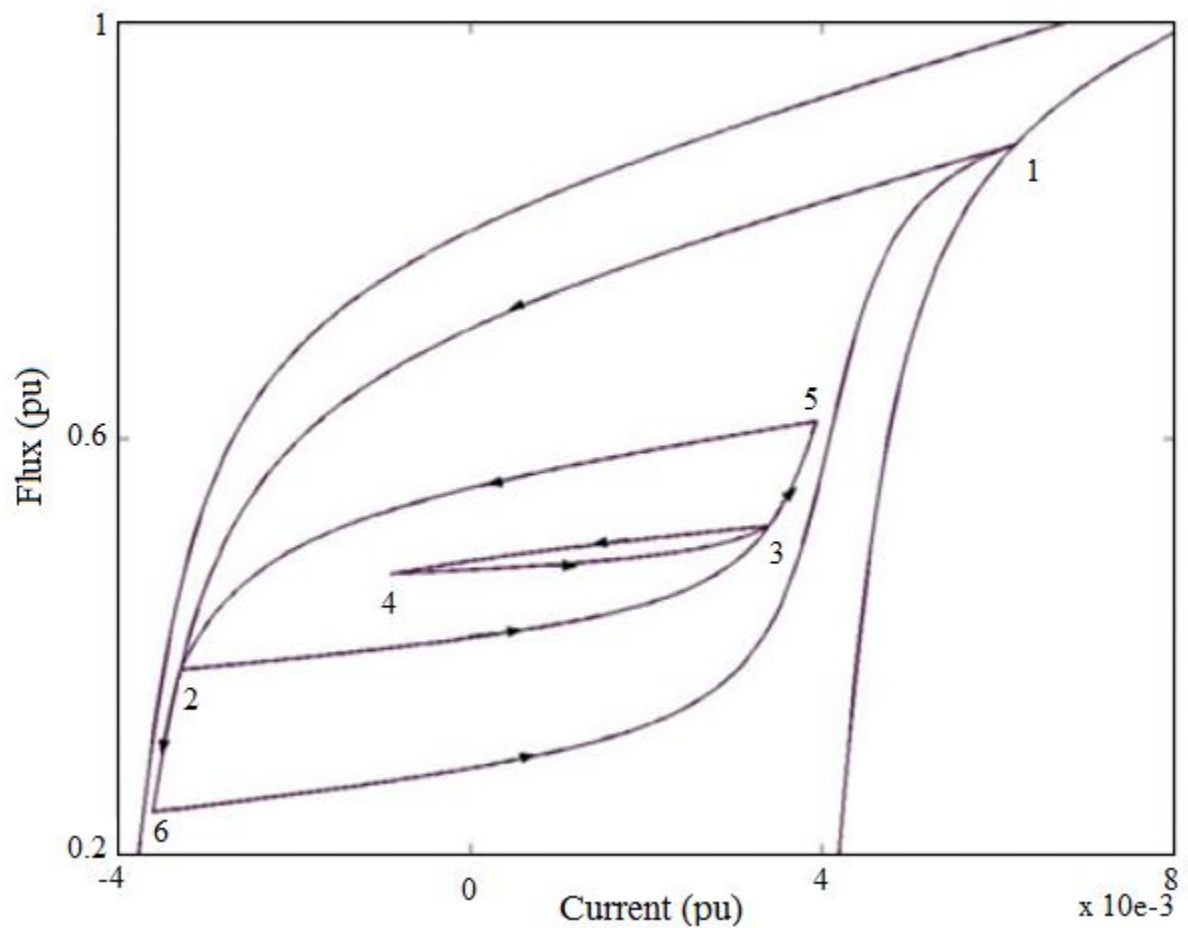


**Figure 3.11 Internal minor loops [22]**

**3.3.2- Model Parameterization and circuit**

Figure 3.12 illustrates the simulation of the hysteresis in a saturable transformer block of PSB. It consists of the DC link of 600V and the timer switch that is turned on to charge the capacitors. The timer switch and S1/S2 are complementary to each other. When timer switch is on, S1 and S2 are off and vice versa. Once the capacitors are charged up to the desired voltage, the timer switch closes while S1 and S2 turn on. S1 is used to fire the thyristor. By controlling the firing of the thyristor, we can control the discharge of the energy into the primary coil of the transformer acting as an excitation coil. In the circuit, damper resistance is used to increase the resistance of the system to control the maximum and minimum peak of the excitation current through the excitation coil.

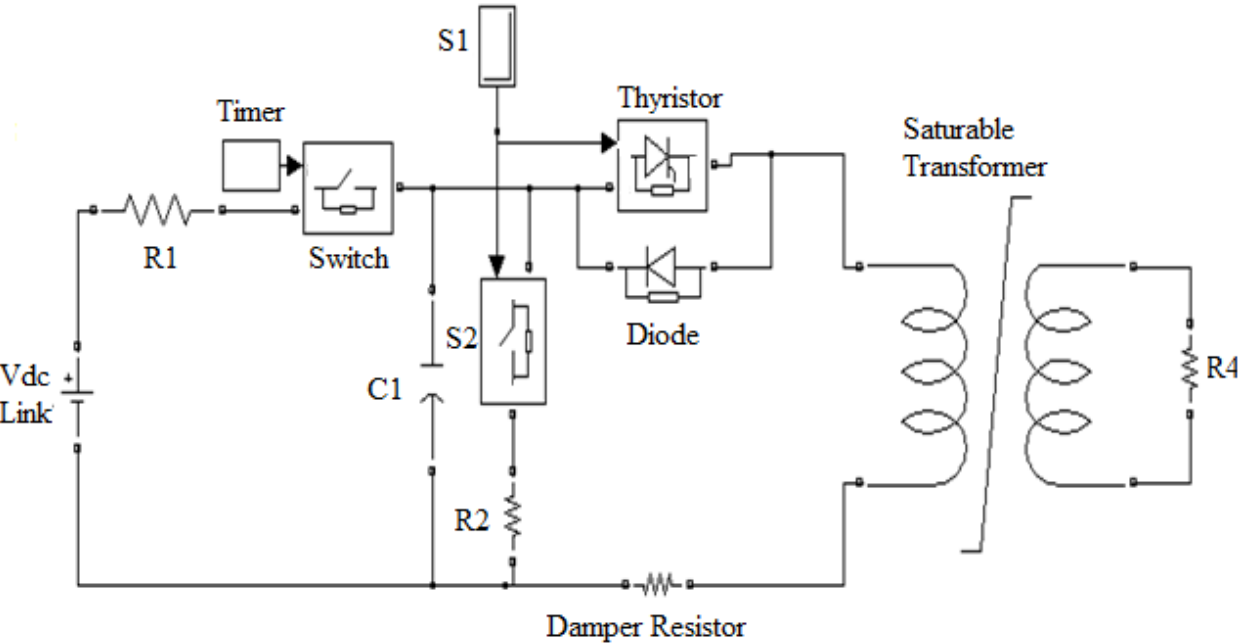


**Figure 3.12 Simulink Circuit**

The hysteresis parameters that are modeled in a saturable transformer are shown in Table 3.1. The resulting waveform of the major loop hysteresis by using these parameters is illustrated in Figure 3.13.

Table 3.1 Hysteresis parameters

Parameter	Value
Segments	512
Remnant Flux Fr (V.s)	2.3e-3
Saturation Flux Fs (V.s)	2.4e-3
Saturation Current (A)	5059
Coercive Current Ic (A)	3626
df/dI at coercive current	1.37e-5
Saturation region currents (kA)	[5.6 5.34 6.9 7.5 82 1.83e12 ]
Saturation region Fluxes (mVs)	[2.4 2.42 2.45 2.55 3.5 6.5]
Nominal Parameters[P (VA) V(V <sub>rms</sub> ), f(Hz)]	[150e6 500e3/√3 60]

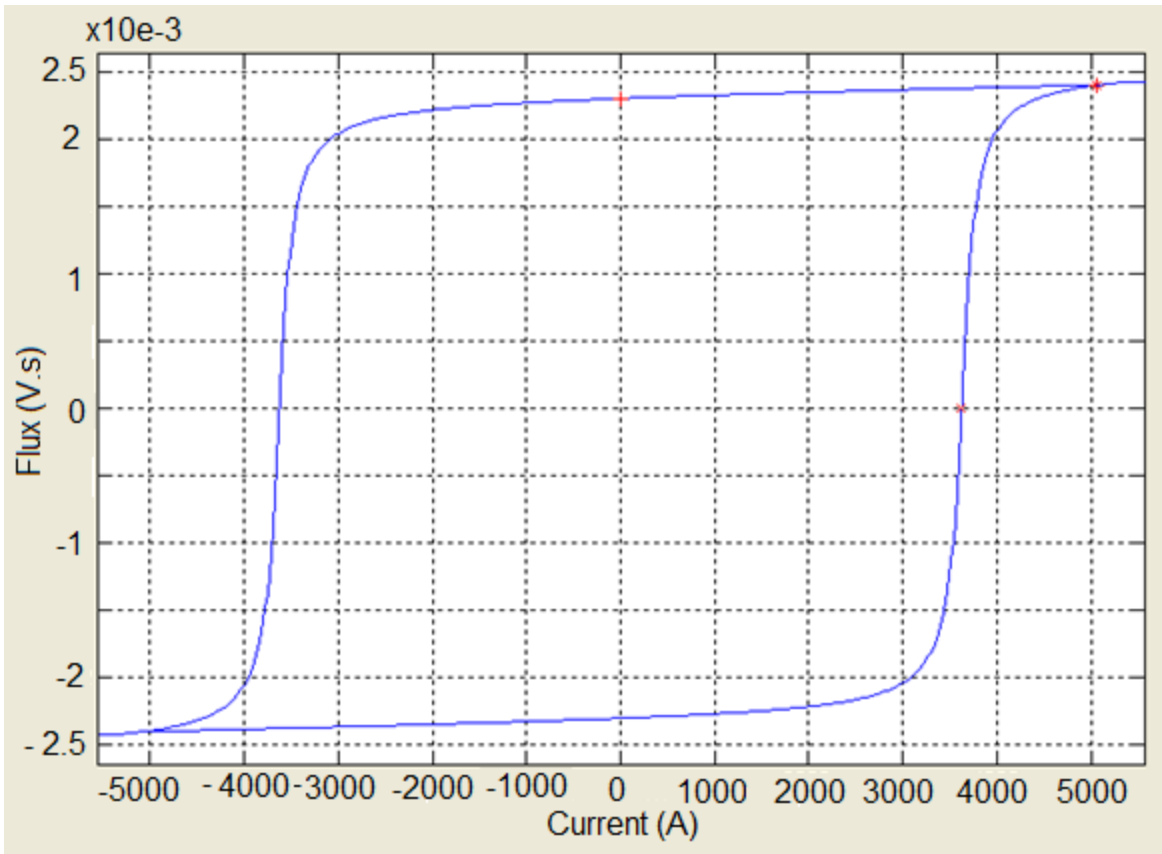


**Figure 3.13 Modeled hysteresis major loops**

### 3.3.3- Results/Waveforms

Figure 3.14 shows the excitation current that consists of eddy currents and magnetizing current. It is the total current coming out of the capacitive bank. Figure 3.15 shows only the magnetizing current where it can see the effect of magnet.

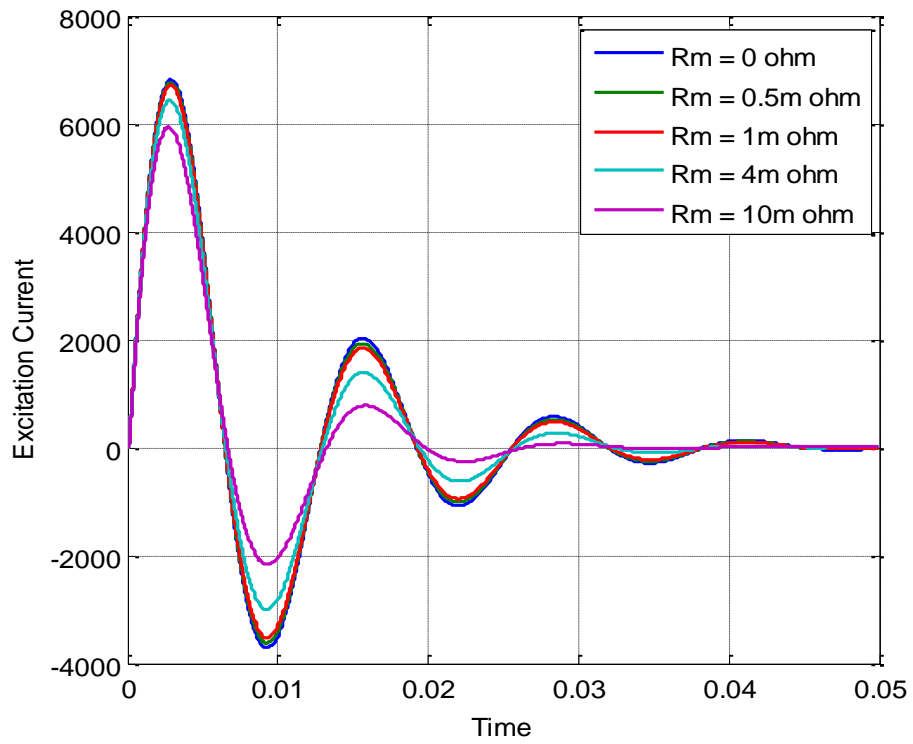


**Figure 3.14: Excitation Current**

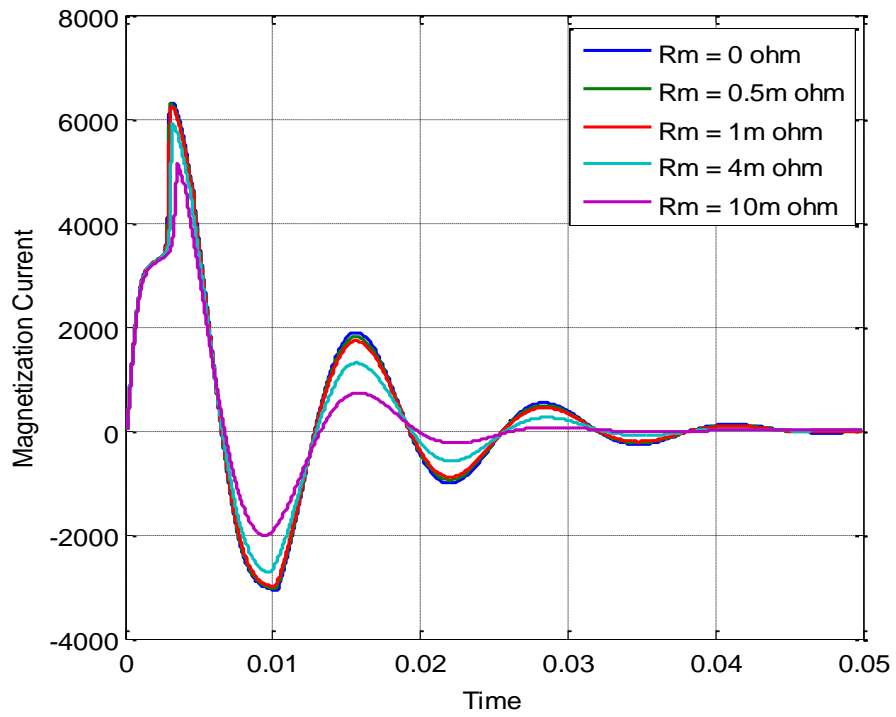


**Figure 3.15: Magnetization Current**

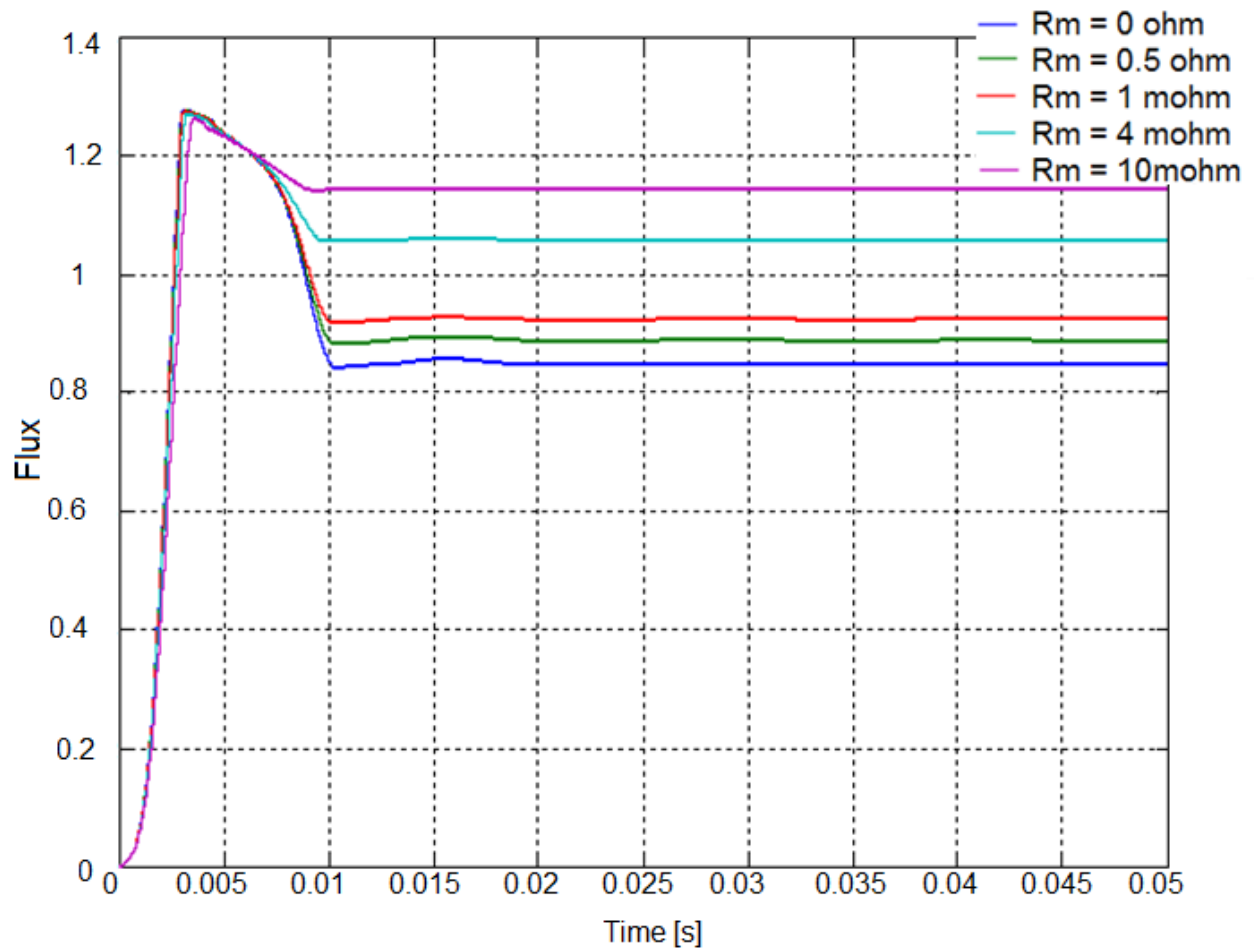


**Figure 3.16: Magnetization Current**

The total amount of flux that is passing through the transformer with respect to time is shown in Figure 3.16 while Figure 3.17 shows the hysteresis effect of the pulsed excitation. The magnetic field is calculated using the current.

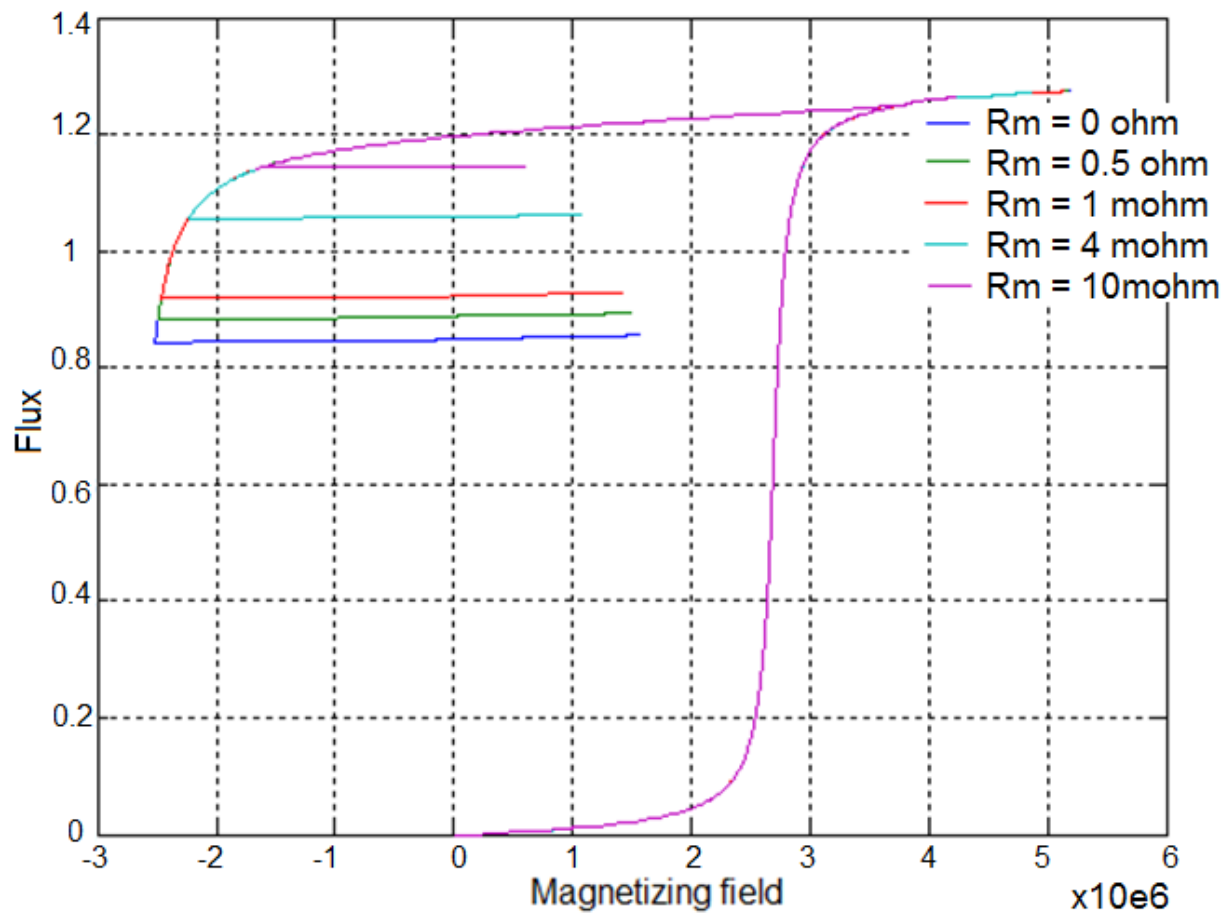


Figure 3.17: Magnetization Current

## Chapter 4

### Experimental Setup

This section explores a pulsed field magnetometer experimental setup consisting of two core components; power electronics and software implementation to control the power electronics circuitry. After the setup, experimental procedure will be defined to distinguish between good and bad raw material and how to establish different recoil lines.

#### 4.1- Hardware (Power Electronics)

There are two main modes of the power electronics: charging and discharging. Figure 4.1 shows the complete power electronics circuitry consisting of both these modes. The charging mode consists of a Step-Up Isolated Transformer, Hammond-PH750MQMJ-FK, which converts the 120 Vac into 480 Vac. It then passes through a diode bridge rectifier, NTE-5331, that converts the AC voltage to DC voltage. To charge the capacitors, the DC voltage has to pass through electrically controlled switch known as contactor. The contactor, Moeller-DILA-22, is a Four Poles Single Throw (4PST) switch with two Normally Closed (NC) and 2 Normally Open (NO) poles. The contactor is controlled by an additional relay which itself is controlled by digital signal outputted by the Data Acquisition (DAQ) Card, NI-USB 6259 by National Instruments. Figure 4.2 shows the control circuitry from the DAQ card to turn on the contactors.

The DAQ card output signal first passes through the phototransistor optoisolator and NPN transistor to turn-on the relay 1. The optoisolator is used to isolate the DAQ card from the rest of the system to prevent damage caused by reverse voltage. The relay then turns-on the contactor and NC poles are open while NO poles are closed which allows the capacitors to start charging slowly. The current passing through the capacitor is about 1.5A due to the series resistance of 400  $\Omega$ . The capacitor voltage is continuously monitored at the DAQ card analog input pin. Once the capacitor reached the desire voltage, charging is stopped as the contactor turns off. The negative terminal of the capacitor then connects to the ground.

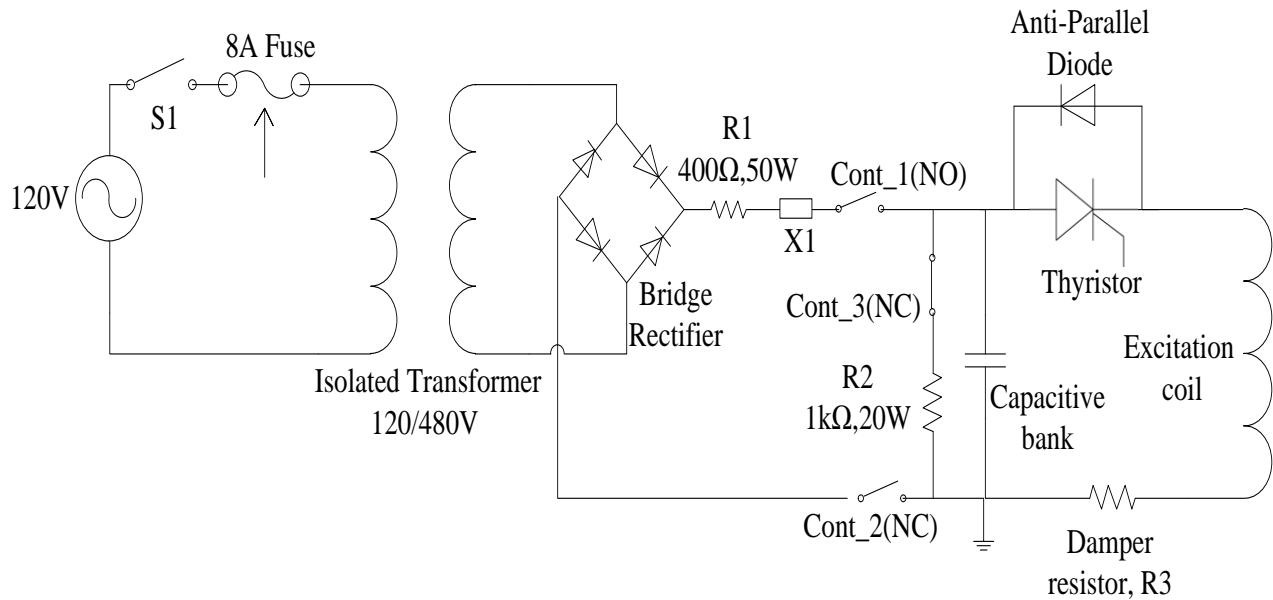


**Figure 4.1: Power Electronics Circuitry**

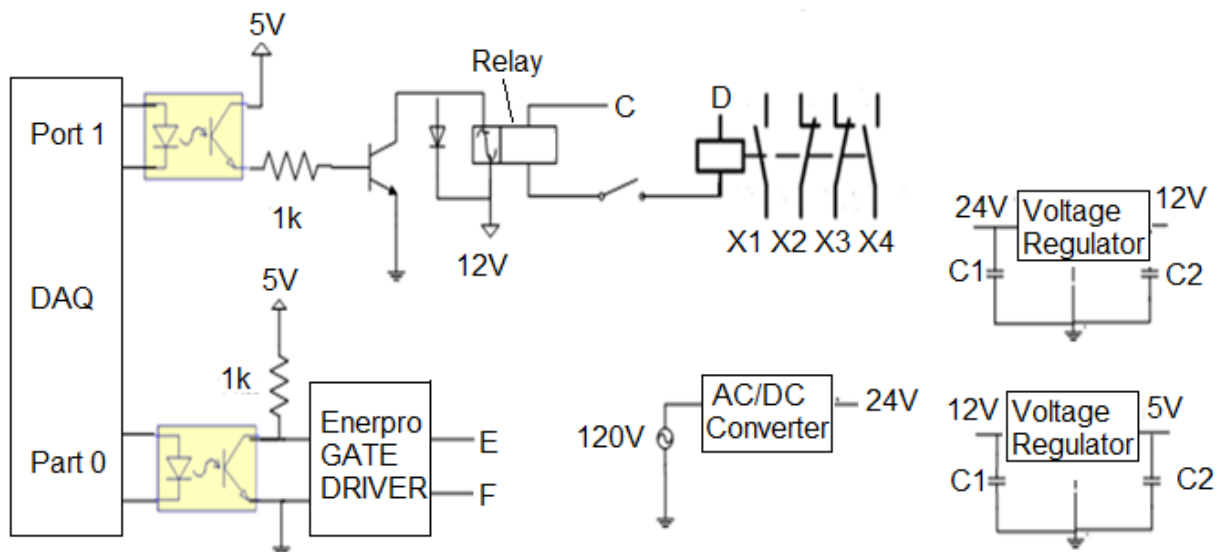


**Figure 4.2: Control Circuitry from data acquisition to control the contactors.**

The discharging mode consists of Westcode thyristor, N1718NS-140 and an anti-parallel diode, W3270NC220, to protect the thyristor from reverse voltage. It is also controlled by Enerpro Firing Board, CBTC-1-1, which itself is controlled by the DAQ card output signal as shown in

Figure 4.2 port 0. When the DAQ output signal is sent, it first passes through the second phototransistor optoisolator and NPN transistor to turn-on the gate driver. The gate driver fires the signal to the gate of the thyristor. As soon as the thyristor turns on, the capacitors are discharged through the excitation coil. A damper resistor of different values ranging from  $0\Omega$  to  $2m\Omega$  is connected in series with the excitation coil in different iterations to calculate the transient excitation current.

The actual coil arrangement for the system has an excitation coil that is made up of 90 turns using square 8 AWG with an inner diameter of about 3 in and the length of 5.3 in. The 8 AWG coil is coated with double Plexiglas insulation. The cylindrical shaped magnet samples are placed at the center of the excitation coil on the delrin rod support. The search coil is wrapped around the magnet using 22 AWG wire with seven numbers of turns while the Helmholtz coil pair is situated outside the excitation coil of diameter 7 in. The Helmholtz coil pair has two numbers of turns each made of up 22 AWG wire as shown in figure 4.3

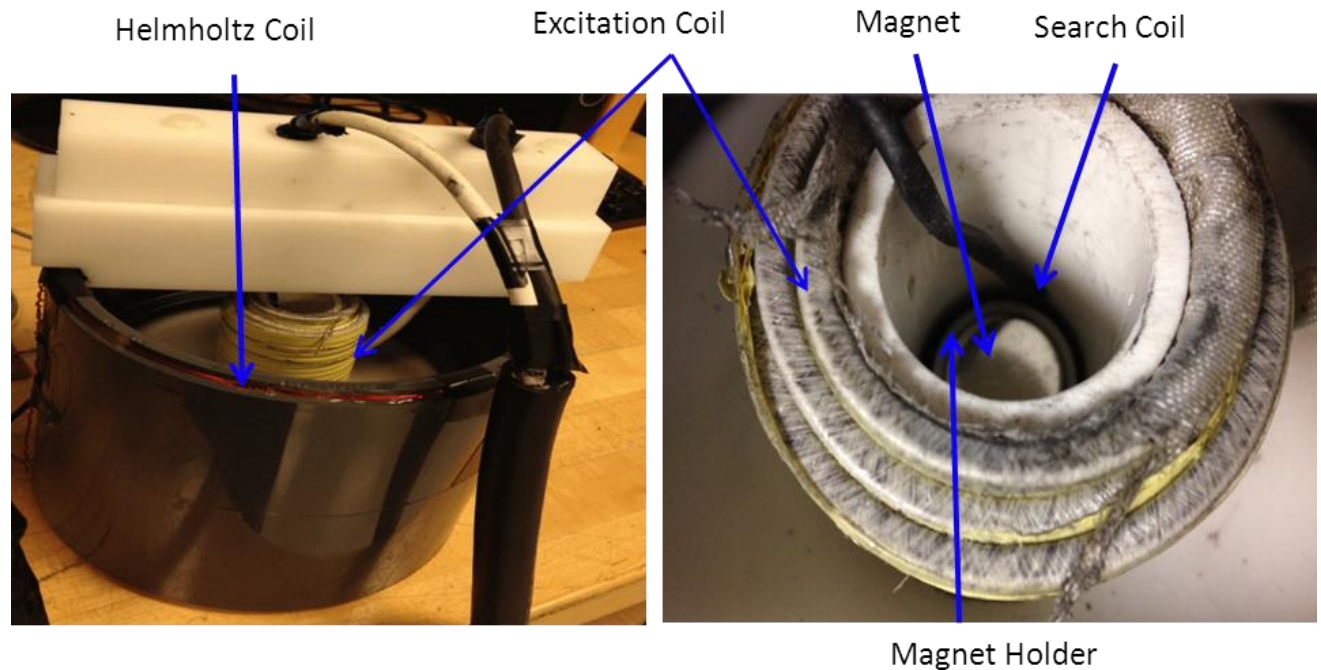


**Figure 4.3: Actual coil arrangement showing excitation coil, search coil and Helmholtz coil with the sample magnet at the center**

The induced voltages from the search coil and Helmholtz coil are first passed through the voltage divider and then through two 7.5V zener diode clipper circuit to clip the voltage in excess of 8.2V without distorting the signal. The gain of voltage divider is chosen in such a way that it ensures the maximum possible voltage from the pickup coils without driving the voltage response of the data acquisition board into saturation.

The output from the clipper circuit goes to the DAQ card to record the data as shown in Figure 4.4. The magnetic field (H-field) is recorded through a Helmholtz coil pair while the magnetic flux (B-field) inside the sample material is obtained through a tightly wound search coil.

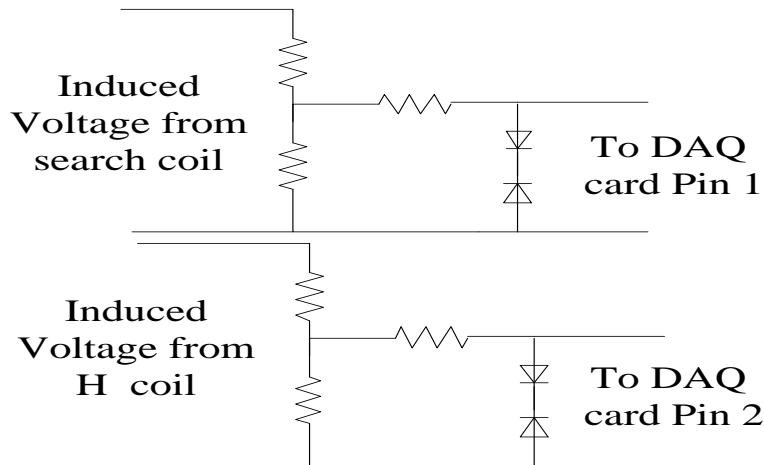


**Figure 4.4: Control Circuitry from data acquisition to control the contactors.**

## 4.2- Software Implementation

There are two aspects of the software implementation for the pulsed hysteresis graph system:

A) LabView for control and measure parameters and B) MATLAB for post processing.

### 4.2.1- LabView

The first phase of software implementation for the pulsed field magnetometer is mainly used to communicate with the power electronics circuitry and measure the induced voltages across the pickup coils. The control user interface is developed in LabView using the data acquisition (DAQ) card, USB-6259, by National Instrument. The maximum sampling frequency is 1.2 MS/s for one channel, or 1 MS/s for multiple channels.

Using the front panel, user can output the digital signal through Port 1 to turn on the first contactor that initiates the charging of the capacitors. The capacitor voltage is measured using the analog input signal, ai2. Once the capacitors are charged till the desired voltage, it stops the charging by turning off the signal from Port 1. If user desires to stop charging before it reaches

the desired voltage, it can be stopped using the “Charge Stop” button. Another output signal from the Port 0 is then sent that turns on the thyristor through the firing board to allow the energy to discharge through the excitation coil. As soon as the Port 0 turns on, two analog input signals are captured at the sampling rate of 125 kHz and the number of data points collected by each signal is 60,000.

All analog input signals are measured under the differential mode. The first analog signal, ai0, represents the induced voltage in the search coil; the second analog signal, ai1, represents the induced voltage in the H coil. All input and output channels have a voltage range of  $\pm 10$  V. All the measured voltages are then plotted in the graph and saved in an excel file which is further post processed in Matlab.

#### **4.2.2- MATLAB**

The second stage of software implementation consists of post processing in MATLAB where the measured data is loaded from excel files. The MATLAB software contains information about the length of the sample and its radius. Both values are given in meters and are required for the computation of the demagnetization factor and the compensation for the eddy current influence in highly conductive samples.

The next portion of the software is the description of the pickup coils (number of turns, coil area, and area-turn product of the coil. The last portion of the software describes the parameters for the data acquisition. Those are the sampling frequency and the number of acquired data points.

The magnetic field and magnetic flux density are then calculated using the induced voltages and these parameters are plotted to establish the hysteresis curve of the sample.

### **4.3- Experimental Procedure**

#### **4.3.1- Calibration of Helmholtz Coil**

Helmholtz coils (H coil) can be used as flux sensing coils, instead of flux generating coils for the measurement of open-circuit magnetization of most permanent magnet materials. The H coils are connected in series, therefore the induced voltages add up. A true Helmholtz coil configuration assumes separation of coils equal to their radius. For the physical realization of the housing of the excitation coil it was not possible to bring the two halves of Helmholtz coil close enough to satisfy the condition where height of the coil is equal to the radius of the coil, nor did it matter much, because the Helmholtz coil is used to record excitation field using calibration coefficients which compensate for non-ideality of the coil [24].

In case of imperfect Helmholtz coil, it can be calibrated by just recording a pulse from a small search coil that is placed in the middle of excitation coil without the presence of any permanent magnet. As the voltages induced in both pickup coils are in the air, the final calculated magnetic field must be of equal magnitude. The magnetic field is calculated separately using induced voltage at the search coil as well as using the H coil and then compared to each other. The magnetic field from the H coil is multiplied by the calibration coefficient, C that is calculated using the following equation.

$$H = \frac{\int V_1 \cdot dt}{\mu_0 N_1 A_1} = C \frac{\int V_2 \cdot dt}{\mu_0 N_2 A_2} \dots (4.1)$$

$$C = \frac{\frac{\int V_1 \cdot dt}{N_1 A_1}}{\frac{\int V_2 \cdot dt}{N_2 A_2}} \dots (4.2)$$

Where

$V_i$  is the induced voltage at the  $i^{\text{th}}$  coil.

$N_i$  is the number of turns in the  $i^{\text{th}}$  coil

$A_i$  is the coil area of the  $i^{\text{th}}$  coil

$C$  is the calibration coefficient

#### **4.3.2- Testing Procedure**

The sample magnets that are obtained are either in magnetized or unmagnetized state. If they are already in the magnetized state, the magnetic flux density in magnet is unknown. The magnetic flux density and magnetic field are calculated by integrating the induced voltages across the coils with no knowledge of the initial conditions. The characterization of the quality of the magnets requires the knowledge of exact initial conditions to accurately establish the hysteresis loop. The symmetrical hysteresis property is utilized to estimate the initial condition. The magnitude of positive saturated magnetic flux density,  $B_s$ , is equal to negative saturated magnetic flux density;  $-B_s$  while the magnitude of magnetic field required to reach saturation is also equal in the positive and negative direction. The offset in the maximum and minimum saturation flux density and magnetic field are removed to establish the final symmetrical hysteresis loop.

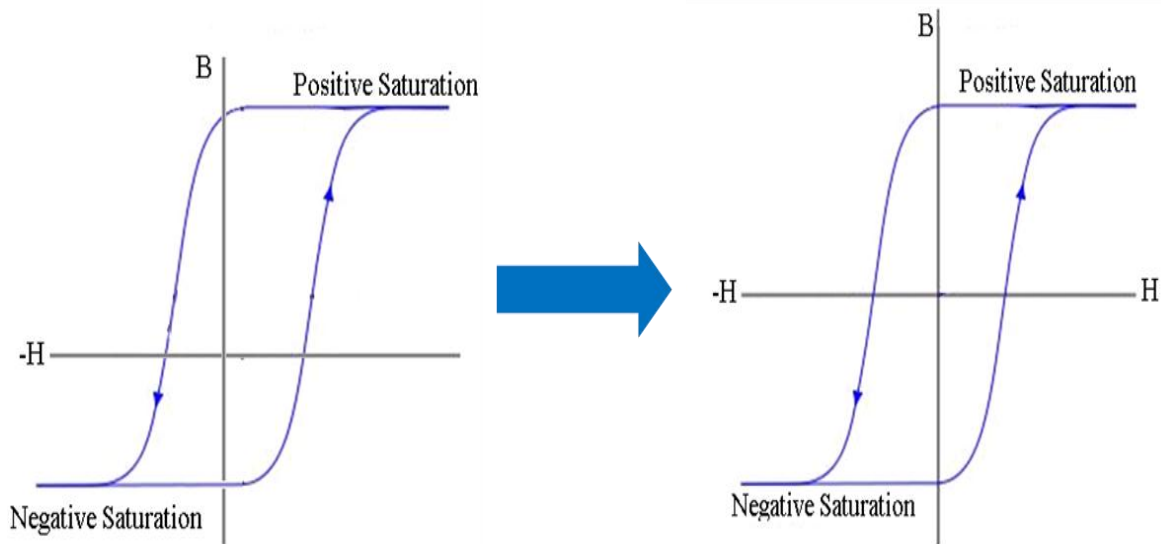


**Figure 4.5: Initial Hysteresis loop without knowledge of initial conditions converted to symmetrical hysteresis after removing the offsets**

The experimental testing sequence to establish the symmetrical hysteresis loop is shown in Figure 4.6 and is described as follows:

- In the first testing position, the direction of magnetic poles alignment and the magnetic flux density in the magnet are unknown. If the magnetic poles are not already aligned, then after the pulsed current is applied to the excitation coil the magnetic poles will try to align in the same direction to the applied field. The magnet reaches saturation point and on the reversal follows some recoil lines. But if the magnetic poles are already aligned to the direction of applied field, the magnet acts as an air.
- In the second testing position, the magnet is flipped such that the magnetic poles are aligned opposite to the direction of applied field. After that, the magnet will realign to the direction of applied field and reach the same saturation point as in first position and then follows the same recoil line.

- In the third testing position, the magnetic poles are already aligned in the same direction to the applied field. After the applied field, the magnet will act as an air region.
- In the fourth testing position, the magnet is flipped again such that the magnetic poles are aligned in an opposite direction to the field applied as in the second testing position. After the applied field, the magnet will again try to realign to the direction of applied field and reach saturation point and then follows the same recoil line.

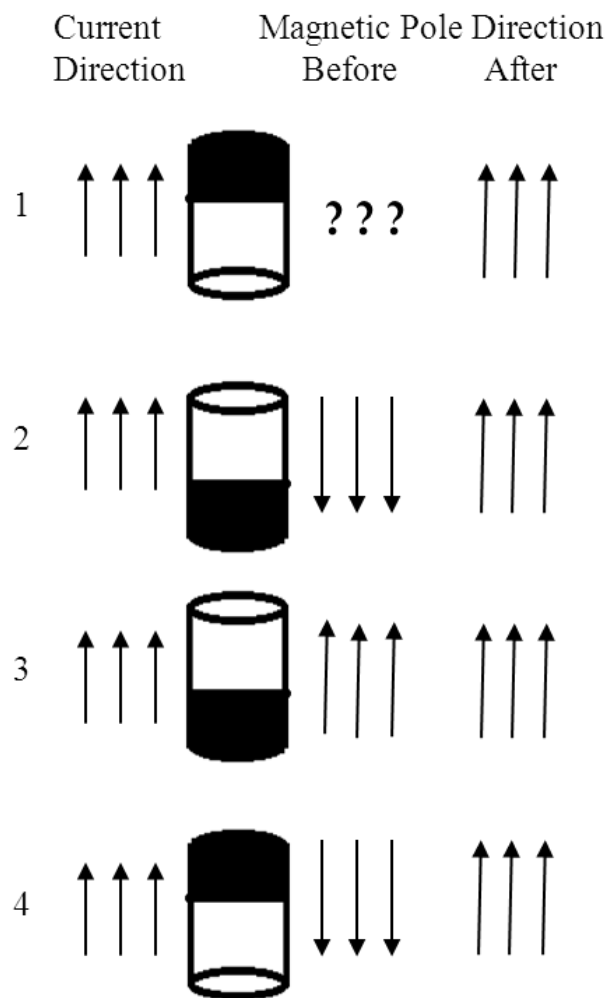


**Figure 4.6 Testing Sequence for the magnet**

### **4.3.3- Testing Procedure for good and bad raw material**

The proposed idea is to operate the magnet just above the knee of the hysteresis. If the bulk of magnets are made up of good material i.e. has no impurities, they will all be operating at the same operating point (above the knee). If the magnet contains bad material, the operating point will fall below the knee of the hysteresis.

As we do not have different set of raw material permanent magnets for the same type of magnet set, the magnets are emulated bad raw material by heating good magnets at high temperatures. We have assumed that the heated permanent magnet emulate some degree of impurities in the raw material as compared to the same permanent magnet at room temperature. The degree of emulated impurity in raw material in the permanent magnetic increases with the increase in the temperature of the magnet i.e. the magnet at 50<sup>o</sup>C emulates bad raw material quality as compared to the same type of magnet at room temperature while the magnet at 70<sup>o</sup>C emulates more bad raw material quality as compared to the same type of magnet at room temperature.

The testing procedure between good and bad raw material is as follows:

- Charge capacitors up to certain voltage such that negative peak of the applied magnetic field forces the operating point of the magnet to fall slightly above or close to the knee of the hysteresis curve.
- If the operating point is slightly below the knee, use the damping resistor to force the operating point slightly above the knee of the hysteresis.

- Test the magnet sample at room temperature to obtain hysteresis loop using the sequence explained in Section 4.3.2.
- Heat the magnet till certain temperature to emulate bad raw material.
- Test the magnet sample using the sequence in Section 4.3.2
- Compare the recoil lines and residual remanence to distinguish between good and bad raw material.

#### **4.3.4- Set of Tests**

Each type of magnets undergo four different sets of testing

- Different capacitance (46.2mF and 38.2 mF )
- Different voltages (300V, 350V, 400V and 425V)
- Different damping resistors (0 $\Omega$ , 500 $\mu\Omega$ , 1m $\Omega$  and 2m $\Omega$ )
- Different temperatures (24<sup>o</sup>C, 50<sup>o</sup>C, 75<sup>o</sup>C and 100<sup>o</sup>C)

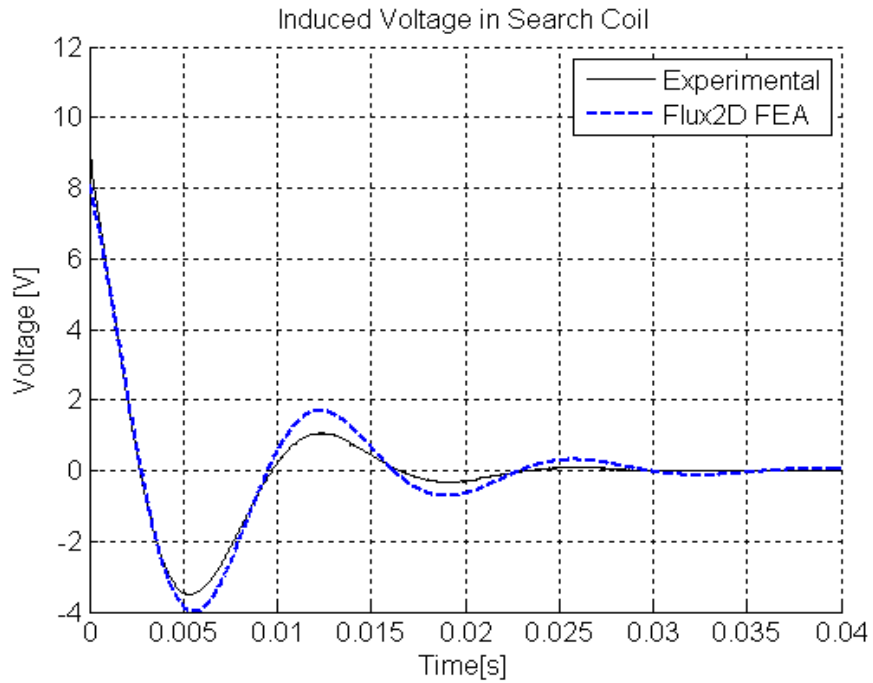
# Chapter 5

## Experimental Results

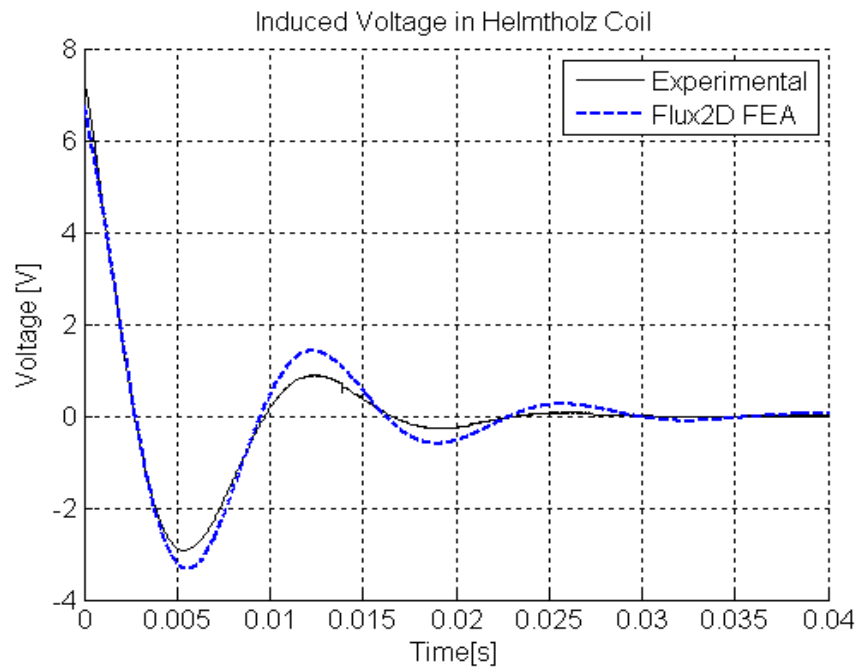
This section will discuss the results obtained for pulsed field magnetometer system with different types of magnets.

### 5.1- Magnetometer

Figure 5.1 shows the comparison between the waveforms obtained experimentally from the pulsed field magnetometer system with the simulation results obtained from FEA analysis. The applied pulsed field was applied through the excitation coil without placing the magnet at the center. The experimental induced voltages across the pickup coils are very close to the reference obtained from the finite element. There is a small variation in the pulse width due to a difference in the inductance of excitation coil. The inductance changes with rapid change in field and it cannot be measured accurately. The peak magnetic flux density and magnetic field intensity also shows very good agreement with the simulated results.



(a) Induced voltage in search coil

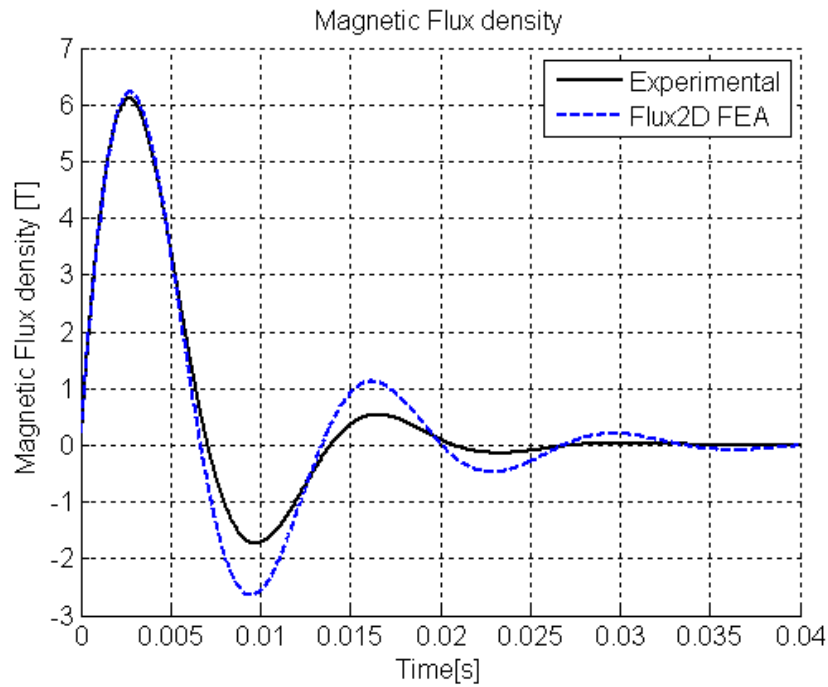


(b) Induced Voltage in H Coil

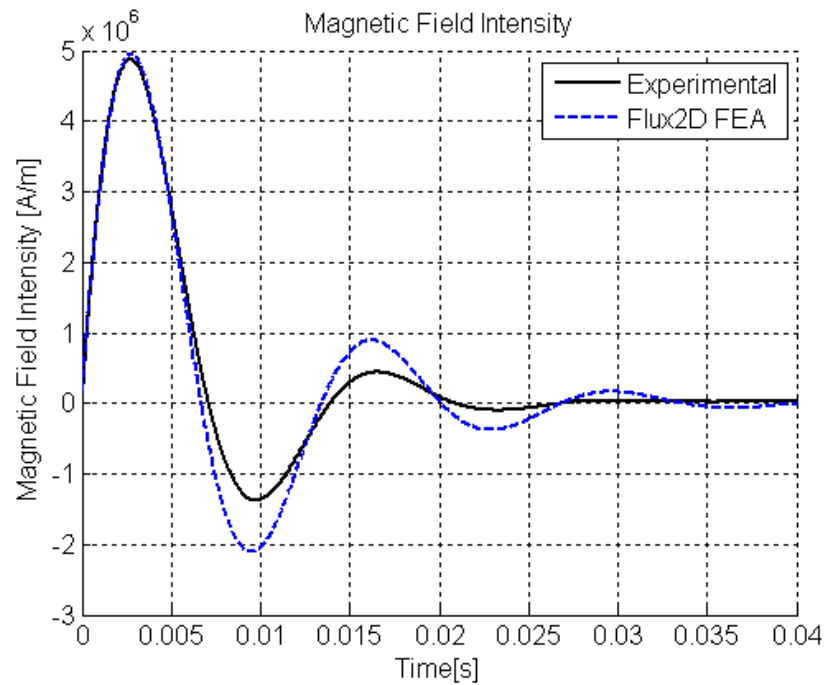
**Figure 5.1: Comparison between Finite Element Analysis and Experimental Results**

**without placing the magnet at the center of the coil i.e. in the air**

Figure 5.1 (cont'd)



(c) Magnetic Flux Density at the center of coil



(d) Magnetic Field Intensity at the center of coil

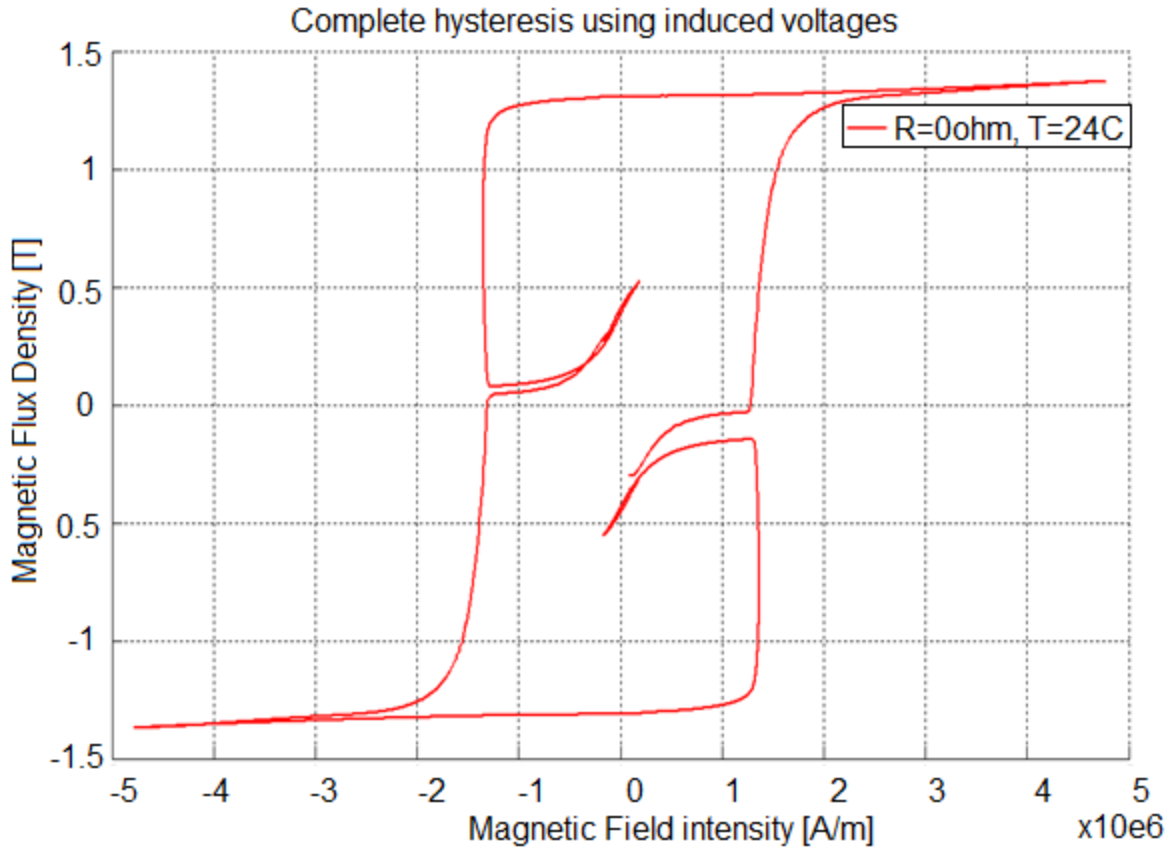
## 5.2- Sample Magnets

Three different types of Neodymium-Iron-Boron Nd-Fe-B magnets were tested as follows:

- Nickel Plated-N42 magnet from K&J Magnetics
- Aluminum coated-AL provided by General Motors
- Black paint coated- NE provided by General Motors

### 5.2.1- Nickel Plated- N42

The testing procedure explained in section 4.3.2 is used to obtain the complete hysteresis. Figure 5.2 show the measured hysteresis obtained using two pulsed currents when the magnetic poles were in the opposite direction for axially magnetized N42- Nickel plated neodymium magnets from K&J magnets. The 46.2mF capacitors are charged up to 425V and then discharged through the excitation coil. The demagnetization factor due to open-loop measurement has been compensated. The magnetic characteristics from the hysteresis loop obtained are compared to the specifications provided by the K&J Magnetics. The results are shown in Table 5.1. The measured hysteresis results for these materials shows excellent results with reference data without any compensation for eddy current effects.



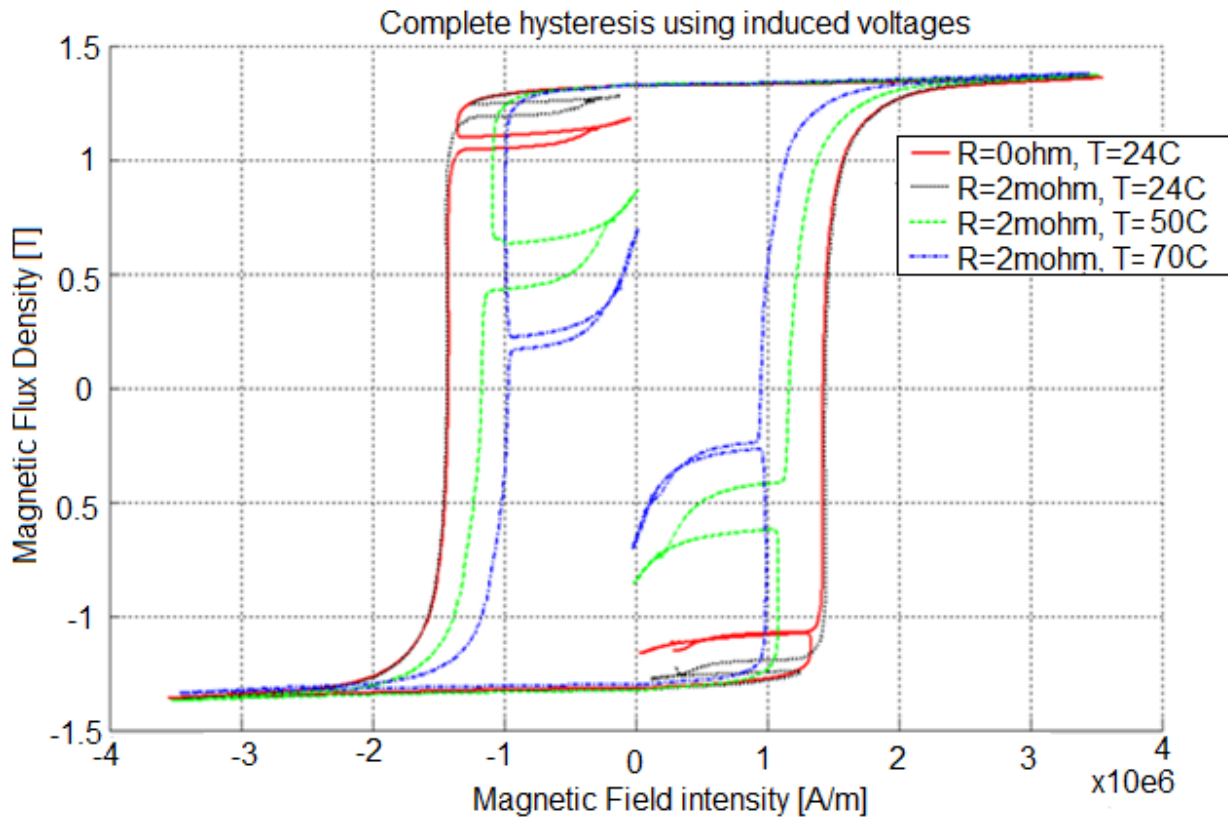
**Figure 5.2: Nickel plated- N42 with 46.2mF capacitance at 425 V**

Table 5.1: Comparison of magnet characteristics between the specs provided by the K&J Magnetics and measured using pulsed field magnetometer

Parameter	Provided	Obtained
Residual Flux Density (Br)	1.30-1.32 T	1.307T
Coercive Force (Hc)	>875.82 At/m	1.257MA/m

The second stage of testing consists of differentiating the quality of raw material of N42 permanent magnet. The magnet is first tested in the pulsed field when the capacitors are charged up to 300V with 0Ω damping resistor. The hysteresis curve is plotted in Figure 5.2. As it can be seen, the recoil line or operating point of the magnet is below the knee. The damping resistor of 2mΩ is added and the testing sequence is repeated and measured hysteresis curve is plotted. The recoil line or operating point is slightly above the knee of the hysteresis. The

magnets are then heated up to 50 °C and 70 °C to induce the effect of bad raw material and pulsed field is generated with 2mΩ damping resistor. Full hysteresis curve for all four experiments are shown in Figure 5.3a, where it can be seen that the operating point of the magnet is lower for the magnet with bad raw material. As the quality gets worse due to higher temperature, the operating point is lowered accordingly. Figure 5.3b shows partial hysteresis that consists of just one pulsed field showing the different recoil lines for each experiment.



(a) Complete Hysteresis

**Figure 5.3: Hysteresis for Nickel Plated-N42 with 46.2mF capacitance at 300V with different damping resistance and temperature**

Figure 5.3 (cont'd)

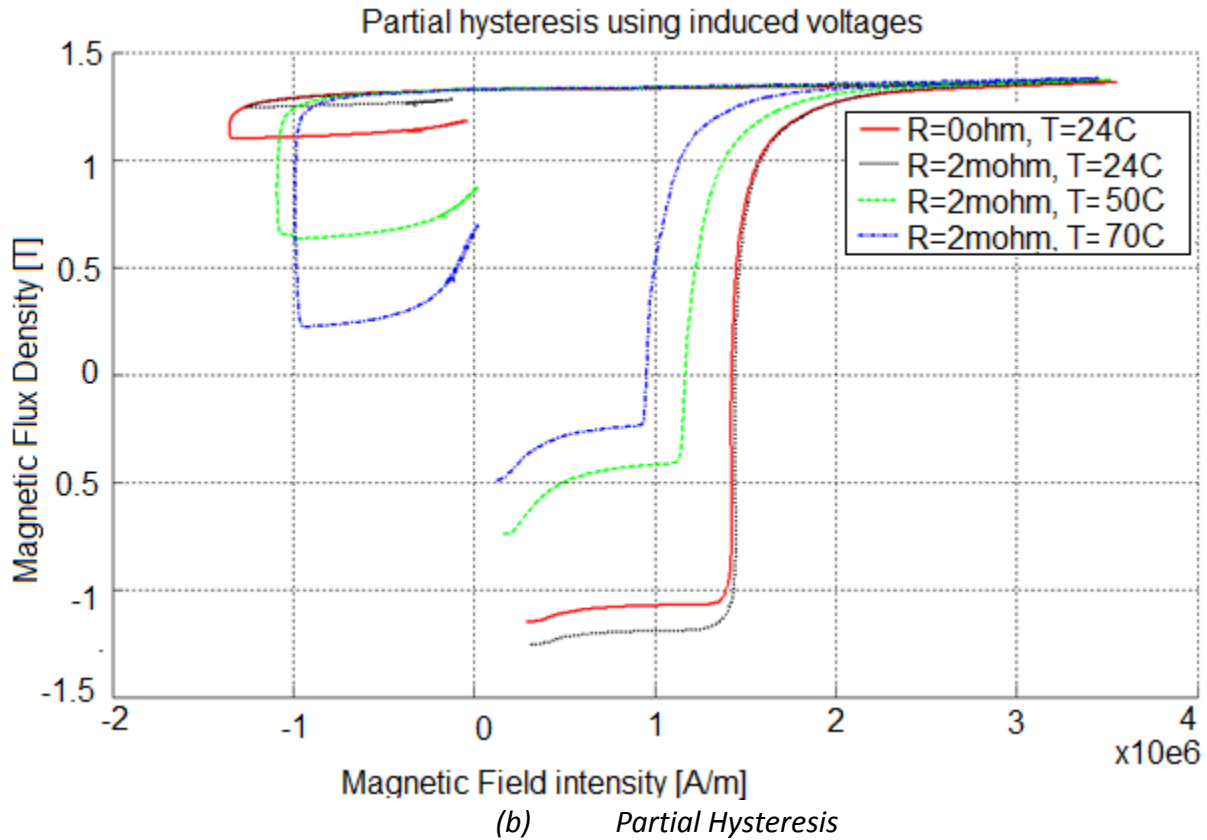


Table 5.2 summarizes the results for Nickel plated magnets where it is shown that the operating point is at 1.28T when 2mΩ damping resistance is added in the circuit. After heating the magnets, the residual remanence decreases with the increase of temperature.

Table 5.2: Comparison of operating points at different temperature and damping resistors for Nickel plated magnets

Experiment	Residual Remanence [T]
0Ω, Temperature 24 <sup>o</sup> C	1.2
2mΩ, Temperature 24 <sup>o</sup> C	1.28
2mΩ, Temperature 50 <sup>o</sup> C	0.80
2mΩ, Temperature 70 <sup>o</sup> C	0.65

### 5.2.2- Aluminum Coated

Figure 5.4 shows the complete hysteresis of Aluminum coated sample magnets with different capacitance of 46.2mF and 38.5 mF while charging the capacitors up to 425 V and 0Ω damping resistance. The measured hysteresis loop is very close to each other at room temperatures. The solid red line represents the 46.2mF capacitance bank discharge where pulsed width is higher than the 38.5mF capacitance bank discharge shown in blue dotted lines. The remanence of the magnet is about 1.25 T and coercivity of 3.2 MA/m. The demagnetization curve for this magnet sample does not fall close to knee of the material when the applied field is in the opposite direction. This shows that these magnets are very strong and requires much higher demagnetization field to fall below the knee as compared to nickel plated-N42 sample magnet.

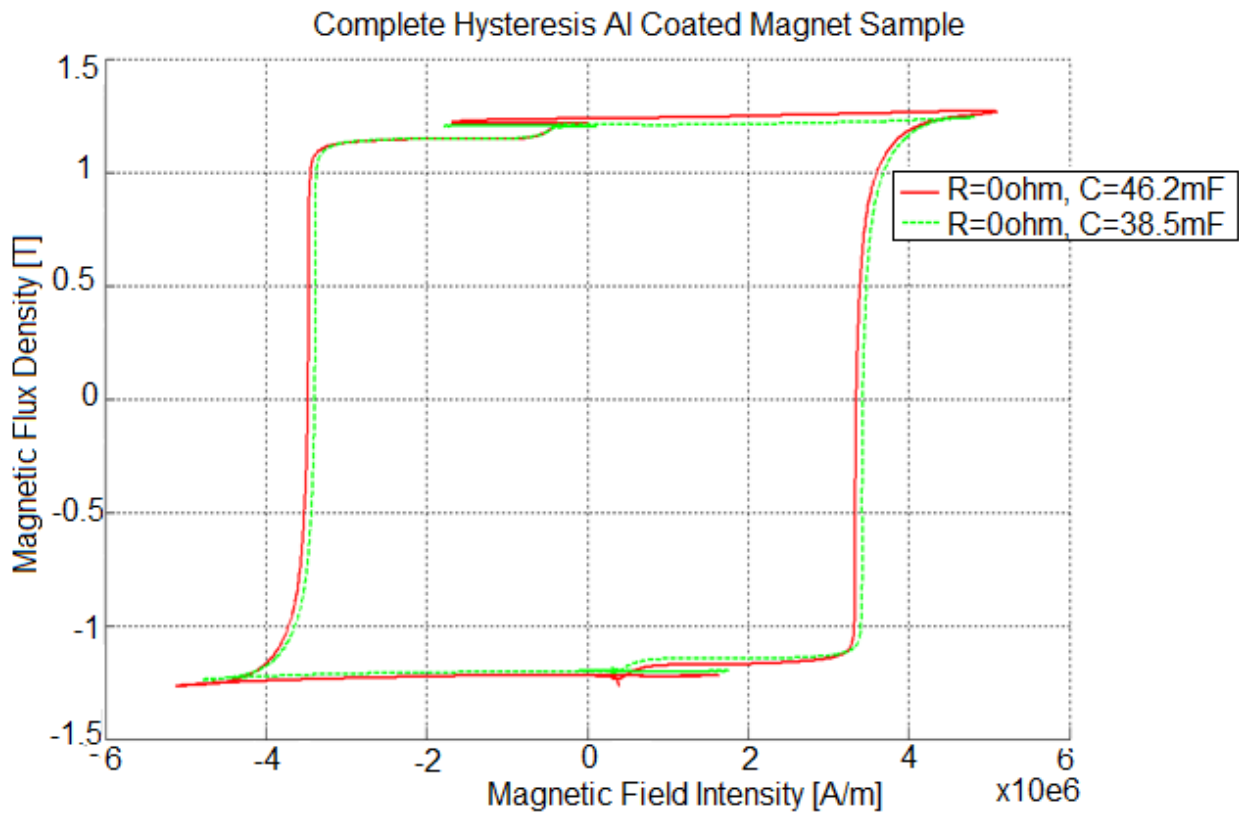
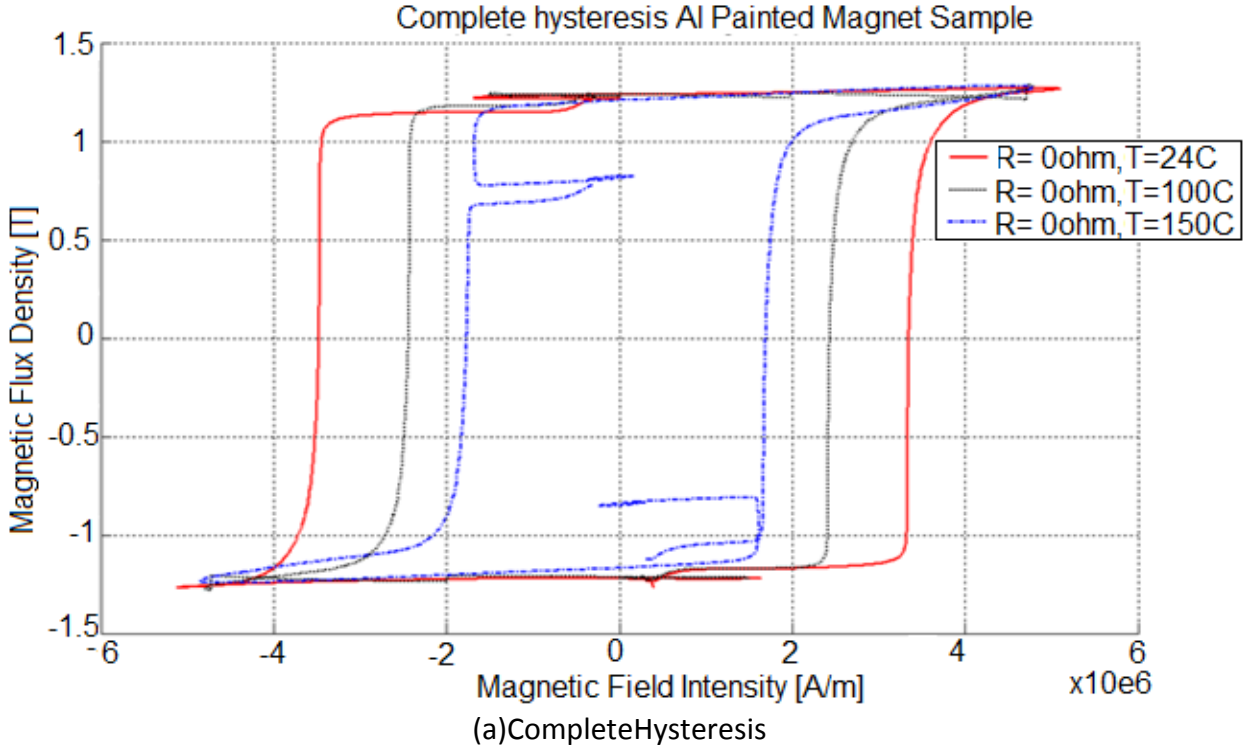


Figure 5.4: Complete hysteresis for Aluminum coated magnet at 425V at room temperature

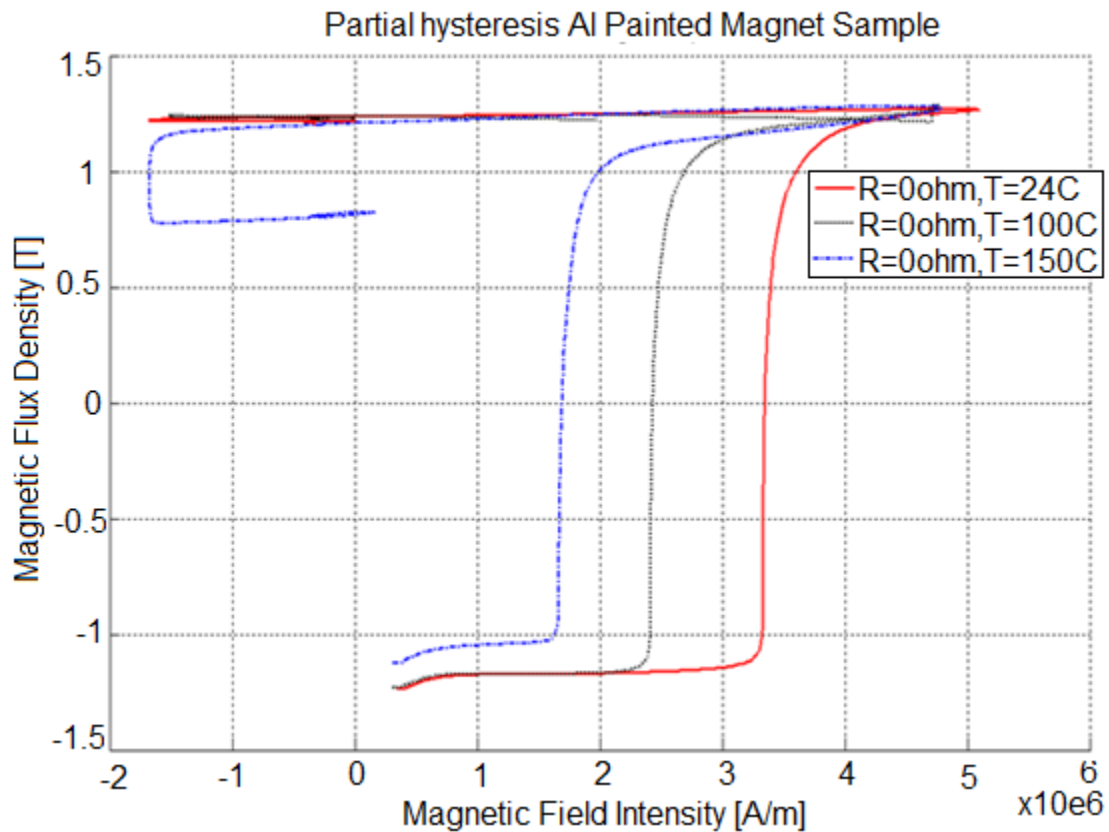
The second stage requires distinguishing between good and bad raw material for these types of magnets. The same method used before is applied here as well where magnet samples are heated to induce bad quality raw materials. The magnets are slowly heated to 100°C and 15°C and also with different capacitance.

Due to the higher negative peak of the applied field in the 38.5mF capacitance as compared to 46.2mF, a better result is seen as the magnets operating point changes at a higher degree. Figure 5.5a and b shows the complete and partial hysteresis of Aluminum coated magnets provided by GM respectively. The results are shown when the capacitors are charged up to 425V with 38.5mF capacitance with 0Ω damping resistance at room temperature and at 150°C.



**Figure 5.5: Hysteresis for Aluminum coated magnet at 425V at different temperatures using capacitance of 38.5mF**

Figure 5.5(cont'd)



(b) Partial Hysteresis

It can be seen using Figure 5.5b that the magnets have to be heated to a very high temperature before a significant difference can be seen in the operating point. Table 5.3 summarizes the results for Aluminum plated magnets where it is shown that at room and lower temperatures, the operating point remains close to 1.22 T i.e. very close to the remanence of magnet. This reveals that only higher amount of impurities can be detected for these types of samples using the exact same device.

Table 5.3: Comparison of operating points at different temperature for Aluminum coated magnets

Experiment	Residual Remanence [T]
Temperature 24 <sup>0</sup> C	1.22
Temperature 100 <sup>0</sup> C	1.23
Temperature 150 <sup>0</sup> C	0.85

### 5.2.3- Black Paint Coated

Figure 5.6 shows the complete hysteresis of Black Paint coated sample magnets with different capacitance of 46.2mF and 38.5 mF while charging the capacitors up to 425 V and 0Ω damping resistance at room temperature and 150<sup>0</sup>C. The measured hysteresis loop is very close to each other at room temperatures. The solid red line represents the 46.2mF capacitance bank discharge where pulsed width is higher than the 38.5mF capacitance bank discharge shown in green dotted lines. The effect of temperature is clearly seen in the measured hysteresis loop as the squareness of the loop is much smaller. The black and blue dotted line represents the discharge using capacitance of 46.2mF and 38.5mF at 150<sup>0</sup>C respectively. The remanence of the magnet is about 1.25 T and 1.15T at room temperature and 150<sup>0</sup>C while the coercivity of 3.4 MA/m and 1.6MA/m.

These magnets are very strong magnets like the Aluminum coated magnets that requires much higher negative applied peak for the demagnetization curve to fall close or lower than the knee of the material.

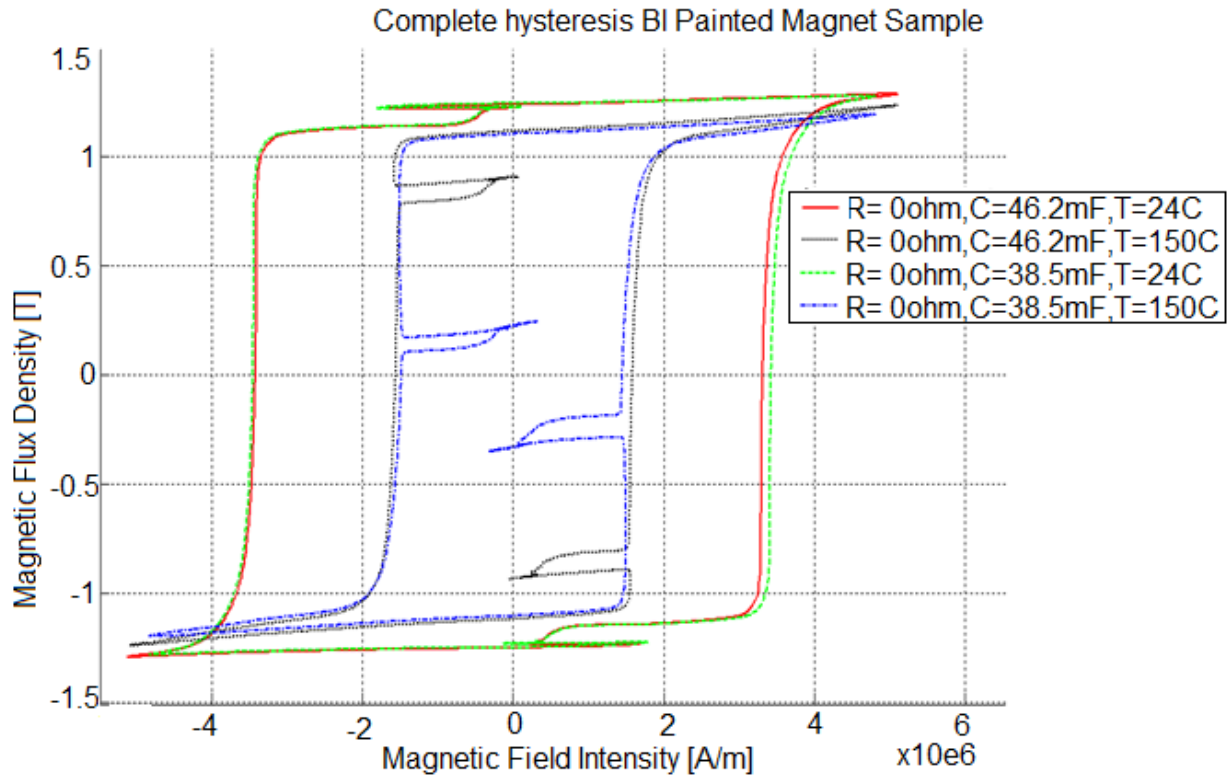
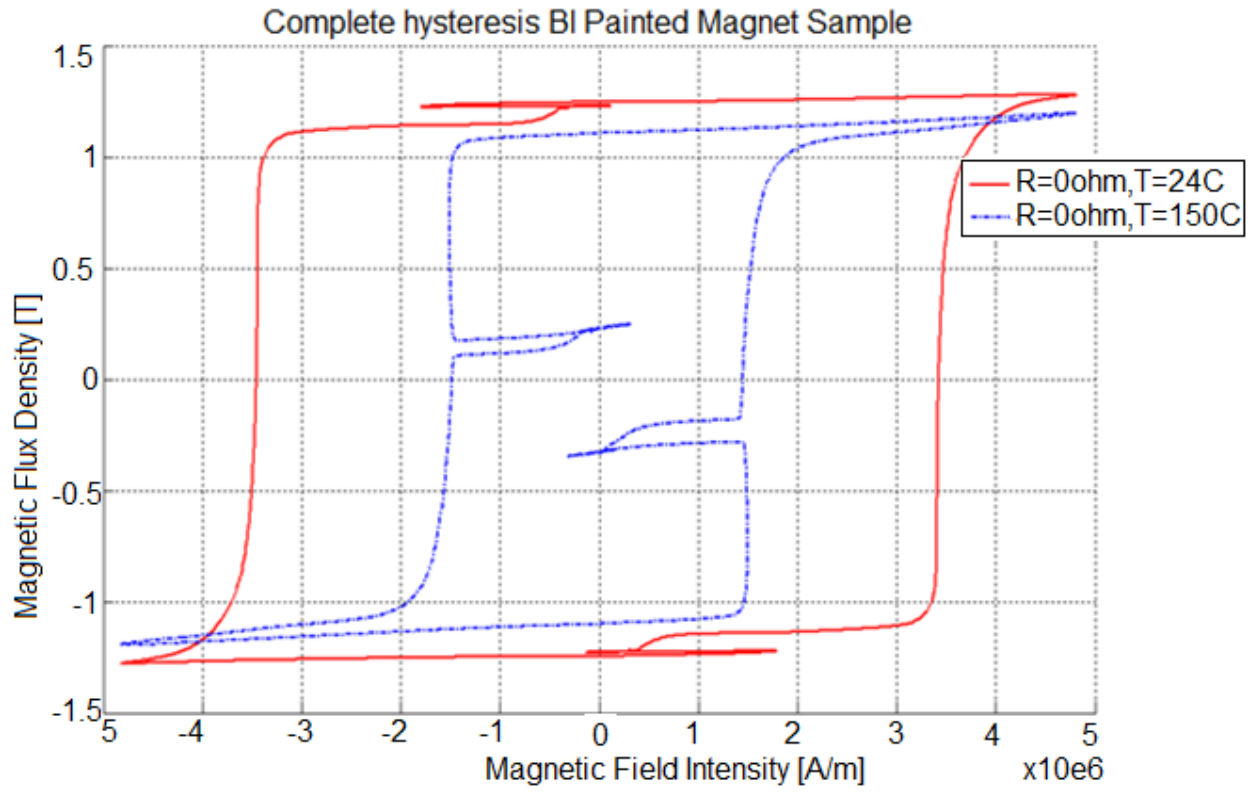


**Figure 5.6: Complete hysteresis for Black paint coated magnet at 425V at different temperatures and capacitance**

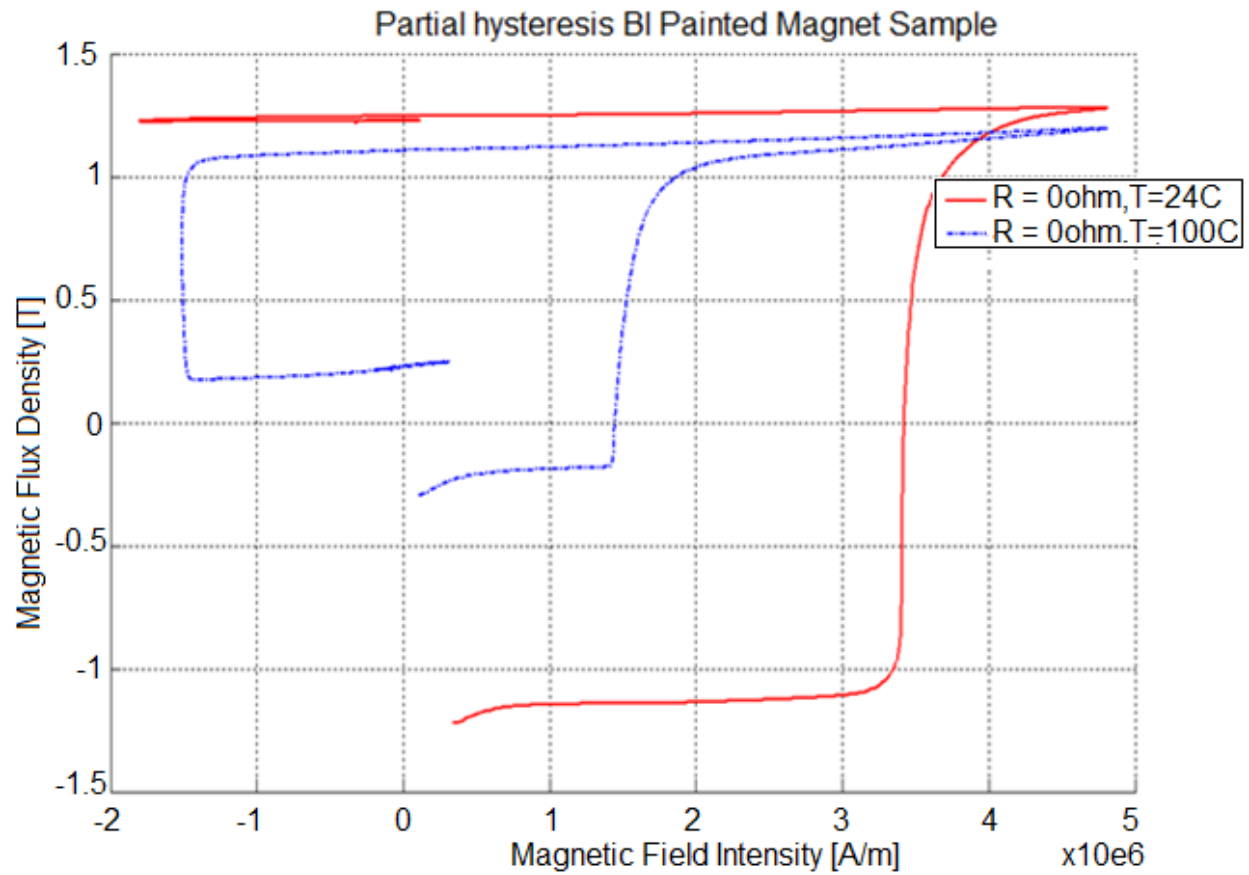
The second stage requires distinguishing between good and bad raw material for these types of magnets where the magnets are slowly heated to 100<sup>o</sup>C and 150<sup>o</sup>C and also with different capacitance. Figure 5.7a and b shows the complete and partial hysteresis of Black painted magnets provided by GM respectively. The results show a similar pattern as the aluminum coated sample magnets where magnets have to be heated to very high temperature before a significant difference can be seen in the operating point. At room and lower temperatures, the operating point is very close to the remanence of magnet. This also shows that only higher amount of impurities can be detected in these types of samples using the exact same device. The results are summarized in Table 5.4.



(a) Complete hysteresis

**Figure 5.7: Complete hysteresis for Black Paint coated magnet at 425V at different temperatures**

Figure 5.7 (cont'd)



(b) Partial hysteresis

Table 5.4: Comparison of operating points at different temperature for Black painted magnets

Experiment	Residual Remanence [T]
Temperature 24 <sup>0</sup> C	1.2
Temperature 100 <sup>0</sup> C	0.3

## Chapter 6

### Conclusions and Future Work

#### 6.1- Conclusions:

Different magnetometers are reviewed before pulsed field magnetometer is chosen due to its simplicity, quick and smaller size. Starting from the basic geometry, coil winding configuration and input currents of the pulsed field magnetometer are calculated using Finite Element Method and MATLAB/Simulink. The whole coil arrangement combined with power electronic circuitry is built. The control is implemented using LabView and the results are post processed using MATLAB. The concept of the proposed method using FEM is compared to those results obtained using experimentally.

The pulsed field magnetometer system device is used to test three different Neodymium-Iron-Boron magnets: Nickel plated, Aluminum coated and Black painted magnets with different testing sequences. The first part of the proposed solution is successfully implement using two current pulsed with magnet position at  $0^{\circ}$  and  $180^{\circ}$ . The measured hysteresis loops are plotted for different set of magnets at different temperature after compensating for open-loop demagnetization factor.

In the second part of the solution, the magnetic field is applied such that the negative peak forces the magnet operating point to fall slightly above or close to the knee of the hysteresis curve. The magnets with both, good and bad, raw material quality are tested with different sequences using the pulsed field magnetometer system. The magnets with bad raw material trail different minor loops and recoil line when compared to the magnets with good raw material.

It has been shown that the operating point of the Nickel plated magnets fall below the knee of the hysteresis curve when the raw material has slight form of impurities. On the other hand, the Aluminum coated and Black painted magnets are much stronger than the Nickel plated magnets. Using the current pulsed field magnetometer system, both of these stronger magnets have to contain many impurities to be able to distinguish between the good and bad qualities of raw material. This is due to the fact that the existing negative applied field is not strong enough to force the magnet to operate close to the knee of the hysteresis loop at room temperature. Small modifications in the present design are needed such that small amount of impurities can be detected in the stronger magnets as well and are further explained in the following section.

On the whole, the pulsed field magnetometer, coupled with minor loops and recoil lines, is used as successful technique to distinguish between good and bad raw material of the permanent magnets used in PMAC machines. After accounting for small modifications in the design, the device can be used to test the bulk of the permanent magnets.

## 6.2- Future Work Modifications:

There are several design modifications that can be made for future work:

1. Aluminum and black coated magnets are much stronger magnets as compared to nickel plate. The negative peak of the current does not create enough magnetic fields, which will force the magnet to operate below or close to the knee of the hysteresis curve. Even heating the magnet at higher temperatures such as  $50^{\circ}\text{C}$ ,  $70^{\circ}\text{C}$ ,  $100^{\circ}\text{C}$ ,  $130^{\circ}\text{C}$  does not force the magnet to reach significantly different operating point. The magnets were required to heat up to  $150^{\circ}\text{C}$  so that the operating point falls below the knee of the hysteresis. This shows that using the exact same pulsed field magnetometer device; it can only detect higher degree of impurities in the sample magnets.

Therefore, the power electronics circuitry needs to be modified in such a way that will increase the negative peak of the current. The rated capacitor voltage that is currently utilized in the experiment is 450V. One option is to find capacitors with higher rated voltage. The drawback for this type is that the capacitor size is going to be larger and the cost is more expensive.

Another and most feasible option is to increase the voltage ratings by adding the same amount of capacitance in series. As the net capacitance will be halved, the same amount of net capacitance is added in parallel mode. There we need to quadruple the same amount of capacitors such that the total rated voltage of the

capacitors can be increased by double amount while the total capacitance remains the same.

2. In the current mode, the magnets are reversed manually that takes usually requires extra time. Another circuit modification is to add 2 DPDT safety switches to reverse the direction of current before thyristor as shown in Figure 6.1. Safety switches have much higher current ratings as compared to high current contactors that tend to open automatically once current exceeds the limit as a safety feature.
3. Add thermocouple that can accurately measure the magnet temperature in the holder and/or put the whole coil arrangement in the oven. We need to make sure that all the parts used to make the pulsed field magnetometer arrangement are able to withstand higher temperatures.

# **BIBLIOGRAPHY**

# BIBLIOGRAPHY

- [1] P. Campbell, *Permanent Magnet Materials and Their Applications*. Cambridge, U. K.: Cambridge University Press, 1994, pp. 90–97.
- [2] F. Fiorillo, "Measurements of magnetic materials," *Metrologia*, vol. 47, no. 2, p. S114, 2010
- [3] J. Lenz, "A review of magnetic sensors," *Proceedings of the IEEE*, vol. 78, no. 6, pp. 973 – 989, jun 1990.
- [4] Springer, *Springer Handbook of Materials Measurement Methods*.
- [5] P. Bretchko and R. Ludwig, "Open-loop pulsed hysteresis graph system for the magnetization of rare-earth magnets," *IEEE Transactions on Magnetics*, vol. 36, no. 4, pp. 2042 –2051, jul 2000.
- [6] R. Krishnan, *Electric Motor Drives: Modeling, Analysis, and Control*, Upper Saddle River, NJ: Prentice Hall, 2001.
- [7] Permanent magnets (magnetically hard) materials-methods of measurement of magnetic properties, IEC standard publication 60404-5, 1993, Geneva: IEC central office.
- [8] Dennison, E.J., "The hysteresisgraph as a quality control tool," *Electrical Electronics Insulation Conference and Electrical Manufacturing & Coil Winding Conference, 1993*.
- [9] S. Foner, "Versatile and sensitive vibrating-sample magnetometer," *Review of Scientific Instruments*, Vol. 30, no. 7, pp. 548–557, 1959.
- [10] Ribeiro, A.L. , "Vibrating sample magnetometer for large permanent magnets," *AFRICON 2007* , vol., no., pp.1-5, 26-28 Sept. 2007
- [11] D. Dufeu, and P. Lethuillier, "High sensitivity 2 T vibrating sample magnetometer," *Review of Scientific Instruments*, vol. 70, 3035 , Jan 1999.
- [12] M. Radparvar, "A wide dynamic range single-chip SQUID magnetometer", *IEEE Trans. on Applied Superconductivity*, vol. 4, pp.87 -91 1994

- [13] R. Grossinger, G. Jewell, D. Howe, and J. Dudding, "Pulsed field magnetometry," in Magnetics Conference, 1993. INTERMAG '93., Digest of International, 13-16 1993, pp. CB-03 –CB-03.
- [14] R. Cornelius, J. Dudding, P. Knell, R. Grossinger, B. Enzberg-Mahlke, W. Fernengel, M. Kupferling, M. Taraba, J. Toussaint, A. Wimmer, and D. Edwards, "Pulsed field magnetometer for industrial use," *IEEE Transactions on Magnetics*, vol. 38, no. 5, pp. 2462 – 2464, sep 2002.
- [15] D. Eckert, R. Grssinger, M. Doerr, F. Fischer, A. Handstein, D. Hinz, H. Siegel, P. Verges, and K. H. Mller, "High precision pick-up coils for pulsed field magnetizationmeasurements," *Physica B: Condensed Matter*, vol. 294-295, pp. 705 – 708, 2001.
- [16] R. Ludwig, P. Bretchko, and S. Makarov, "Magnetic and eddy current effects in an open-loop pulsed hysteresis graph system for magnetization of rare-earth magnets," *IEEE Transactions on Magnetics*, vol. 38, no. 1, pp. 211 –220, jan 2002.
- [17] S. Kato and G. Kido, "Pulsed field magnetometer for low-temperature study of high-performance permanent magnets," *IEEE Transactions on Magnetics*, vol. 36, no.5, pp. 3634–3636, Sep. 2000.
- [18] R. Grssinger, M. Kpferling, P. Kasperkovitz, A. Wimmer, M. Taraba, W. Scholz, J. Dudding, P. Lethuillier, J. C. Toussaint, B. Enzberg-Mahlke, W. Fernengel, and G. Reyne, "Eddy currents in pulsed field measurements," *Journal of Magnetism and Magnetic Materials*, vol. 242-245, no. 2, pp. 911 – 914, 2002.
- [19] G. Jewell, D. Howe, C. Schotzko, and R. Grossinger, "A method for assessing eddy current effects in pulsed magnetometry," *IEEE Transactions on Magnetics*, vol. 28, no. 5, pp. 3114 –3116, sep 1992.
- [20] Flux 10.3 2D Application User guide Volume 1-4. CEDRAT GROUP, 2009.
- [21] E. B. Becker, G. F. Carey, and J. T. Oden, *Finite Elements: An Introduction*, vol. I. Englewood Cliffs, New Jersey: Prentice-Hall, 1981.
- [22] Casoria, S., P. Brunelle, and G. Sybille, "*Hysteresis Modeling in the MATLAB/Power System Blockset*," *Electrimacs 2002*, École de technologie supérieure, Montreal, 2002.
- [23] G. Sybille, P. Brunelle, H. Le-Huy, L.A. Dessaint, K. Al-Haddad, Theory and application of Power System Blockset, a MATLAB/Simulink-based simulation tool for power systems, in: *Proceedings of the IEEE PES Winter Meeting Conference*, 2000.

- [24] S. Trout, "Use of helmholtz coils for magnetic measurements," *IEEE Transactions on Magnetics*, vol. 24, no. 4, pp. 2108 –2111, july 1988.